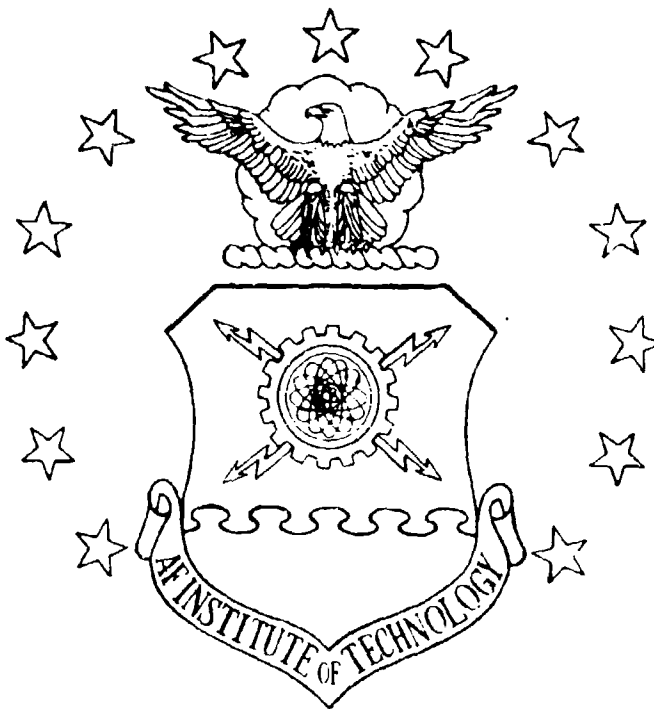


1

AD-A154 722



THE EFFECT OF STRESS AND HOT CORROSION
ON NICKEL-BASE SUPERALLOYS

THESIS

Stephen J. Balsone
First Lieutenant, USAF

AFIT/GAE/AA/85M-1

Accession
NTIS GR
DTIC TAB
Unannoun
Justific

By

This document has been approved
for public release and sale; its
distribution is unlimited.

S DTIC ELECTE **D**
JUN 4 1985
E

DTIC FILE COPY

DEPARTMENT OF THE AIR FORCE
AIR UNIVERSITY

AIR FORCE INSTITUTE OF TECHNOLOGY

Wright-Patterson Air Force Base, Ohio

AFIT/GAE/AA/85M-1

①

SECRET
JUN 4 1985
E

THE EFFECT OF STRESS AND HOT CORROSION
ON NICKEL-BASE SUPERALLOYS

THESIS

Stephen J. Balsone
First Lieutenant, USAF

AFIT/GAE/AA/85M-1

Accession For	
NTIS GRA&I	<input checked="" type="checkbox"/>
DTIC TAB	<input type="checkbox"/>
Unannounced	<input type="checkbox"/>
Justification	
By _____	
Distribution/	
Availability Codes	
Dist	Avail and/or Special
A/1	

Approved for public release; distribution unlimited

AFIT/GAE/AA/85M-1

THE EFFECT OF STRESS AND HOT CORROSION
ON NICKEL-BASE SUPERALLOYS

THESIS

Presented to the Faculty of the School of Engineering
of the Air Force Institute of Technology
Air University
In Partial Fulfillment of the
Requirements for the Degree of
Master of Science in Aeronautical Engineering

Stephen J. Balsone
First Lieutenant, USAF

March 1985

Approved for public release; distribution unlimited

ACKNOWLEDGEMENTS

I wish to thank my faculty advisor, Lt Col G.W. Watt, for his time and assistance in completing this work. It was his original idea to conduct such a study, and his guidance and metallurgical knowledge proved invaluable. I have learned a great deal from him. Thanks also to Dr T. Nicholas of the Metals Behavior Branch, Air Force Materials Laboratory. Without his enthusiastic support and technical assistance in the lab, this work would have never been conducted. I wish to thank Dr M. Khobaib of The University of Dayton for his advice and help in analyzing the experimental results. I am indebted to the Coatings Division, General Electric's Aircraft Engine Business Group, Evendale, Ohio, for supplying test material. Their interest in this program and help in outlining the scope of the study is much appreciated. Finally, I wish to express my deepest thanks to my wife Susan and son Andy for their understanding during the course of this work. Now, they can get the attention that they deserve.

Stephen J. Balsone

TABLE OF CONTENTS

	page
Acknowledgements 11
List of Figures iv
List of Tables vi
Abstractvii
I. Introduction 1
Background 1
Objective 7
Approach 7
II. Description of Test Apparatus 15
A. Inconel 718 15
B. René 77 and René 80 21
III. Test Procedure 25
A. Inconel 718 25
B. René 77 and René 80 30
IV. Experimental Results and Discussion 34
A. Inconel 718 34
1. Creep Behavior 34
2. Metallographic Analysis 48
3. Summary 68
B. René 77 and René 80 70
1. Metallographic Analysis 70
2. Summary 83
V. Conclusions and Recommendations 87
Bibliography 90
Appendix: Tabulated creep data 92
Vita106

LIST OF FIGURES

<u>Figure</u>	<u>page</u>
FIG. 1. Effect of salt thickness on hot corrosion rates	10
FIG. 2. Typical creep curve showing the three stages of creep	13
FIG. 3. Effect of temperature on the yield strength of IN 718	17
FIG. 4. Inconel 718 round bar tensile specimen	19
FIG. 5. Experimental test apparatus	20
FIG. 6. Schematic of extensometer assembly	22
FIG. 7. Inconel 718 specimens (A) as received; (B) after salt coating; (C) after hot corrosion attack; and (D) after oxidation	27
FIG. 8. René 77 and René 80 pin placement for testing	32
FIG. 9. Creep curves for IN 718 at a stress level of 10 Ksi	35
FIG. 10. Creep curves for IN 718 at a stress level of 15 Ksi	36
FIG. 11. Creep curves for IN 718 at a stress level of 20 Ksi	38
FIG. 12. Creep curves for IN 718 at a stress level of 30 Ksi	39
FIG. 13. Effect of molten salt of the creep behavior of IN 718	40
FIG. 14. Effect of reduced diameter on creep at 15 Ksi	42
FIG. 15. Effect of reduced diameter on creep at 20 Ksi	43
FIG. 16. Effect of stress level on minimum creep rate for IN 718	45
FIG. 17. Duplicate creep test at a stress level of 20 Ksi	47
FIG. 18. Scanning electron micrographs (500X) showing (a) oxidation and (b) hot corrosion attack of IN 718	49
FIG. 19. Method for determining the depth of hot corrosion attack	51
FIG. 20. Effect of stress level on the depth of hot corrosion attack	52
FIG. 21. Scanning electron micrographs (1000X) showing microstructure of IN 718 (a) in fully heat-treated condition and (b) after creep testing at 20 Ksi for 72 hours at 1472°F	55
FIG. 22. Effect of stress level on the hot corrosion attack of IN 718 during creep testing (500X)	57

FIG. 23.	Scanning electron micrographs (1000X) showing typical hot corrosion attack of IN 718 at (a) 20 Ksi and (b) 15 Ksi, for 72 hours at 1472 ^o F	60
FIG. 24.	Schematic drawings of grain boundary sliding and intergranular cracking	62
FIG. 25.	Scanning electron micrographs (a) 500X and (b) 1000X showing intergranular penetration and grain boundary cracking	64
FIG. 26.	Elemental analysis of hot corrosion products for IN 718.	66
FIG. 27.	Elemental analysis of hot corrosion products for IN 718.	67
FIG. 28.	Weight change of salt coated specimens after 72 hours at 1652 ^o F	71
FIG. 29.	Depth of hot corrosion attack of salt coated specimens after 72 hours at 1652 ^o F	73
FIG. 30.	Scanning electron micrographs (1000X) showing hot corrosion attack of Rene'77	74
FIG. 31.	Scanning electron micrographs (1000X) showing hot corrosion attack of Rene'80	75
FIG. 32.	Elemental analysis of hot corrosion products for Rene'77	77
FIG. 33.	Elemental analysis of hot corrosion products for Rene'80	79
FIG. 34.	Elemental analysis of sulfide particles found in Rene'77 and Rene'80 after hot corrosion attack	82
FIG. 35.	Rene'77 pins showing the effect of salt thickness on the degree of hot corrosion attack	84
FIG. 36.	Effect of salt thickness on the hot corrosion attack of Rene'77	85

LIST OF TABLES

<u>Table</u>	<u>page</u>
TABLE 1. Nominal Composition of Inconel 718	16
TABLE 2. Heat Treatment for Inconel 718	16
TABLE 3. Nominal Composition of René 77 and René 80	24
TABLE 4. Heat Treatment for René 77 and René 80	24
TABLE 5. Test Matrix for Inconel 718	29
TABLE 6. Test Matrix for René 77 and René 80	31

ABSTRACT

The nickel-base superalloys used for jet engine structural components are subjected to high stresses and severe environmental conditions. At the high temperatures inside the jet engine, molten salts tend to form, and thin films of salt coat the internal components. Also present is a very corrosive gas phase containing O_2 , SO_2 , and SO_3 . Such a combination of stress and corrosive environment results in reduced component life and eventual failure. As a consequence, research on high temperature material properties and environmental degradation is a vital part of the technology base for engine life prediction and alloy development.

This study examines the effect of a molten salt environment on the high temperature creep properties of Inconel 718. Sustained-load creep tests were conducted at a temperature of $1472^\circ F$ ($800^\circ C$) in laboratory air at stress levels in the range of 10 Ksi to 30 Ksi. Round bar tensile specimens were coated with a 90% Na_2SO_4 / 10% NaCl salt mixture by spraying a heated specimen with an aqueous salt solution. Creep data were then collected over a 72 hour test period. Tests conducted with salt coated specimens were compared with tests conducted with uncoated specimens. Specimens were subsequently sectioned and mounted, and a metallographic analysis of the corrosion attack was conducted.

Evidence shows a degradation of the high temperature creep properties of Inconel 718 due to the presence of molten salt. This is due primarily to oxide penetration into metal which has been depleted of

alloying elements and, subsequent cracking along oxide-metal interfaces. In addition, grain boundary sliding and void formation along the grain boundaries occurred in the alloy-depleted zone of corrosion attack. This report examines the effect of stress in the corrosion process and the microstructural changes and mechanisms which occur during corrosion-mechanical property interactions.

Static hot corrosion tests on specimens of René 77 and René 80, were also conducted. Cylindrical pins were salt coated and tested for 72 hours at a temperature of 1652°F (900°F) in laboratory air. Weight-change calculations and measurements of the depth of corrosion attack were made, and a metallographic analysis was done.

Handwritten notes:
... corrosion-mechanical property
... results

THE EFFECT OF HOT CORROSION ON NICKEL-BASE SUPERALLOYS

I. INTRODUCTION

BACKGROUND

The design of today's high performance gas turbine engines involves highly complex technologies. The rotating components operate at very high speeds at elevated temperatures and high stresses. Many technological hurdles had to be overcome to reach the high levels of performance and efficiency demanded by today's aircraft. However, military mission requirements keep demanding aircraft which can fly higher and faster. In response to this, the gas turbine engine has been transformed over and over. Scientists and engineers have been tasked with the job of meeting stringent performance requirements under the constraints of existing materials and manufacturing techniques. The drive for reduced weight, higher thrust, and greater efficiency has increased the strength and temperature requirements past the limit of many materials. This has led to the use of nickel-base superalloys as a material class capable of withstanding the severe operating conditions of the gas turbine engine.

Nickel-base superalloys are high-temperature, heat-resistant alloys that are able to retain high strength in the temperature range of 1400°F (760°C) to 1900°F (1038°C). These complex alloys also have good oxidation and corrosion resistance and superior resistance to creep and

rupture at elevated temperatures. Nickel-base superalloys are precipitation hardenable alloys. The major phases present are (1) γ (gamma) phase - the continuous matrix of nickel-base austenite; (2) γ' (gamma-prime) phase - the major precipitate phase; and (3) carbides - mainly $M_{23}C_6$ and MC, where M stands for a metallic element. The gamma phase is strengthened by solid-solution elements such as chromium, molybdenum, tungsten, cobalt, columbium, titanium, and aluminum. Iron in the austenitic matrix lowers the cost and improves workability and weldability, but it also considerably lowers the strength and oxidation resistance of the alloy. The gamma-prime phase can be precipitated in nickel-base superalloys by precipitation hardening heat treatments. The gamma-prime precipitate in high nickel matrices is typically the intermetallic phase $Ni_3(Al,Ti)$. If cobalt is present, it can substitute for some nickel as $(Ni,Co)_3(Al,Ti)$, and if columbium is present, it can form the intermetallic phase Ni_3Cb . The gamma-prime phase has extraordinary long-term stability, and a high volume fraction of gamma-prime gives the alloy remarkable high temperature strength. The third phase is metallic carbides which form in the grain boundaries and within grains. MC carbides are monocarbides formed by titanium, columbium, or tungsten. These carbides are very stable and are believed to form just below the solidification temperature. In $M_{23}C_6$ carbides, the metallic element is usually chromium, but this element can be replaced by iron, tungsten, molybdenum, or cobalt depending on the alloy. $M_{23}C_6$ carbides form during lower temperature heat treatments and during service in the temperature range of 1400°F (760°C) to 1800°F (982°C). They can form either from the degeneration of MC carbides or from soluble carbon in the alloy matrix and usually precipitate in the

grain boundaries.

Since carbides are harder and more brittle than the alloy matrix, their distribution along the grain boundaries will affect the high-temperature strength, ductility, and creep properties. If there are no carbides along the grain boundaries, voids will coalesce along them during high temperature deformation, and excessive grain boundary sliding will take place. Studies in which the carbon content was reduced to very low levels have demonstrated sharply reduced creep life and ductility.⁽¹⁾ Conversely, if continuous chains of carbides extend along the grain boundaries, grain boundary sliding will be inhibited. As a result, excessive stresses will build up during deformation and lead to premature failure along the continuous fracture paths at the carbide interface. A discontinuous chain of carbides along the grain boundaries is the optimum condition since carbides in this form will hinder grain boundary cracking and at the same time will not restrict ductility due to deformation and sliding in the grain boundary region.⁽²⁾

In the selection of a superalloy for jet engine structural components, two important criteria are mechanical properties and environmental degradation. The high temperatures, large rotating velocities, vibratory stresses, and corrosive environment require a material to exhibit good fatigue, creep, and stress-rupture properties, as well as good oxidation and corrosion resistance. Corrosion-mechanical property interactions have been studied by many investigators in the blade operating temperature range of 1200°F (649°C) to 1900°F (1038°C). These results have shown that the environment can significantly degrade the material properties. Floreen and Kane⁽³⁾⁽⁴⁾

reported that oxygen can produce a 100-fold increase in the crack growth rate in some superalloys compared to tests in vacuum or inert environment. They have also shown that minor amounts of sulfur-bearing species in the environment can produce severe degradation of the crack growth properties of high strength alloys. These two types of environmental attack are widely observed and are known as oxidation and sulfidation.

Sulfidation, or hot corrosion, is a form of accelerated oxidation attack occurring in the presence of sulfur and alkali salts in gas turbine engines.⁽⁵⁾ There is general agreement that sodium sulfate, Na_2SO_4 , is the major corrosive constituent. Sodium sulfate is found naturally in sea salt or can be formed by the reaction of sodium in the air with sulfur from burning jet fuel. Hot corrosion occurs due to the presence of a condensed thin film of sodium sulfate on the surface of internal components and is particularly severe in the temperature range of 1400°F (760°C) to 1900°F (1038°C). This corrosive environment along with the high temperatures and large stresses results in a degradation of material properties and reduced component life. Allen and Whitlow⁽⁶⁾ stated that superalloys in combustion turbine environments could experience high-frequency fatigue failure if design values of vibratory and maximum steady stress are based on mechanical properties obtained in air. At high mean stresses, fatigue failure occurred in orders of magnitude fewer cycles than for corresponding loading conditions in air. In another case, Whitlow, et al.,⁽⁷⁾ reported that the presence of a molten salt resulted in more than an order of magnitude reduction in the low-cycle fatigue life of a superalloy. Yoshihira, et al.,⁽⁸⁾ showed that for salt coated specimens, stress-rupture strength was drastically

reduced. These investigations clearly demonstrate the importance of understanding the hot corrosion process and how it affects the material properties. Research in this area has led to methods for minimizing the effect of hot corrosion on superalloys. These include the development of more corrosive resistant alloys and the application of protective coatings.

The nickel-base superalloys are highly alloyed and as a result, determining the corrosion mechanism is very difficult. A unique mechanism may not exist, but rather one that varies from alloy to alloy and with salt composition is more likely to occur. However, some similarities do exist, and variations of a general mechanism have been proposed. Oxide ions in the molten Na_2SO_4 film break down the protective oxide layer formed on the alloy surface. Sulfur diffuses inward, and the formation of sulfides, mainly CrS , depletes the alloy of chromium and other elements which thereby increases the oxidation attack. The breakdown of the protective surface oxides, consisting mainly of Cr_2O_3 and TiO_2 , and the depletion of corrosion resistant alloying elements in the base metal are the phenomena common to most proposed mechanisms. Some mechanisms emphasize the role of sulfur in depleting chromium, the strongest oxidation resistant alloying element. Spengler and Viswanathan⁽⁹⁾ proposed that once chromium sulfides are formed in the alloy, subsequent oxidation of these sulfides can release the sulfur, allowing further diffusion into the metal and the formation of new chromium sulfides. Thus, the sulfidation of nickel-base superalloys in the presence of molten Na_2SO_4 is a self-sustaining reaction. Their research showed that sulfur penetration into a nickel-chromium alloy persisted even after the sulfur-bearing

environment had been removed. Goebel, et al.,⁽¹⁰⁾ stated that the most essential feature of the hot corrosion mechanism is the oxide ion activity of the molten Na_2SO_4 . As sulfur diffuses from the Na_2SO_4 into the alloy, the oxide activity in the molten salt increases, and the Na_2SO_4 becomes a basic flux for the surface oxides. This liquid flux dissolves the normally protective oxides thereby increasing the oxidation attack. The basic fluxing reactions and the formation of internal sulfides cause a more severe depletion of chromium than that which occurs during normal oxidation. Bornstein and DeCrescente⁽¹¹⁾ arrived at similar conclusions. This type of aggressive oxidation continues as Na_2SO_4 is resupplied to the surface or until the sulfur diffusing from the Na_2SO_4 into the alloy is exhausted.

Aggressive environmental-material interactions are commonly associated with intergranular fracture. Many investigators have documented that the presence of a molten salt quickly changed the fracture mode from transgranular in a non-aggressive environment to intergranular. Evidence shows this to be the result of diffusion of an embrittling species such as oxygen or sulfur into the grain boundaries ahead of the crack tip and eventual fracture of the weakened boundaries.⁽⁴⁾ Separation along the weaker fracture paths at the grain boundaries occurs because they represent relatively accessible microstructural inhomogeneities to oxygen and sulfur.⁽⁷⁾ Thus, improving the general corrosion resistance of an alloy, such as by increasing the chromium content, will not reduce crack growth rates if diffusion of aggressive species along grain boundaries is the cause. Compositional changes in the grain boundary and near grain boundary phases are more likely to modify the diffusion rates of embrittling

species along grain boundaries.⁽¹²⁾ This illustrates the need to understand the corrosion mechanisms if the corrosion resistance of materials under stress is to be improved.

OBJECTIVE

The objective of this investigation is to determine the effects of a molten salt environment on the high temperature creep properties of a nickel-iron-base superalloy. This study will attempt to determine the role stress plays in the hot corrosion process and to determine the mechanism(s) which occur during corrosion-mechanical property interactions.

APPROACH

A total of thirteen (13) sustained-load creep tests were conducted using smooth round bar specimens of Inconel 718 (IN 718) having a diameter of either 0.25 inches or 0.125 inches. These tests were conducted at a temperature of 1472^oF (800^oC) and at stress levels of 30 Ksi, 20 Ksi, 15 Ksi, and 10 Ksi. At least two tests were run at each of these four stress levels. One test was conducted in laboratory air to generate baseline creep data. A second test was run using a specimen which had been coated with a thin layer of salt. The results of this test conducted in a molten salt environment were then compared to those of the baseline test generated with the uncoated specimen at the same

stress level. Creep data were collected over a 72 hour test period. All specimens were sectioned and prepared for metallographic analysis. The depth of penetration of the corrosion attack was measured, and an elemental analysis was conducted on the corrosion products.

Static corrosion tests were also conducted using small cylindrical pins of René 77 and René 80. Twenty-three (23) pins were tested at a temperature of 1652^oF (900^oC) in laboratory air for 72 hours. Salt coated and uncoated pins were tested to characterize the oxidation and hot corrosion attack in an unstressed condition. In addition, the effect of salt layer thickness was examined by varying the salt coverage on five (5) of the twenty-three pins. Weight-change calculations were made, and the depth of corrosion attack was measured.

One of the inherent problems of laboratory research is designing experiments to yield results which simulate those seen in actual service. This is especially true when designing hot corrosion experiments. For many years the gas turbine industry has conducted "burner rig" tests to study and rank alloys based on their corrosion resistance. Thin coupons or small pins are tested in combustion gas streams at elevated temperatures. A hot corrosion environment is usually simulated by burning a sulfur-containing fuel with air often containing a specified concentration of sodium chloride, NaCl. However, in such burner rig tests used to simulate actual turbine engine operating environments, it is difficult to determine the exact conditions to which the material has been exposed. Thus, in an attempt to more clearly control the experimental variables, several laboratory test procedures have been used to study hot corrosion.⁽¹⁰⁾

It is convenient to group most laboratory hot corrosion experiments

into the following three categories:

(1) a test specimen is completely or partially immersed in a molten pool of Na_2SO_4 exposed to an oxidizing environment;

(2) a test specimen is coated with a specified amount of Na_2SO_4 and exposed to an oxidizing environment;

(3) the Na_2SO_4 is applied to a test specimen at periodic intervals either by immersion or spraying in an oxidizing environment.

In this study, test specimens were coated with a thin layer of salt by spraying a heated specimen with a saturated salt solution. Only a single application prior to testing could be done because after the specimen was mounted in the creep testing frame and the tube furnace lowered to enclosed the specimen, there was no access to the specimen until the test was completed. Goebel, et al.,⁽¹⁰⁾ reported that a single salt application does allow for the development of hot corrosion mechanisms for the situation where Na_2SO_4 is deposited on the surface of an alloy. Allen and Whitlow⁽⁶⁾ also reported that corrosion produced using these laboratory techniques duplicated the hot corrosion attack frequently observed on combustion turbine blades retrieved from service.

Figure 1 shows the effect of salt thickness on hot corrosion rates for a nickel-base superalloy as reported by Fang and Shores.⁽¹³⁾ The figure clearly shows that the most severe corrosive condition was not complete immersion but at a Na_2SO_4 salt coverage of approximately 2.5 mg/cm^2 (in an $\text{O}_2 + 0.15\% \text{ SO}_2$ gas environment). Although Fang and Shores

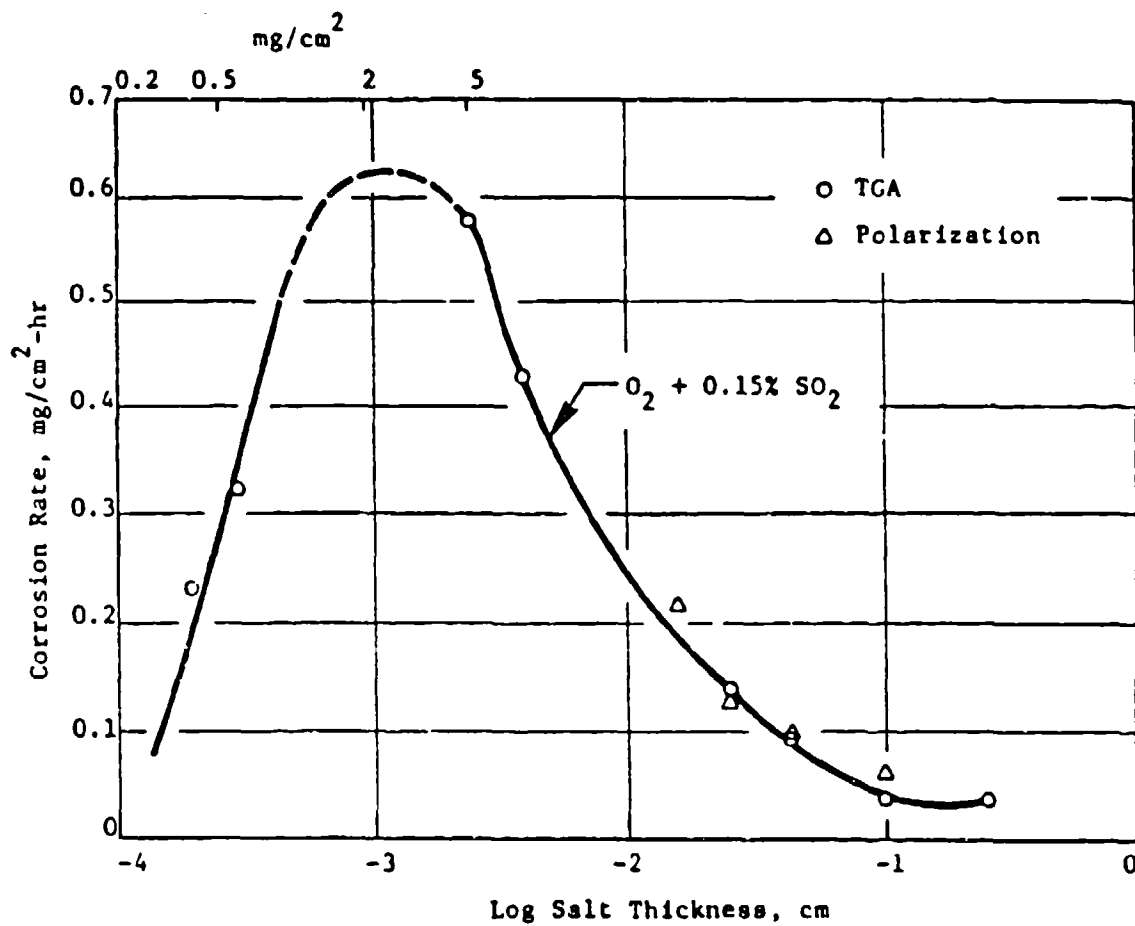


FIG. 1. Effect of salt thickness on hot corrosion rates (ref. 13).

conducted their experiments in a different gas environment and on a different superalloy, their results were used as a guide in defining the test condition used in this study. A salt coverage of 5.0 mg/cm^2 was selected for this study so that it would produce a corrosion attack slightly less than the most severe on the "thick" side of the curve. This was chosen to prevent the single salt application from exhausting its corrosive action during the course of a test.

As was stated earlier, sodium sulfate, Na_2SO_4 , has been determined to be the major corrosive constituent. However, Whitlow, et al.,⁽¹²⁾ have stated that chloride ions, Cl^- , play a role in the degradation of rupture properties and that sodium sulfate at 750°C alone had no effect on creep behavior. Their observed rupture life data indicated that the time to rupture in the presence of molten salt decreased with increasing chloride content. Such observations have led investigators to include a chloride containing salt in their molten salt experiments. A mixture of 90% Na_2SO_4 / 10% NaCl by weight was chosen for this study. This mixture has a melting point of approximately 1400°F (760°C). This is the same salt composition used by Yoshida, et al.,⁽⁸⁾ in their investigation.

Most corrosion experiments in past years have been conducted under no stress. Such an example is burner rig testing in which the test specimens are most often suspended freely. In many cases, the experiments were used to rank new alloy compositions according to their corrosion resistance based on visual examination and weight-change measurements. However, such high temperature corrosion tests may not be useful in predicting the corrosion behavior of components in actual service. The specific role of stress in the hot corrosion process is not clear, and recent studies have begun to address this question.

Floreen and Kane⁽³⁾⁽⁴⁾ reported that environments which markedly increase the crack growth rate did not produce significant corrosion attack or degradation of material properties in unstressed specimens. Even in some of the very aggressive sulfur-containing environments, unstressed samples showed no general corrosion damage and no visible subsurface attack. Whitlow, et al.,⁽¹²⁾ showed that the decrease in time to rupture due to the presence of a molten salt appears to diminish with decreasing stress and suggested that below a threshold stress level, rupture life is insensitive to corrosion. Crack initiation and propagation may be due to stress enhancing the localized diffusion of embrittling species such as oxygen and sulfur down grain boundaries along a stress gradient. As a result of studies such as these, more emphasis is being placed on corrosion testing under stress and the effect corrosion has on material properties. This is the driving force behind a study such as this one.

In this study, the material property selected for investigation was creep resistance. Creep is the progressive deformation of a material at constant stress due to elevated temperature exposure.⁽¹⁴⁾ To determine the creep curve of a material, a constant tensile load is applied to a specimen maintained at a constant temperature, and the elongation of the specimen is determined as a function of time. In this study, the load was maintained constant throughout the test. Thus, as a specimen elongated and decreased in cross-sectional area, the axial stress increased. The initial stress which was applied to the specimen is the reported value of stress for the test.

Figure 2 is a schematic of a typical creep curve. The creep curve is divided into three stages. The first stage of creep is known as

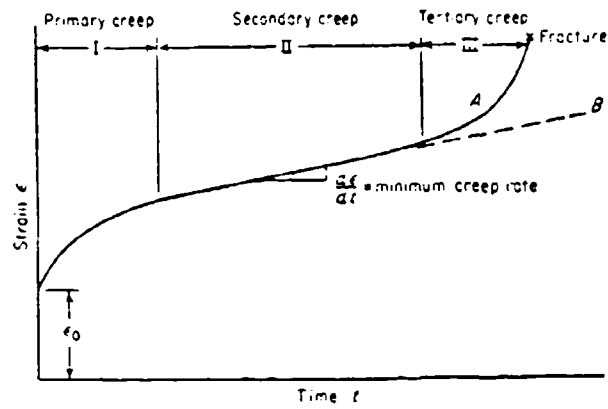


FIG. 2. Typical creep curve showing the three stages of creep.
 Curve A, constant load test; curve B, constant stress test.

primary creep and is a region of decreasing creep rate in which the creep resistance of the material increases due to the specimen deformation. The strain represented by ϵ_0 occurs instantaneously upon loading the specimen. Most of this strain is elastic and is recoverable upon unloading. The second stage of creep, known as secondary creep or steady-state creep, is a region of essentially constant creep rate which results from a balance between the processes of strain hardening and recovery. The slope of this linear region is the minimum creep rate for the material and is often given in material property data. The third stage of the creep curve is called tertiary creep and occurs when there is significant intergranular sliding and cracking and internal void formation. There is frequently a reduction in cross-sectional area due to necking during tertiary creep, and the creep rate increases rapidly with time until fracture occurs. The three stages of creep vary with changes in stress and temperature and in many cases, are not well defined.

II. APPARATUS

All testing was conducted at the Metals Behavior Branch, Air Force Materials Laboratory, Wright-Patterson AFB, Ohio. All metallographic work was completed at the Structural Metals Branch, Air Force Materials Laboratory, Wright-Patterson AFB, Ohio.

A. INCONEL 718

The smooth round bar tensile specimens used in this study were taken from commercial plate of Inconel 718 (IN 718). The composition of the material is given in Table 1. IN 718 is an air-melted, precipitation hardening nickel-iron-base alloy. It is strengthened by a gamma-prime precipitate containing columbium (also known as niobium), titanium, and aluminum. The heat treatment used for this alloy is given in Table 2. This heat treatment produces optimum rupture, creep, and fatigue properties. IN 718 has high yield, tensile, and creep rupture strength up to a temperature of 1200°F (650°C). Because of these properties, it has been used in gas turbine engines up to temperatures of 1200°F. However, the iron in IN 718 considerably lowers its strength and corrosion resistance at higher temperatures. Figure 3 shows that at temperatures greater than 1200°F, the tensile yield strength drops off dramatically. Due to these material property limitations, IN 718 is not found in applications in the temperature range where hot corrosion is a major consideration. Hot corrosion occurs predominantly in the temperature range of 1400°F (760°C) to 1900°F (1038°C). However, IN 718 was selected for this study so that significant hot corrosion attack

TABLE 1: Nominal Composition of Inconel 718 (wt pct)

Ni	Cr	Fe	Cb	Mo	Ti	Al	C
bal	23.4	20.3	4.8	2.9	0.8	0.5	0.12

TABLE 2: Heat Treatment for Inconel 718

- * solution at 1775^oF (968^oC) for 1 hour;
furnace cool to 1325^oF (718^oC)
- * age at 1325^oF (718^oC) for 8 hours;
furnace cool to 1150^oF (621^oC)
- * age at 1150^oF (621^oC) for 10 hours;
* air cool to room temperature

TENSILE YIELD VS TEST TEMP

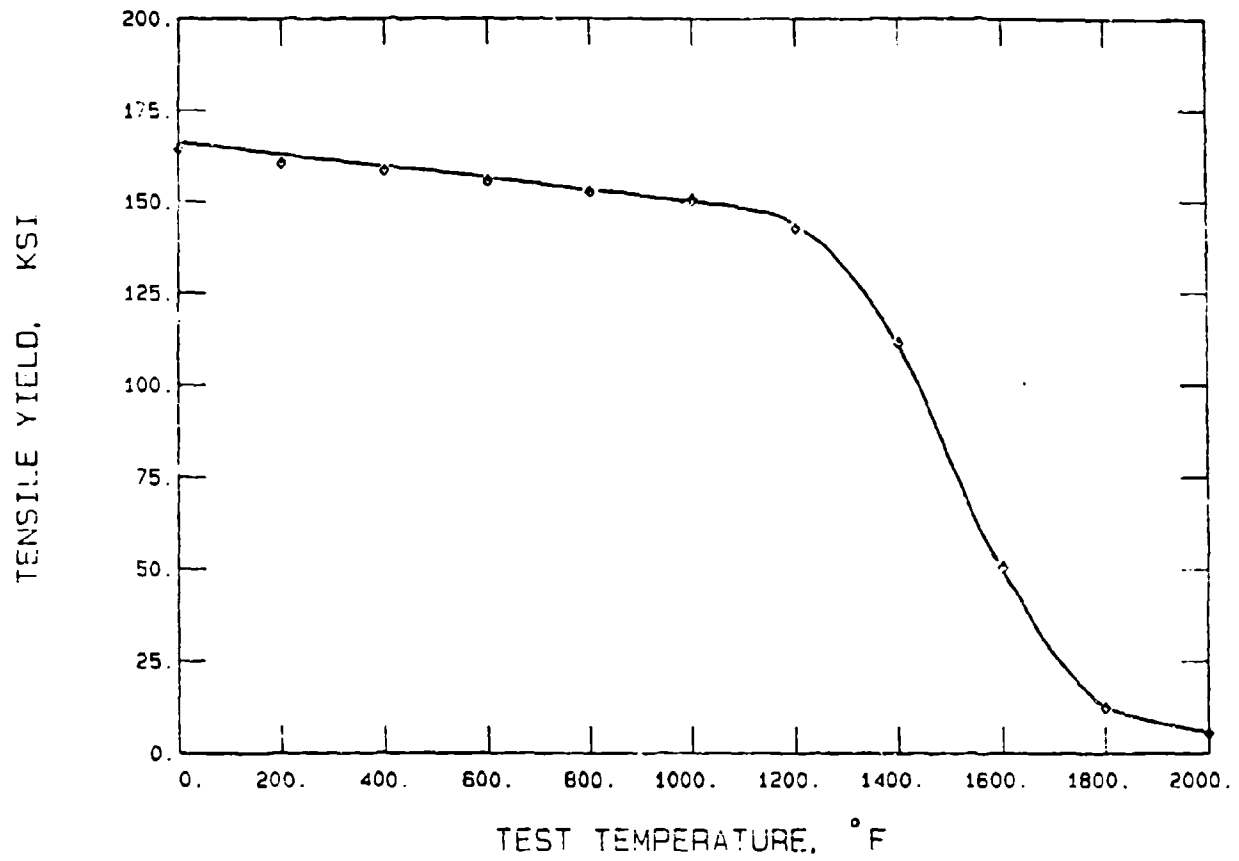


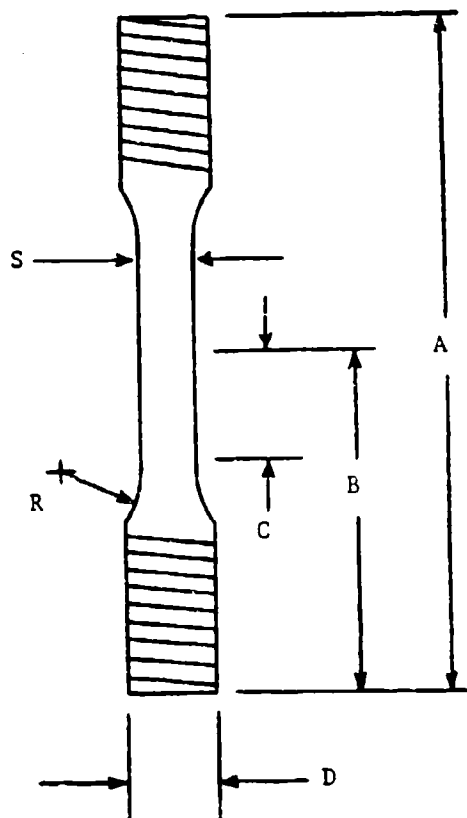
FIG. 3. Effect of temperature on the yield strength of IN 718 (ref. 15).

would occur in a relatively short test time. Studying an alloy whose material properties limit its use in applications where hot corrosion occurs "magnifies" the hot corrosion process and the deformation mechanisms which take place. The smooth round bar tensile specimens were machined from the plate transverse to the rolling direction and have a gage length of 1.25 inches and a diameter of either 0.25 inches or 0.125 inches. Overall dimensions of the test specimens are shown in Figure 4.

The experimental apparatus consisted of the following equipment:

- (1) an **Arcweld** creep frame
- (2) tube furnace
- (3) **West** temperature controller
- (4) extensometer assembly with **Daytronics** LVDT
- (5) **Daytronics** 9000 signal conditioner
- (6) **Tektronix** 4051 microproces.

The high temperature creep testing was done in an **Arcweld** creep frame having a 1200 lb capacity and a 20 to 1 lever-arm ratio. The creep frame was equipped with a tube furnace capable of providing ohmic heating to a temperature of 1652°F (900°C). The furnace was mounted using a counterweight so that it could be easily raised and lowered to gain access to the test specimen. Figure 5 shows the experimental apparatus. The furnace is controlled by a time-proportioning **West** temperature controller using a K-type thermocouple for closed-loop feedback control. The thermocouple was mounted adjacent to the center of the gage length of the specimen. Three other thermocouples mounted near the test specimen were used to monitor the temperature distribution along the gage length of the specimen.



A	4.00
B	2.00
C	0.625
D	0.50
R	0.50
S	0.25

dimensions in inches

FIG. 4. Inconel 718 round bar tensile specimen.

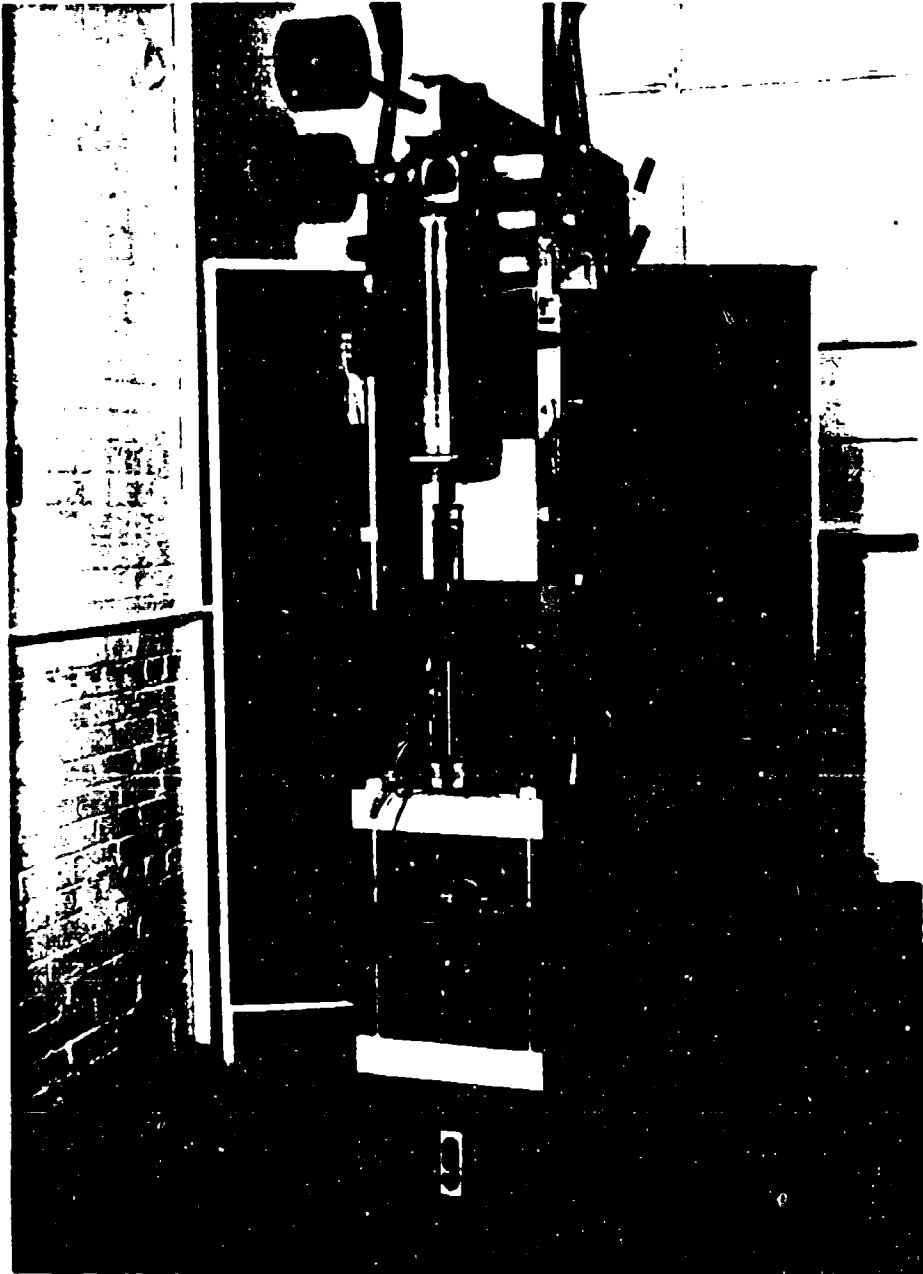


FIG. 5. Experimental test apparatus.

The creep elongation measurements were recorded using a specially designed extensometer consisting of two rods in two concentric tubes. The extensometer tubes extended along the load train of the creep frame and down through the bottom of the tube furnace. The axial deflection was measured using a Daytronic LVDT (linear variable differential transducer) located at the lower end of the rod-in-tube assembly outside the furnace. A schematic of the extensometer assembly is shown in Figure 6. The micrometer was used to calibrate the LVDT output prior to each test.

Output from the three thermocouples monitoring the temperature along the specimen and the output from the LVDT were fed to a Daytronics 9000 signal conditioner. The signal conditioner was calibrated to display the temperature readings and specimen elongation and to provide the interface to recording devices. The specimen elongation versus time was monitored continually using an Omega strip chart recorder. The elongation data was also recorded at one hour intervals in digital form using a Tektronix 4051 microprocessor. The Tektronix 4051 could be programmed to record test parameters at specified time intervals. This arrangement allowed for continuous day-night testing, and the computer-acquired data was stored on magnetic tape in a format which permitted data reduction and plotting to be done using computer programs at a later date.

B. RENÉ 77 AND RENÉ 80

The corrosion pins of René 77 and René 80 used in this study were similar to those widely used by the gas turbine industry in burner rig

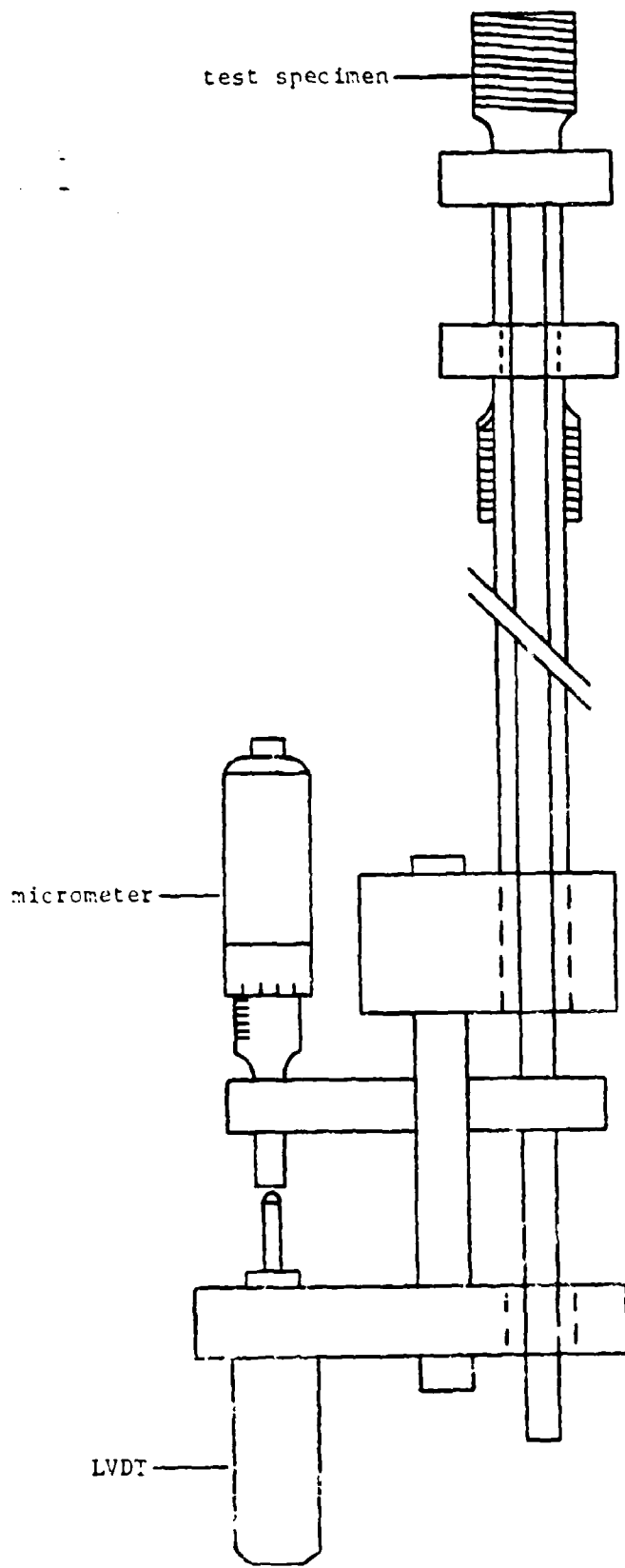


FIG. 6. Schematic of extensometer assembly.

testing. The cylindrical pins were approximately 1.5 inches in length and 0.125 inches in diameter. The composition of the two alloys and heat treatments are given in Table 3 and Table 4. René 77 and René 80 are cast, precipitation hardenable, nickel-base alloys containing chromium and cobalt, with titanium and aluminum acting as the gamma-prime precipitation hardening elements. Tungsten and molybdenum are added for solution strengthening. These alloys have excellent creep-rupture strength up to 1900°F combined with good elevated temperature ductility, hot corrosion resistance, and long-term stability. The main usage for these alloys is in vacuum cast turbine blades and vanes. Unlike Inconel 718, René 77 and René 80 operate in conditions which favor hot corrosion attack. For this reason, these alloys were selected for this study in order to characterize hot corrosion on alloys designed for applications in which this type of corrosion is a major consideration.

The furnace used for the high temperature testing was a Lindberg Hevi-Duty metallurgical furnace controlled by a Barber-Colman solid-state temperature controller capable of reaching temperatures of 1850°F (1010°C). Testing was performed in three environments. Laboratory air was used to study the oxidation characteristics of the two alloys, and the two salt compositions were used to study the hot corrosion resistance. The first salt mixture had a composition of 90% Na₂SO₄ / 10% NaCl by weight. The second was a salt of pure 100% Na₂SO₄.

TABLE 3: Nominal Composition of René 77 and René 80 (wt pct)

	Ni	Cr	Co	Mo	Ti	Al	C	other
René 77	bal	14.2	15.0	4.2	3.4	4.3	0.07	---
René 80	bal	14.0	9.5	4.0	5.0	3.0	0.17	4.0 W

TABLE 4: Heat Treatment for René 77 and René 80

René 77

- * solution at 2125°F (1160°C) for 2 hours in vacuum;
furnace cool to 1975°F (1085°C)
- * age at 1975°F (1085°C) for 4 hours in vacuum;
furnace cool to 1700°F (925°C)
- * age at 1700°F (925°C) for 24 hours in vacuum;
furnace cool to 1400°F (760°C)
- * age at 1400°F (760°C) for 16 hours in vacuum

René 80

- * solution at 2200°F (1204°C) for 2 hours in vacuum;
furnace cool to 2000°F (1093°C)
- * age at 2000°F (1093°C) for 4 hours in vacuum;
furnace cool to 1925°F (1052°C)
- * age at 1925°F (1052°C) for 4 hours in vacuum;
furnace cool to 1550°F (843°C)
- * age at 1550°F (843°C) for 16 hours in vacuum

III. PROCEDURE

A. INCONEL 718

A round bar tensile specimen of IN 718 was prepared for testing by first cleaning it in warm, soapy water to remove any remaining machining oil. The gage section of the specimen was then buffed with 600 grit silicon carbide paper. This was done to remove the smooth, shiny machined surface finish in order to allow the salt film to coat the specimen. If the surface was not roughened, the salt spray would bead and roll off the specimen. The specimen was washed again to remove the silicon carbide residue and dried with acetone. The weight of the specimen was then recorded, the diameter measured using a micrometer, and the surface area of the gage section calculated.

The cleaned specimen was then ready to be salt coated. If the specimen was to be tested without a salt coating, this spraying step was omitted, and the specimen was ready to be mounted in the extensometer. However, a specimen to be salt sprayed was placed on a hot plate and heated to approximately 347°F (175°C). Specimen temperature was critical since if the specimen was too cold, the spray would not vaporize. If the specimen was too hot, vaporization occurred violently on contact, and spallation of the salt occurred. The salt spray was a saturated aqueous solution of 90% Na₂SO₄ / 10% NaCl by weight. The salt solution was sprayed on the heated specimen using a plastic non-aerosol trigger pump similar to those used on household cleaners. The pump

nozzle was adjusted to give a very fine spray at a spraying distance of approximately 10 inches. The specimen was sprayed until a very thin layer of dried salt was deposited on the gage section as the water quickly vaporized from the surface. The specimen was then returned to the hot plate. Thin layers of salt were overlaid to achieve a coating of approximately 5.0 mg/cm^2 of salt calculated by weighing the salt coated specimen after each spraying. Figure 7 shows an uncoated and a coated specimen. Any salt deposited in the threads of the test specimen was washed away by immersing the threads in warm water.

The salt solution was made from technical grade Na_2SO_4 and NaCl crystals. Ninety grams of Na_2SO_4 and ten grams of NaCl were added to a beaker of warm distilled water. The solution was stirred until all of the salt was dissolved. The solution was then allowed to cool to room temperature. As the solution cooled and the solubility of the salt decreased, salt precipitated out of solution. Distilled water at room temperature was then slowly added until the precipitated salt redissolved. This procedure was used to ensure a nearly saturated salt solution.

Once a specimen was successfully coated to approximately 5.0 mg/cm^2 of salt, it was carefully mounted in the extensometer assembly. The extensometer grips were tightened using a torque wrench to 70 in-lbs. This prevented an overly tight grip from initiating a premature failure under load at the grip knife-edge. Conversely, a grip not tightened to 70 in-lbs would slip down the specimen during the elongation of the testing. Care had to be taken not to flake any salt off the specimen during mounting in the extensometer assembly.

The specimen and extensometer assembly were installed in the load

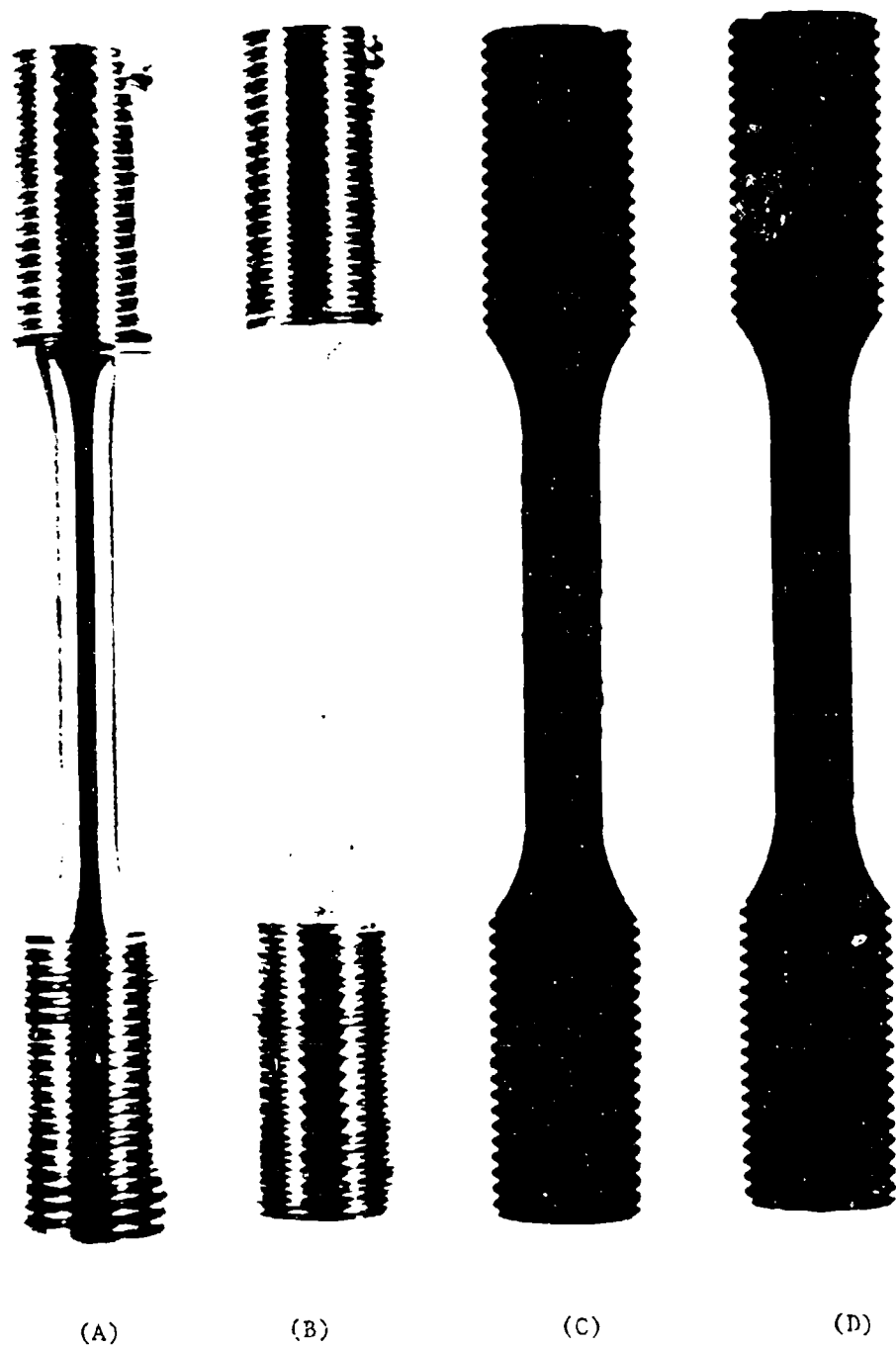


FIG. 7. Inconel 718 specimens (A) as received; (B) after salt coating; (C) after hot corrosion attack; and (D) after oxidation.

train of an Arcweld creep frame using threaded grips. All threads were coated with a liberal amount of magnesium hydroxide (commercial milk of magnesia) to prevent the parts from "freezing" together during the high test temperature and to permit easy disassembly. The LVDT was installed, and the LVDT output calibrated using the micrometer on the extensometer assembly. The gage length for the test (used later to calculate the percent strain) was measured and recorded as the distance between the extensometer grips. The gage length was nominally one inch. Three K-type thermocouples were wired to the extensometer assembly and positioned near the specimen along the gage length. A fourth thermocouple was mounted near the midpoint of the specimen gage length and connected to the temperature controller. All tests were conducted at 1472°F (800°C), and the temperature variation along the gage length was within 4°C. Visual examination after testing salt coated specimens revealed little evidence of much of the salt creeping onto the extensometer grips.

Sustained-load creep tests were conducted at stress levels of 30 Ksi, 20 Ksi, 15 Ksi, and 10 Ksi. Table 5 lists the complete test matrix. All tests were stopped short of failure at 72 hours except for the runs at 30 Ksi which failed in approximately 25 hours due to the high stress level. Figure 7 shows test specimens after a typical 72 hour test at a temperature of 1472°F. After testing, all specimens were rinsed gently in warm water to dissolve any remaining salt on the specimen surface and dried with acetone. All specimens were then sectioned at the midpoint of the gage section. The cross-sections were mounted, polished, etched, and examined by optical microscopy. In addition, the corrosion attack was examined using the scanning electron

TABLE 5: Test Matrix for Inconel 718

specimen ID	diameter (inches)	salt coverage ₂ (mg/cm ²)	stress level (Ksi)	test time (hrs)
84-253	0.25	none	30	25
84-254	0.25	none	20	72
84-255	0.25	5.16	20	72
84-256	0.25	none	10	72
84-257	0.25	5.18	10	72
84-258	0.25	4.54	30	25
84-259	0.25	5.53	15	72
84-260	0.25	none	15	72
84-261	0.25	5.74	20	72
84-236	0.125	none	15	72
84-237	0.125	5.65	15	72
84-238	0.125	5.87	20	72
84-239	0.125	none	20	72

microscope (SEM), and an elemental analysis was conducted using associated X-ray energy spectroscopy (XES). Depth of corrosion attack measurements were made using a Gaertner toolmaker's microscope with a travelling stage. The cross-sections were viewed at 100X, and the amount of sound metal along a diameter was measured.

B. RENÉ 77 AND RENÉ 80

To prepare the corrosion pins for testing, the specimens were cleaned, roughened with 600 grit silicon carbide paper, cleaned, and dried with acetone as described for an IN 718 specimen. Each pin was then weighed, the diameter measured using a micrometer, and the surface area of each pin calculated.

The pins were salt coated using the same technique as that for a IN 718 specimen. Table 6 lists the test matrix for the René 77 and René 80 corrosion pins. Note that two salt compositions were used, 90% Na_2SO_4 / 10% NaCl by weight and 100% Na_2SO_4 . All specimens were placed horizontally on a firebrick in the test furnace. Each pin was supported on its ends by slipping each end of the pin into a thermocouple bead. Figure 8 shows the pin placement for testing. All tests were conducted at a temperature of 1652°F (900°C) for a period of 72 hours. Table 6 shows that a set of five René 77 pins coated with salt ranging from a coverage of approximately 0.5 mg/cm² to 10.0 mg/cm² was used to examine the effect of salt thickness on the degree of hot corrosion.

At the conclusion of the testing, all specimens were gently rinsed in warm water to remove any remaining salt on the pin surface and dried with acetone. The pins were weighed, and weight-change measurements

TABLE 6: Test Matrix for René 77 and René 80

René 77

specimen ID	salt coverage (mg/cm ²)	salt composition(*)
A1	none	
A2	4.21	90/10
A3	5.43	100
B1	none	
B2	5.13	90/10
B3	5.11	100
C1	none	
C2	5.61	90/10
C3	5.54	100
T1	0.55	90/10
T2	2.93	90/10
T3	4.97	90/10
T4	7.59	90/10
T5	9.52	90/10

René 80

A1	none	
A2	4.45	90/10
A3	5.66	100
B1	none	
B2	5.34	90/10
B3	5.49	100
C1	none	
C2	5.52	90/10
C3	5.66	100

(*) 90/10 = 90% Na₂SO₄ / 10% NaCl by weight

100 = 100% Na₂SO₄

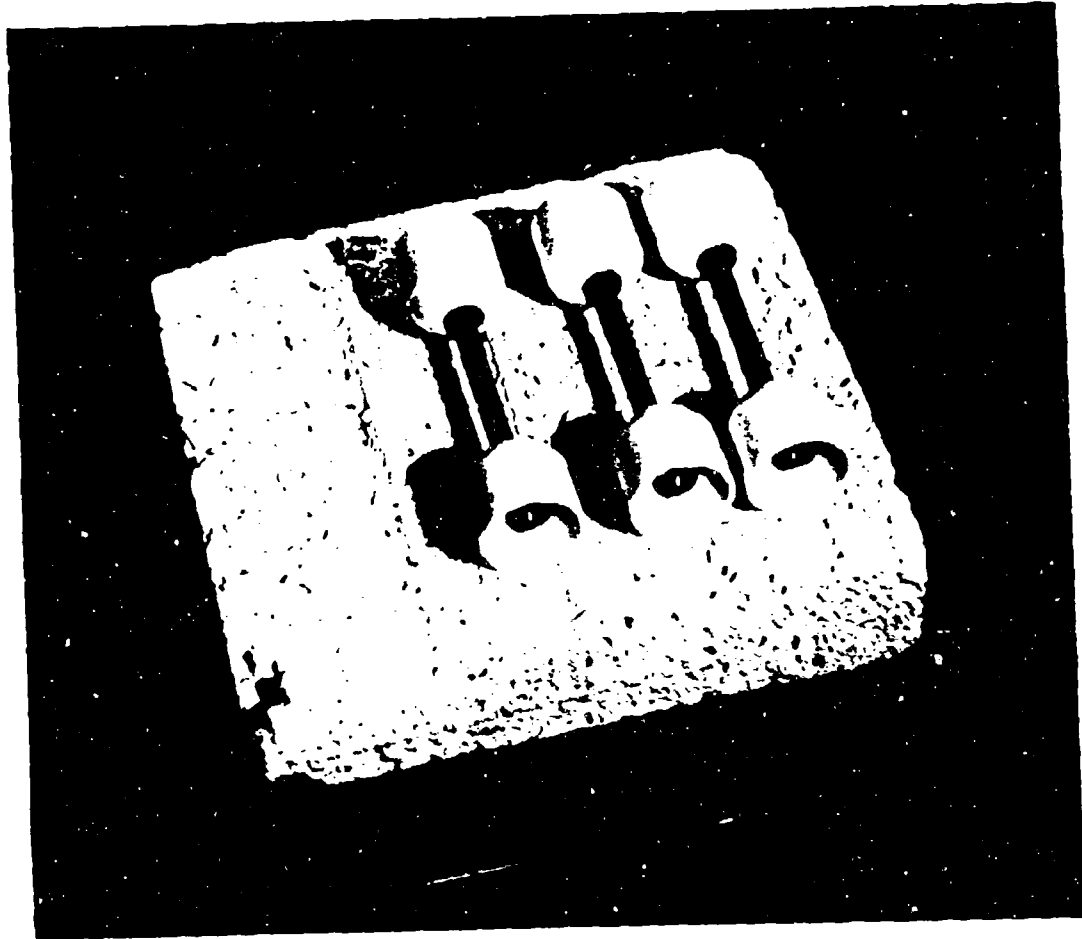


FIG. 8. René 77 and René 80 pin placement for testing.

were calculated. All specimens were then sectioned at midpoint, and the cross-sections mounted, polished, and etched for metallographic analysis. Optical and scanning electron microscopy was conducted to characterize the corrosion attack.

IV. EXPERIMENTAL RESULTS AND DISCUSSION

A. INCONEL 718

1. CREEP BEHAVIOR

Sustained-load creep tests were conducted at a temperature of 1472°F (800°C) at various stress levels using round bar tensile specimens having a diameter of 0.25 inches. Specimens were either salt coated or uncoated. Figure 9 shows the creep data at a stress level of 10 Ksi. The creep curves for the salt coated and uncoated specimens were identical within the experimental scatter. The creep curves for both specimens show a predominant secondary creep region with no tertiary creep occurring within the 72 hours duration of the test. Both specimens experienced a strain of approximately 0.75% in 72 hours. Strain was calculated by dividing the elongation by the gage length recorded prior to testing.

Figure 10 shows the results of the creep tests conducted at a stress level of 15 Ksi. The data show a slight increase in the amount of creep experienced by the salt coated specimen after approximately 45 hours. Although there may be some question whether the difference in the creep curves is primarily due to experimental scatter, it might be interpreted that the presence of molten salt resulted in a reduction of the creep resistance of the material. Steady-state creep predominated up to approximately 45 hours, and at that point, the curves show a slight increase in the rate of creep indicating the onset of tertiary creep. The salt coated specimen underwent approximately 1.5% strain in

IN 718

800° C

10 KSI

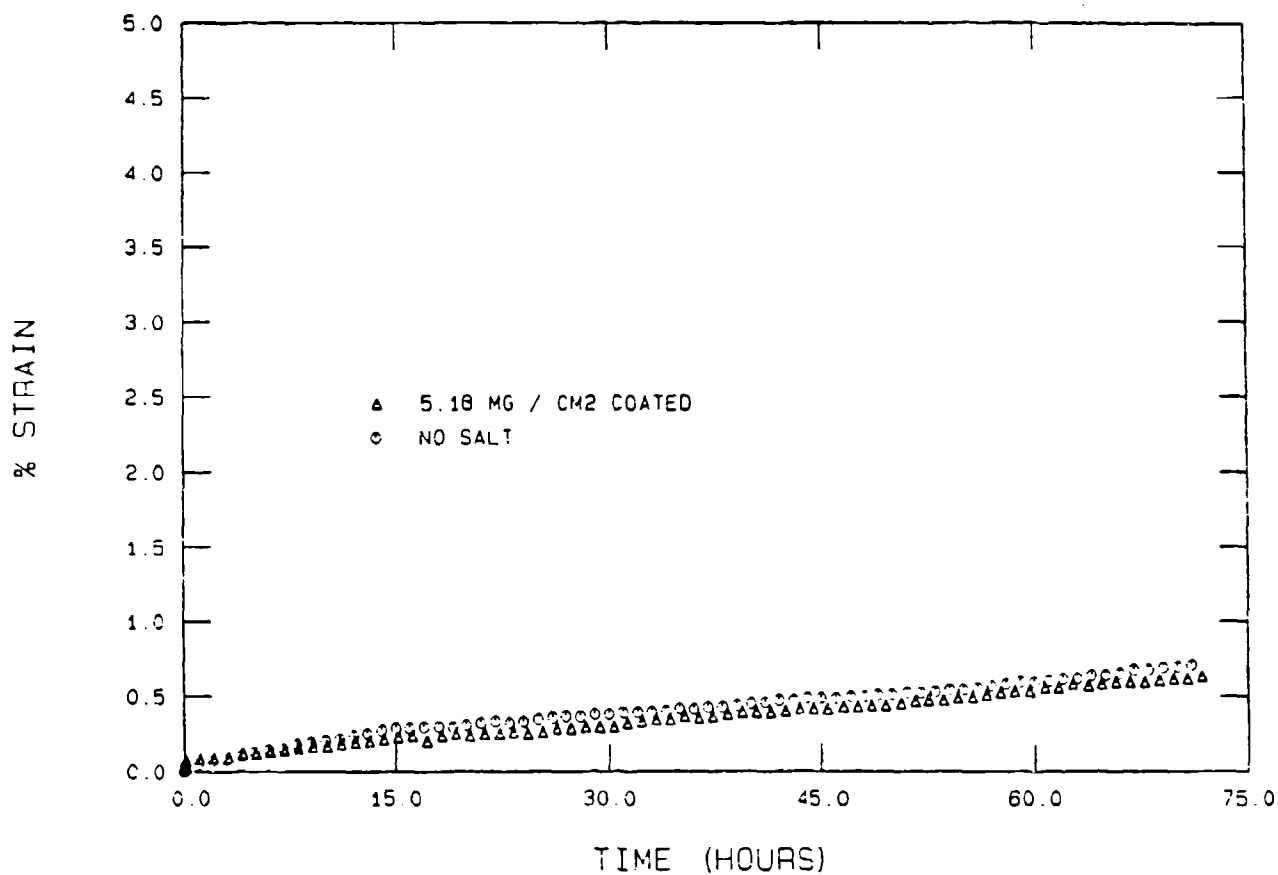


FIG. 9. Creep curves for IN 718 at a stress level of 10 Ksi.

IN 718

800°C

15 KSI

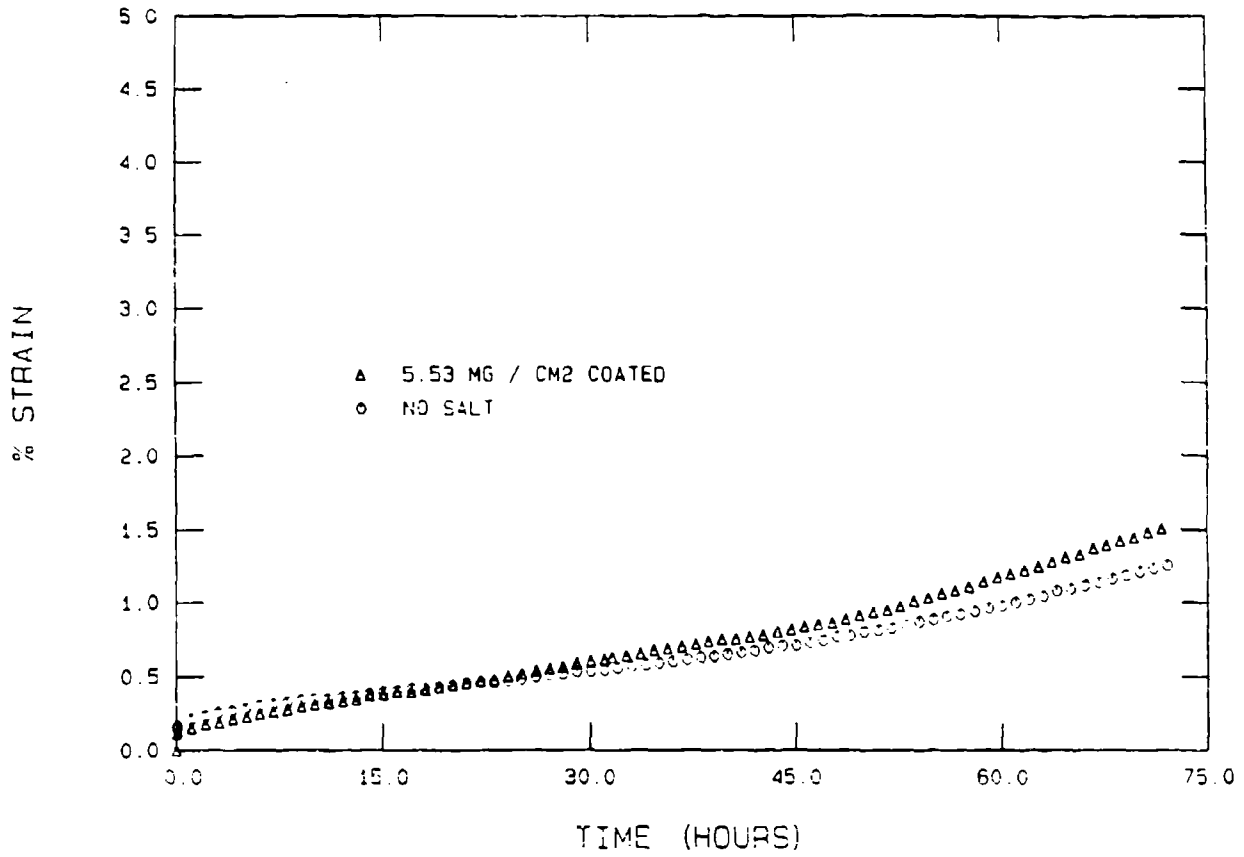


FIG. 10. Creep curves for IN 718 at a stress level of 15 Ksi.

72 hours while the uncoated specimen had a strain of 1.25% in 72 hours.

Figure 11 shows a significant degradation of creep properties due to the presence of molten salt at a stress level of 20 Ksi. The molten salt environment began to influence the creep behavior after approximately 30 hours. The region of steady-state creep is not well-defined, and tertiary creep clearly predominates after 30 hours. The salt coated specimen underwent a strain of 5.0% while the uncoated specimen showed 3.0% strain in 72 hours. The experimental scatter in the early portion of the tests is due primarily to straining of the test specimens during mounting in the extensometer assembly and load train of the creep frame.

Figure 12 shows the effect of molten salt on the creep behavior at a stress level of 30 Ksi. The salt coated specimen failed in approximately 25 hours due to the high stress. The last recorded elongation measurement prior to failure was at a strain of 4.75%. The uncoated specimen was tested for 25 hours and underwent 1.75% strain. This test on the uncoated specimen was stopped after 25 hours in order that the metallographic examination of both the coated and uncoated specimens would be based on the same time at temperature. Due to the high stress level, the steady-state creep region did not exist, and both specimens experienced substantial tertiary creep.

Figure 13 consolidates the creep curves in Figures 9 through 12 showing the effect of molten salt on the high temperature creep behavior of round bar tensile specimens of IN 718 having a 0.25-inch diameter. The presence of a molten salt environment degraded the creep resistance of IN 718 at stress levels sufficiently large to cause substantial tertiary creep to occur within the 72 hour test period. Specimens

IN 718 800° C 20 KSI

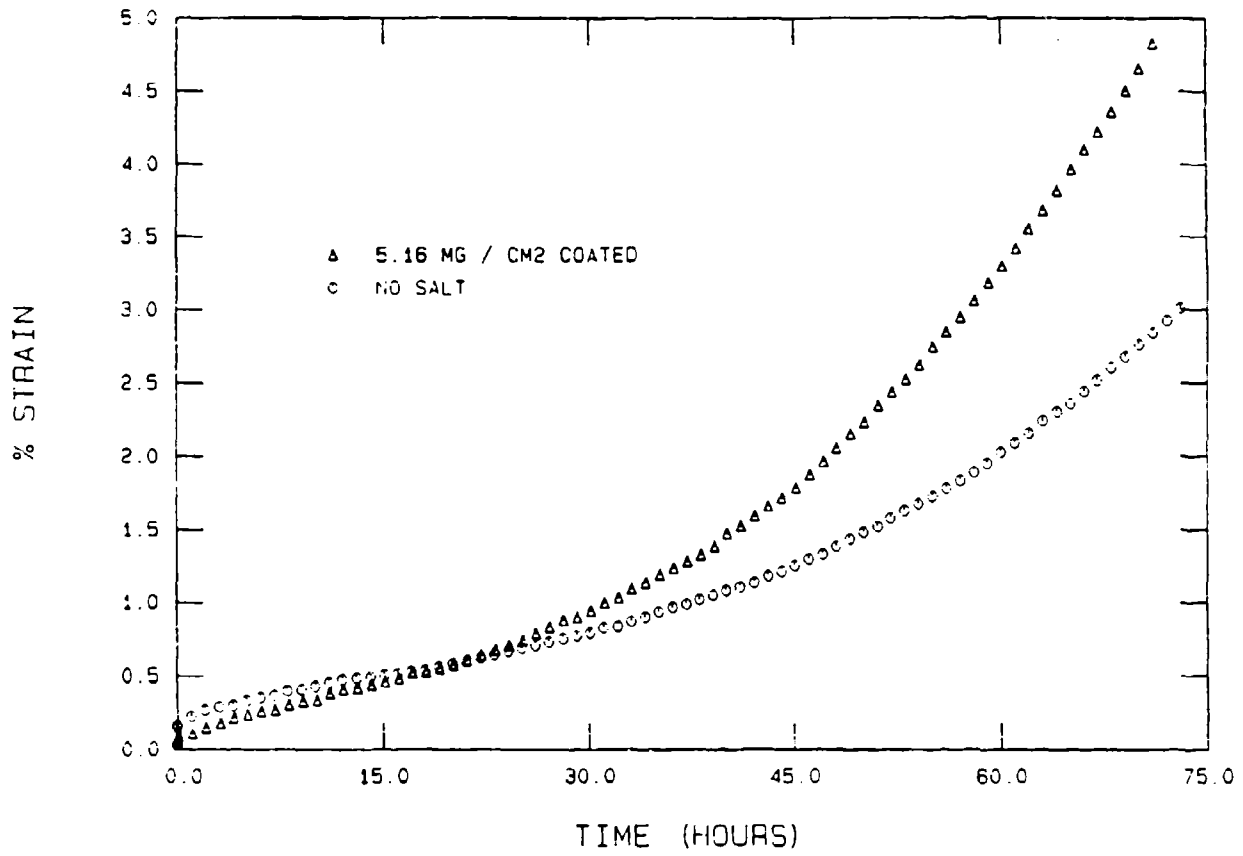


FIG. 11. Creep curves for IN 718 at a stress level of 20 Ksi.

IN 718 800° C 30 KSI

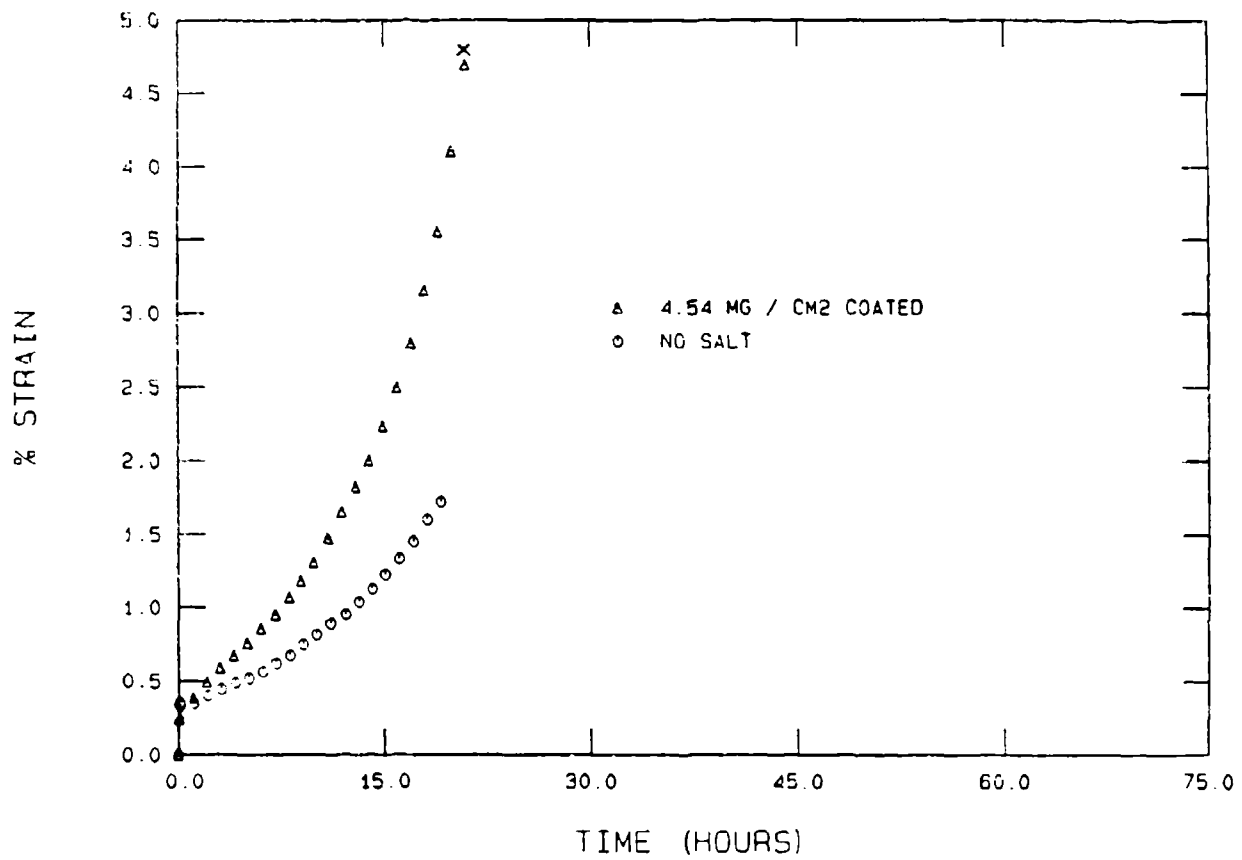


FIG. 12. Creep curves for IN 718 at a stress level of 30 Ksi.

EFFECT OF MOLTEN SALT ON CREEP

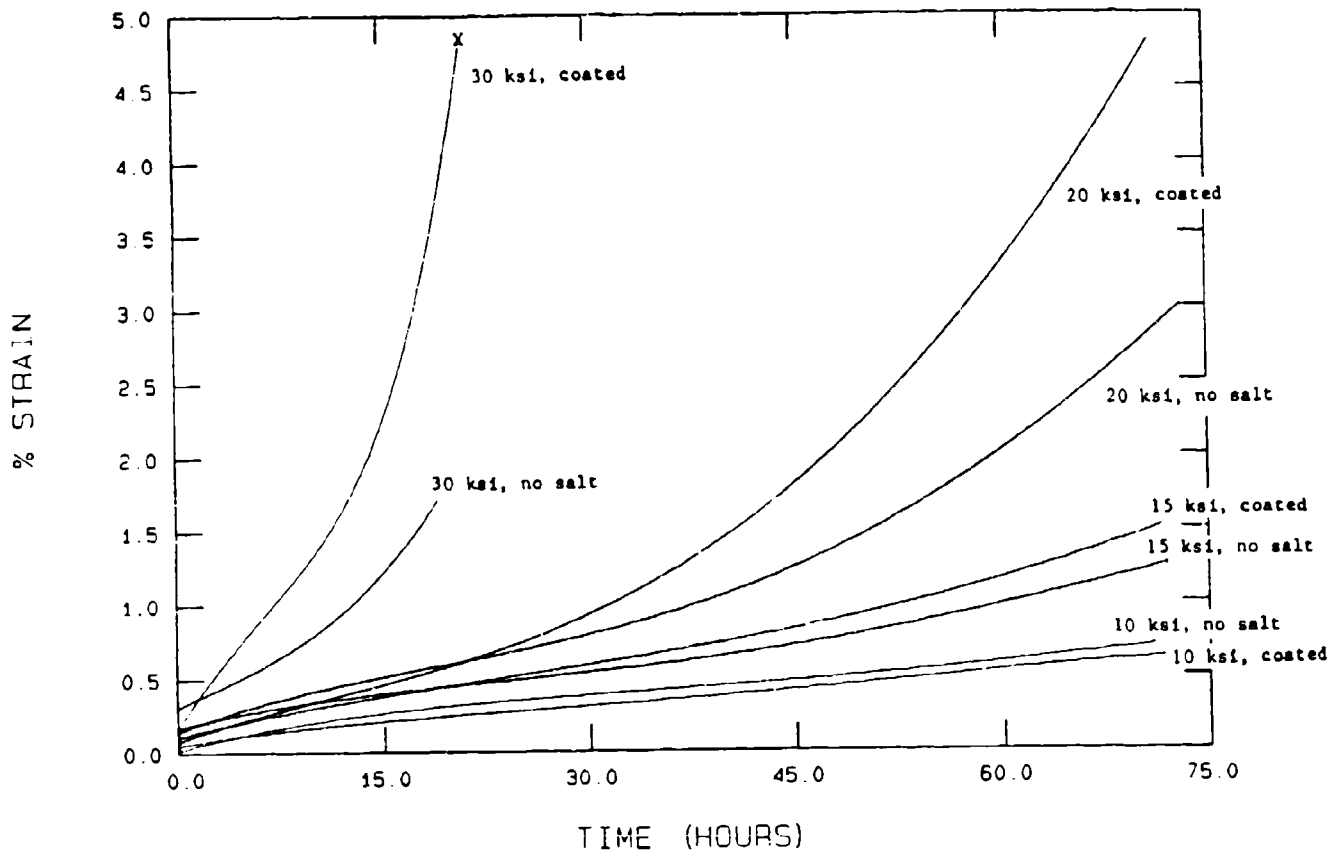


FIG. 13. Effect of molten salt of the creep behavior of IN 718.

tested at 20 Ksi and 30 Ksi experienced predominantly tertiary creep from the onset, and the effect of the molten salt was most severe for these test conditions. At the lower stress levels, the effect of the molten salt was markedly less. At 15 Ksi there was little influence on the creep behavior by the salt environment up to approximately 45 hours. At 10 Ksi there was virtually no effect on the creep behavior due to the presence of molten salt. These specimens underwent primarily steady-state creep throughout the length of testing. There seemed to be no effect of the molten salt environment during steady-state creep, and a significant loss of creep resistance occurred only during the third stage of creep.

It was postulated that reducing the diameter of the specimens would result in a larger environmental effect due to their smaller cross-sectional area. Thus, several sustained-load creep tests were conducted using tensile specimens of IN 718 having half the diameter of the previous specimens, or 0.125 inches. Tests were conducted at a stress level of 15 Ksi to attempt to "magnify" the apparent effect of the molten salt on the larger 0.25-inch diameter specimens at this stress level and to reduce the influence of any experimental scatter. The results shown in Figure 14 clearly show no increased separation of the creep curves for the coated and uncoated 0.125-inch diameter specimens. There was little reduction in creep resistance due to the presence of molten salt. Note that these test specimens did not undergo significant tertiary creep. Figure 15 shows the results of tests conducted with both diameter specimens at a stress level of 20 Ksi. These data show that the 0.125-inch diameter specimens suffered a larger environmental degradation in creep resistance than did the 0.25-inch

REDUCED DIAMETER IN718 15KSI

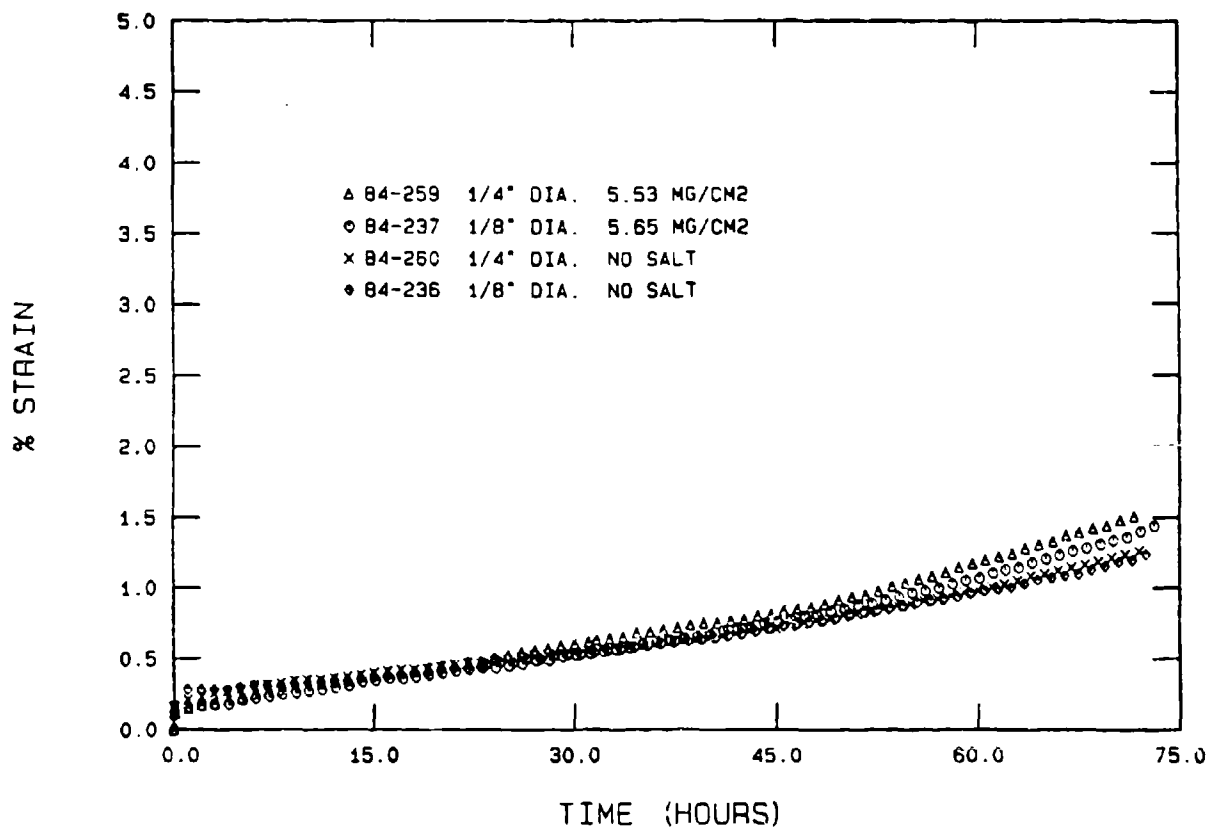


FIG. 14. Effect of reduced diameter on creep at 15 Ksi.

REDUCED DIAMETER IN718 20KSI

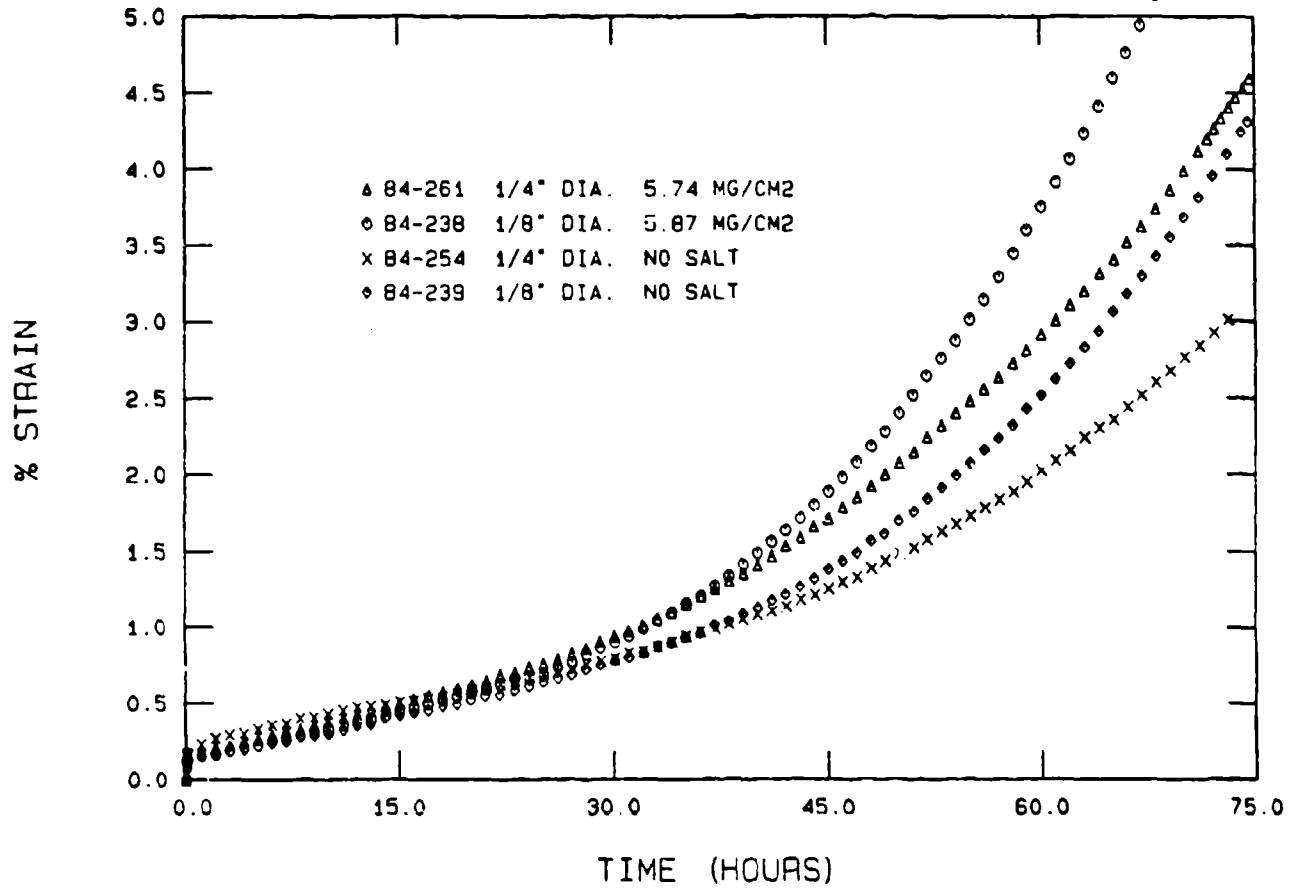


FIG. 15. Effect of reduced diameter on creep at 20 Ksi.

diameter specimens tested at the same stress level for both the salt coated and uncoated specimens. In both cases, the percent strain in 72 hours was approximately 1.7% greater for the salt coated specimens than for the uncoated specimens of corresponding diameter. The molten salt environment and laboratory air environment reduced the creep resistance of the 0.125-inch diameter specimens which experienced predominantly tertiary creep during testing.

Figure 16 shows the minimum creep rate at the various stress levels for salt coated and uncoated specimens. The data show higher minimum rates of creep for salt coated specimens than for uncoated specimens. Creep rate is actually a strain rate given in the units of percent strain per hour. At a constant temperature, the stress level and the strain rate can be related according to the flow law

$$\sigma = K \dot{\epsilon}^n$$

where σ is the stress, $\dot{\epsilon}$ is the strain rate, K is a constant, and n is called the strain rate coefficient. By taking the logarithm of both sides and rearranging, the above equation becomes

$$\log \sigma = n \log \dot{\epsilon} + \log K$$

Thus, on a log-log plot, this equation is a straight line whose slope is n, the strain rate coefficient. Figure 16 shows that the data for salt coated and uncoated specimens fall on two distinct lines of differing slope. The slope of the uncoated data, or the strain rate coefficient, is 0.61. The strain rate coefficient for the salt coated data is 2.70.

MINIMUM RATE OF CREEP

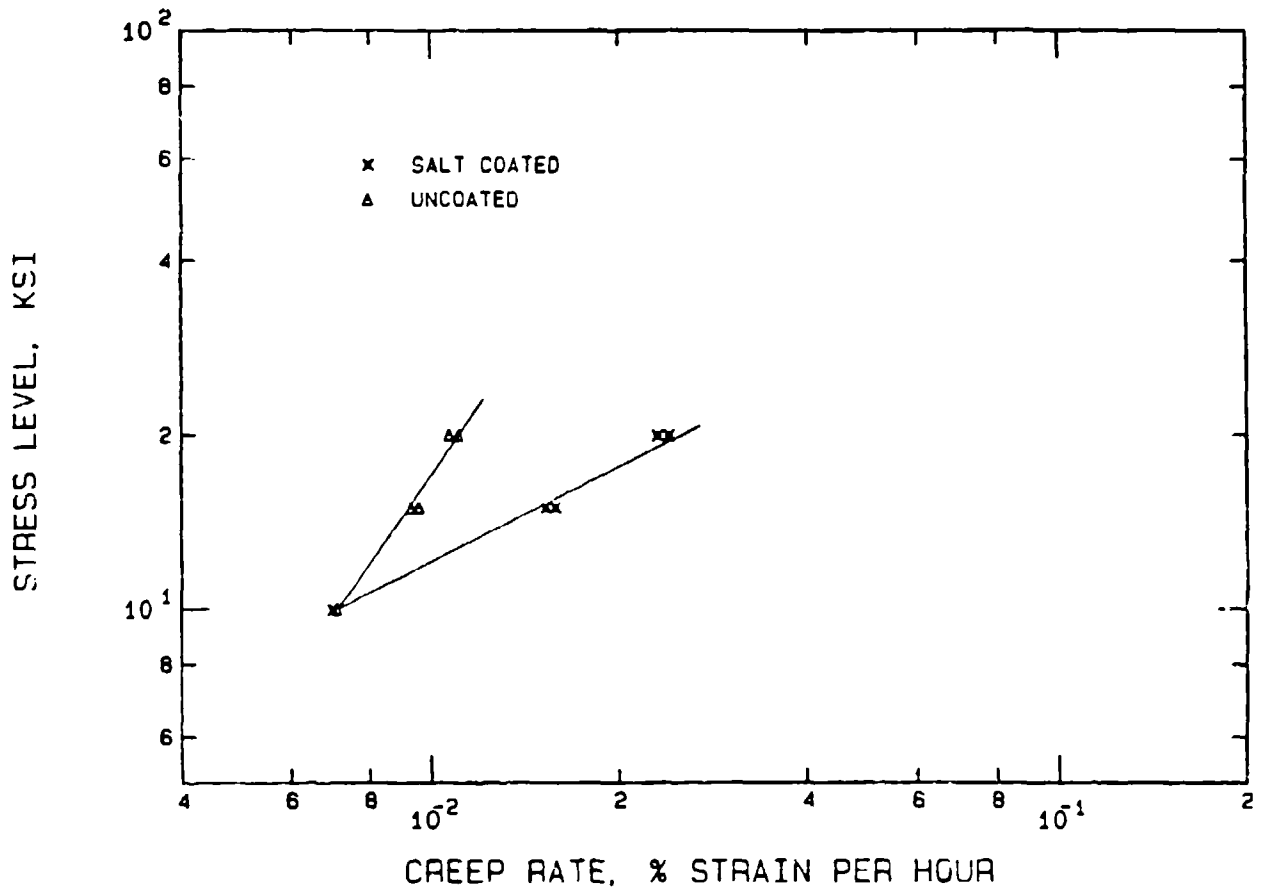


FIG. 16. Effect of stress level on the minimum creep rate for IN 718.

The difference in the strain rate coefficients indicates that different creep mechanisms occurred for the salt coated specimens versus the uncoated specimens. However, it was difficult to determine exactly the minimum creep rate for specimens which did not exhibit a well-defined steady-state creep region, and the actual value of stress corresponding to that point in the test where the minimum creep rate occurred was unknown. As a result, the slopes of the straight lines in Figure 16 are not exact, and the statement that the creep mechanisms are different for coated and uncoated specimens cannot be made without some scepticism.

A duplicate test was conducted to establish the reproducibility of the experimental data and to determine the degree of experimental scatter associated with the experimental technique. Figure 17 shows the result of the duplicate test conducted at a stress level of 20 Ksi. The creep curves were virtually identical up to approximately 45 hours. This indicates that the test technique produced reproducible results and that the experimental scatter was minimal. However, even though the scatter due to the experimental technique was small, significant scatter was introduced by the corrosive attack of the molten salt. At times greater than 45 hours, the effect of the molten salt increased as the specimens experienced tertiary creep, and the reproducibility of the test decreased. This illustrates the localized nature of corrosive attack, and such scatter in corrosion testing is unavoidable since little control over the localized corrosive attack of the salt is possible.

DUPLICATE TEST IN718 20KSI

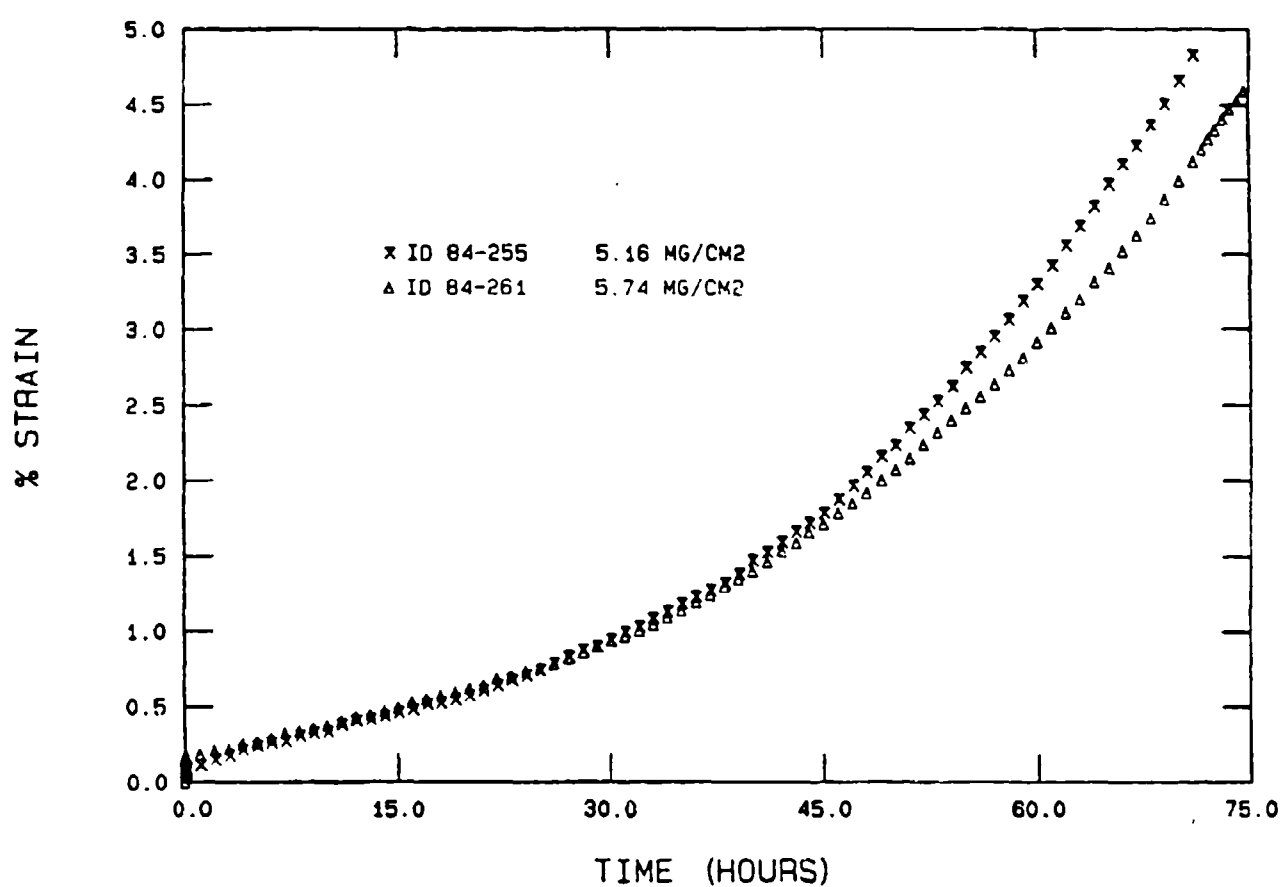


FIG. 17. Duplicate creep test at a stress level of 20 Ksi.

2. METALLOGRAPHIC ANALYSIS

The round bar tensile specimens of Inconel 718 were prepared for metallographic examination after creep testing. Figure 18 shows dramatically the hot corrosion attack by a thin molten salt film. Figure 18(a) shows a portion of the cross-section of a typical specimen tested without salt in laboratory air. The specimen has a very adherent protective oxide layer at its surface. This thin, non-porous oxide layer forms and then acts as a barrier to prevent further oxidation of the base metal by oxygen in the air. Note how little of the metal directly beneath the oxide layer has been depleted of alloying elements. Figure 18(b) shows a region of corrosion attack on a cross-section of a specimen which had been salt coated. This hot corrosion attack was typical of all salt coated specimens in this study and can be divided into four distinct zones as shown. Zone I is a relatively thick oxide layer which is very porous and non-adherent. This flaky oxide layer was often stripped from the specimen during sectioning and mounting for metallographic analysis and does not appear in all photomicrographs showing hot corrosion attack. Zone II is a region of porous metal which has been depleted of alloying elements and which shows massive "fingerlike" penetration of oxide. Severe cracking along the oxide fingers is typical in this region. Zone III is a layer of metal depleted of its alloying elements. This zone contains sulfide particles. No sulfide or sulfur-enriched phases were found in exterior layers. The presense of these subsurface sulfide particles was



(A)



(B)

FIG. 18. SCANNING ELECTRON MICROGRAPHS (500x) SHOWING
(A) OXIDATION AND (B) HOT CORROSION ATTACK OF IN 718

consistent with the observations of Floreen and Kane⁽⁴⁾. Also present in Zone III are internal voids which appear to form along grain boundaries. Lastly, Zone IV is the base metal which has been unaffected by hot corrosion attack.

In order to quantitatively characterize the extent of the hot corrosion attack, depth-of-penetration measurements were made. Figure 19 is a schematic representation of a standard metallographic method used in this study to determine the depth of hot corrosion attack. Using a toolmaker's microscope (at 100X) with a travelling stage, the amount of unaffected base metal along each of four diameters 45 degrees apart in the cross-section was measured. These values were averaged, and the result was subtracted from the initial diameter of the round bar measured with a micrometer prior to testing. After subtracting, the result was divided by two to give the depth of penetration along a radial line from the original surface to the unaffected base metal. The depth of corrosion attack was found to be relatively uniform around the circumference of each specimen. Depth-of-penetration measurements were not made on the uncoated specimens since the depth of oxidation attack was negligible.

Figure 20 shows the depth of penetration of the corrosion attack versus stress level for salt coated specimens. The depth of corrosion attack increased with increasing stress level. The measurement made of the specimen tested at 30 Ksi gave a depth of penetration of only 3.1 mils. This was due to the shortened test time which did not allow the corrosion attack to occur as in specimens tested for the full 72 hours. It is also interesting to examine the effect of specimen diameter on the depth of penetration. As noted earlier, the creep tests conducted at a

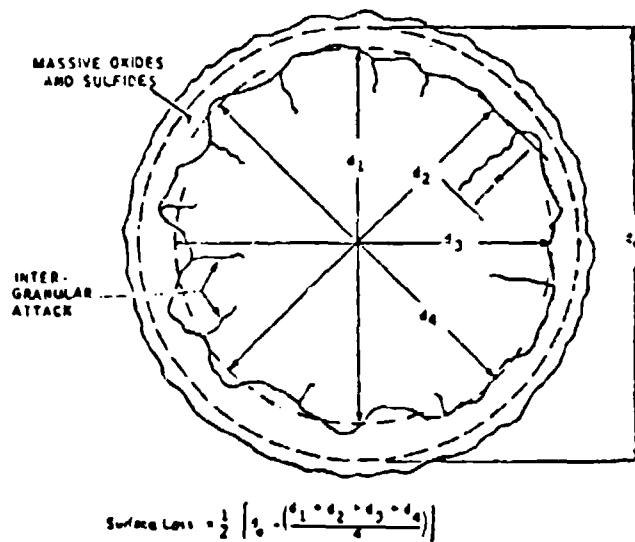


FIG. 19. Method for determining the depth of hot corrosion attack.

DEPTH OF CORROSION ATTACK

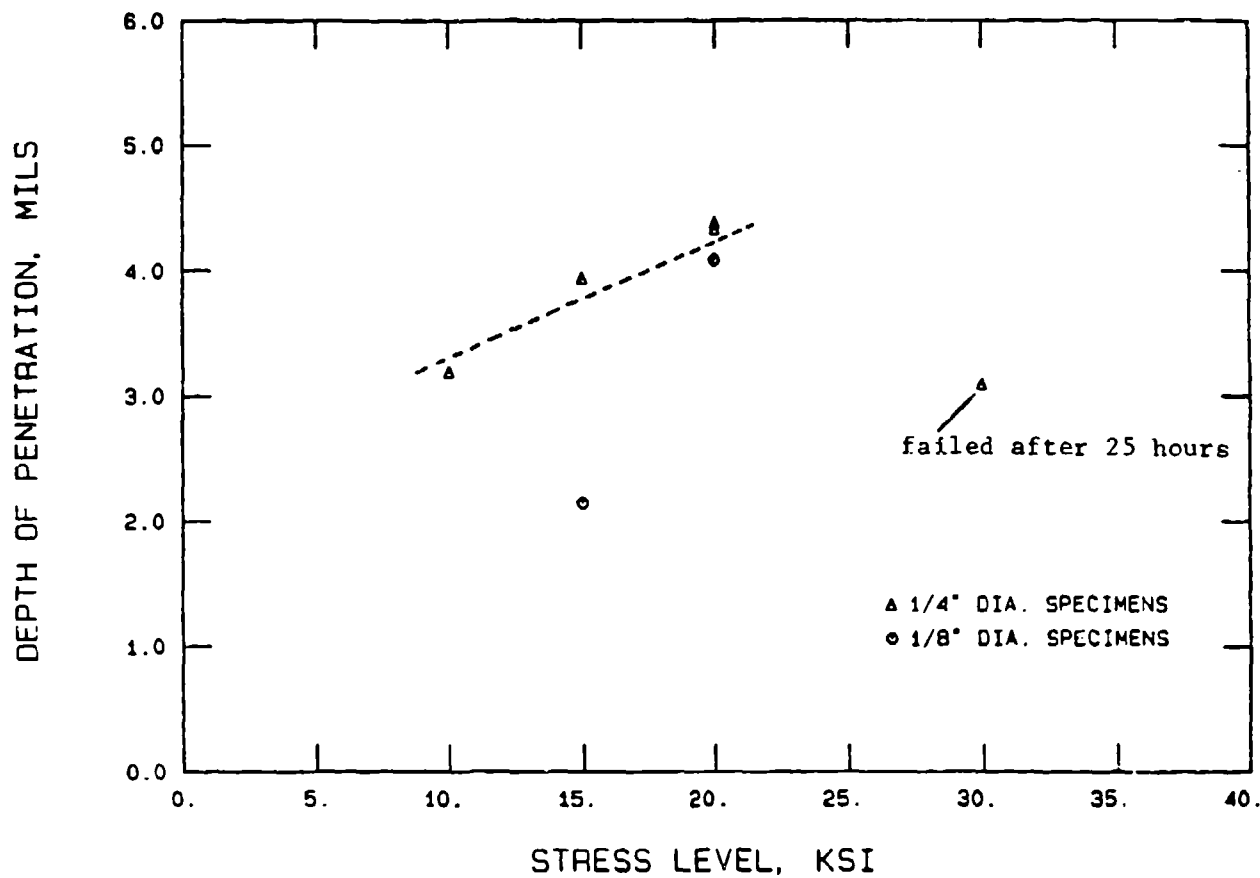


FIG. 20. Effect of stress level on the depth of hot corrosion attack.

stress level of 15 Ksi exhibited virtually identical creep curves for specimens of both 0.25 inches in diameter and 0.125 inches in diameter. Figure 20 shows, for this case, that the depth of penetration for the 0.125-inch diameter specimen was less than that for the 0.25-inch diameter specimen. This was due to the test-to-test variability in the amount of corrosion attack that is typical of mechanisms of a localized nature even though test conditions were the same. The depth of penetration for the 0.25-inch diameter specimen was approximately 3.95 mils which results in 6.14% of the original cross-sectional area of the round bar specimen being affected by corrosion attack. The depth of penetration for the 0.125-inch diameter specimen was 2.15 mils, and thus 6.61% of the original cross-sectional area of the round bar specimen was affected by corrosion attack. These specimens which underwent nearly the same percentage of corrosion attack exhibited virtually identical creep behavior. At a stress level of 20 Ksi, the depth of the hot corrosion attack for specimens of both diameters was approximately 4.28 mils. As a result, the reduced diameter specimen suffered a greater loss of creep resistance due to the molten salt than did the 0.25-inch diameter specimen. For the 0.125-inch diameter specimen, 13.23% of the original cross-sectional area was attacked by corrosion, while only 6.73% of the original cross-section of the 0.25-inch diameter specimen was affected by corrosion attack. Although based on only a few number of specimens, it appears that the degree of environmental degradation of the creep resistance by molten salt is related to the ratio of the cross-sectional area affected by corrosion attack to the original cross-sectional area of the specimen.

In this study, the creep testing was conducted at a temperature of

1472°F (800°C). As was discussed earlier, this test temperature is outside the commercially useable temperature range for IN 718. In fact, it is higher than the temperature of both the primary and secondary age hardening steps in the heat treatment for this alloy (see Table 2). As a result, test specimens were actually overaged during the creep testing at a temperature of 1472°F for 72 hours. Figure 21 shows the microstructure of IN 718 before and after creep testing at 1472°F for 72 hours. Figure 21(a) shows a microstructure of extremely fine gamma-prime phase distributed homogeneously throughout the grains of the nickel matrix. The gamma-prime precipitate is primarily the intermetallic Ni_3Cb with some aluminum and titanium substituting for the columbium (also known as niobium). Small carbide particles, mainly $Cr_{23}C_6$, are also present in the grain boundaries. This microstructure is typical of fully heat-treated, precipitation strengthened IN 718. Figure 21(b) shows the same microstructure which has been overaged during the creep testing at a stress level of 20 Ksi. Substantial formation of a needlelike structure has occurred. This structure has been documented to be an orthorhombic Ni_3Cb phase which forms during long periods of exposure at elevated temperatures.⁽²⁾⁽¹⁶⁾ This phase is detrimental to high temperature strength, and its formation limits the use of IN 718 in any long-term applications to temperatures below approximately 1200°F. There is evidence from this study that the formation of the orthorhombic Ni_3Cb needles begin to nucleate at grain boundaries and that the transformation may be stress enhanced.

Khobaib⁽¹⁷⁾ has conducted sustained-load creep tests with uncoated IN 718 specimens identical to those used in this study at 1400°F at a stress level of 35 Ksi. Under these test conditions, IN 718 exhibited

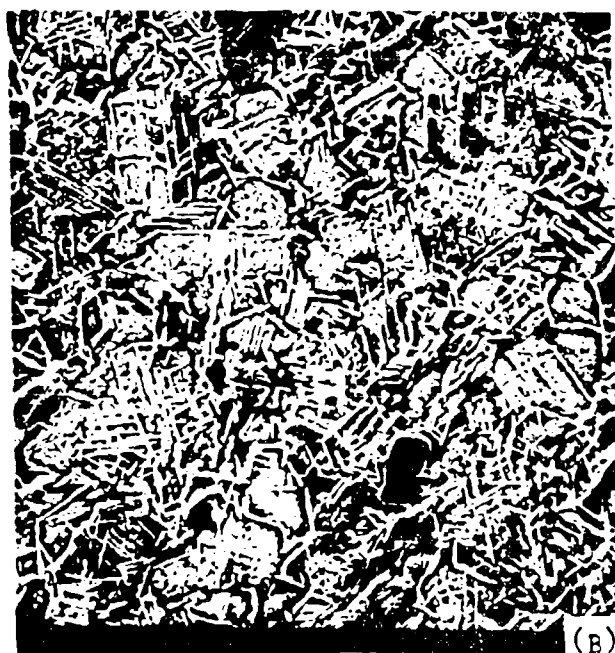
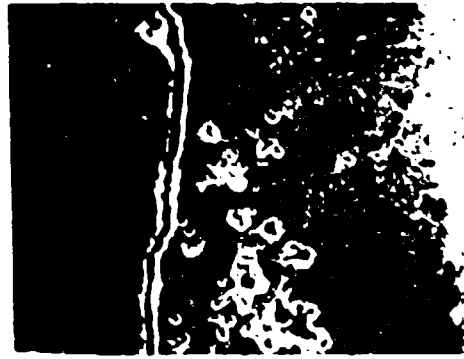


FIG. 21. SCANNING ELECTRON MICROGRAPHS (1000x) SHOWING MICROSTRUCTURE OF IN 718 (A) IN FULLY HEAT TREATED CO'NDITION AND (B) AFTER CREEP TESTING AT 20 ksi FOR 72 HOURS AT 1472°F

approximately 3.0% strain in 320 hours. Metallographic examination revealed that the specimens contained only moderate amounts of transformed orthorhombic Ni_3Cb phase, primarily at the grain boundaries. Thus, even after 320 hours at 1400°F and at 35 Ksi, the amount of orthorhombic Ni_3Cb was considerably less than that seen in this study. The uncoated specimen tested in this study at 1472°F at 30 Ksi underwent 1.75% strain in just 25 hours. The results of Khobaib's work and those of this study indicate that the presence of the orthorhombic Ni_3Cb phase contributes to significant reduction of the creep resistance of IN 718. The reduction in yield strength of IN 718 from a test temperature of 1400°F to 1472°F also contributes to the reduced creep resistance.

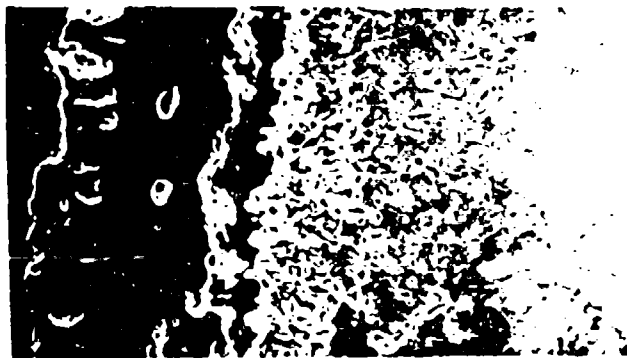
Figure 22 shows the effect of stress on the hot corrosion attack of salt coated specimens. The photomicrographs of Figure 22 are arranged so that the interface between the surface oxide layer and the underlying metal is in line for each stress level. At a stress level of 30 Ksi, the same four zones of corrosion attack previously described are present as shown in Figure 22(a). Zone I is the outermost layer of porous oxide. Its exact thickness is difficult to determine since some of this oxide layer is stripped away when the specimen is sectioned and mounted in order to examine the extent of hot corrosion attack as in Figure 22. However, some oxide did remain intact in this photomicrograph. Note the "fingerlike" penetration of oxide into the metal directly below the surface oxide layer. This region of oxide fingers and metal depleted of alloying elements is the second zone typical of the hot corrosion attack seen in this study. Moving farther inward, Zone III is a region of metal depleted of its alloying elements. This layer contains small globular sulfide particles. Zone IV is the base metal which was



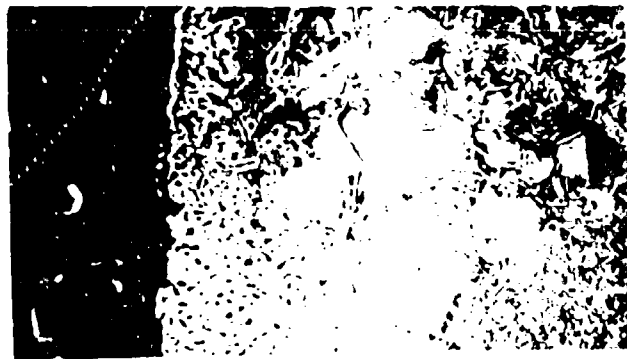
(A) 30 KSI



(B) 20 KS



(C) 15 KSI



(D) 10 KSI

FIG. 22. EFFECT OF STRESS LEVEL ON THE HOT CORROSION ATTACK OF IN 718 DURING CREEP TESTING (500x)

unaffected by hot corrosion attack. Note the significant formation of the orthorhombic Ni_3Cb needles in the base metal after only 25 hours exposure at 1472°F . The large voids which formed in Zones I and II are due to the large strains prior to failure of this test specimen.

Figure 22(b) is a photomicrograph of the hot corrosion attack of the salt coated specimen tested at a stress level of 20 Ksi. The oxide layer formed on the surface of this specimen was completely stripped away during metallographic preparation and is absent in the photo. Zone II shows deep oxide penetration and severe cracking along the interfaces of the oxide fingers and the depleted metal. In this specimen tested for 72 hours at 20 Ksi, the region of oxide penetration is much thicker than that in the specimen tested for 25 hours at 30 Ksi. Figure 22(b) shows the formation of internal voids in Zone III of depleted metal. Also present in this layer are sulfide particles. Again, the base metal contains a significant amount of orthorhombic Ni_3Cb needles. Note that the amount of corrosion attack in the specimen tested at a stress level of 30 Ksi appears nearly the same as that in the specimen tested at 20 Ksi even though the test time was one-third as long.

The corrosion attack of the salt coated specimen tested at a stress level of 15 Ksi is shown in Figure 22(c). This photomicrograph clearly shows the formation of the thick, porous, non-adherent oxide layer. Zone II shows the inward penetration of the oxides as seen previously. However, at a stress level of 15 Ksi, the depth of the oxide penetration is somewhat smaller than that of the specimen tested at a stress level of 20 Ksi, and the amount of cracking in this zone is less. Zone III shows fine sulfide particles throughout the metal depleted of alloying elements. As was seen in the specimen tested at 20 Ksi, internal voids

are also present in Zone III of this specimen.

Figure 22(d) shows the hot corrosion attack of the specimen tested at a stress level of 10 Ksi. The oxide layer has been removed during sectioning and mounting of the specimen cross-section. Zone II shows considerable void formation and little oxide penetration in the fingerlike manner seen in specimens tested at higher stress levels. Zone III is not well defined, and this zone which at the higher stress levels contained sulfide particles did not appear to contain them at a stress level of 10 Ksi.

At this point, it is interesting to examine the formation of the orthorhombic Ni_3Cb needles in the base metal. Note that in Figure 22(d) the amount of transformed Ni_3Cb in the specimen tested at a stress level of 10 Ksi is markedly less than that transformed in the specimen tested at 20 Ksi. Both specimens were tested for 72 hours at a temperature of $1472^{\circ}F$. It appears that the formation of orthorhombic Ni_3Cb at $1472^{\circ}F$ in IN 718 is stress enhanced. Note also that the amount of transformed Ni_3Cb appears to be the same for both specimens tested at stress levels of 30 Ksi and 20 Ksi. This is true in spite of the fact that the specimen tested at 30 Ksi was exposed to temperature for only 25 hours. Figure 22(d) also shows that the formation of the orthorhombic Ni_3Cb tends to nucleate along grain boundaries.

The results of the creep testing showed that reduction in creep resistance due to the presence of molten salt occurred during tertiary creep. This stage of creep was characterized by internal void formation and intergranular cracking in the depleted zone of hot corrosion attack. Figure 23 illustrates the severe cracking and cavities in Zone II and Zone III of the hot corrosion attack. The leftmost edge of the

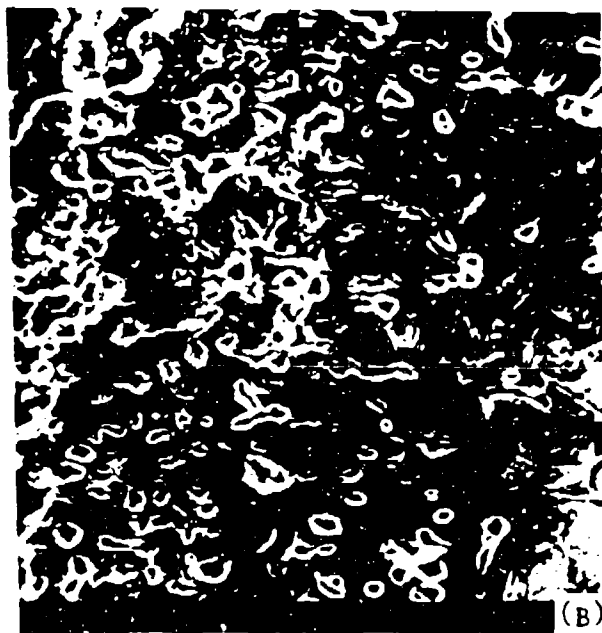


FIG. 23. SCANNING ELECTRON MICROGRAPHS (1000x) SHOWING TYPICAL HOT CORROSION ATTACK OF IN 718 AT (A) 20 KSI, AND (B) 15 KSI, FOR 72 HOURS AT 1472°F

photomicrographs is the interface between the surface oxide layer (Zone I) and the underlying region of intertwined oxide and metal (Zone II). The depth of corrosion attack appears to be greater for the 15 Ksi stress level than for the 20 Ksi stress level. This illustrates that although the overall depth of penetration of the hot corrosion attack increased with increasing stress level as shown in Figure 20, localized regions did exist where the depth of corrosion attack was greater than the average value calculated as shown in Figure 19.

As shown in Figure 23, the massive penetration of oxide into the depleted metal resulted in a region of intertwined oxide and metal. Under the strain during creep, cracking occurred along the interfaces between the oxide and metal in Zone II. In Zone III internal voids and cracking occurred in a region where oxide fingers had not penetrated. Zone III consisted of sulfide particles distributed throughout the metal which had been depleted of its alloying elements. The voids and cracking in this region did not initiate along oxide-metal interfaces, but rather seemed to occur at grain boundaries. Grain boundary sliding in this depleted zone is probably responsible for initiating these cavities. Two types of intergranular cracking occur in creep. These are wedge-type cracking and the formation of oval cavities at grain boundaries⁽¹⁴⁾. Figure 24 illustrates schematically various ways that wedge-type cracks, known as w-type, nucleate at grain boundary triple-points due to grain boundary sliding. Oval voids, called r-type, also form along grain boundaries due to grain boundary sliding and are believed to occur at slip plane and grain boundary intersections or at fine particles in the grain boundary. Because the alloying elements had been depleted in Zone III, no second phase particles are present at the

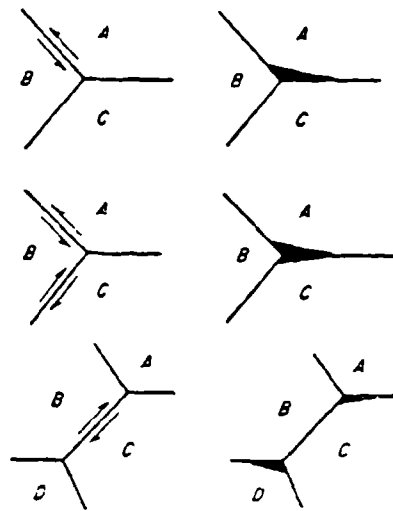


FIG. 24. Schematic drawings of grain boundary sliding and intergranular cracking.

grain boundaries. In addition, no carbides are present at the grain boundaries in this depleted zone because it appears that as the chromium content in the alloy is lowered by sulfur and oxygen, the carbides, mainly Cr_{23}C_6 , dissolve. Without the particles to pin the grain boundaries and inhibit the relative motion of the grain boundaries, sliding can occur with relative ease.

Figure 25 shows further evidence of grain boundary sliding and crack formation along grain boundaries. Excessive sliding sufficient to initiate and open cracks only occurred along grain boundaries where the alloying elements along the grain boundaries had been depleted as shown in Figure 25. This intergranular penetration is typical of aggressive environmental attack. Yoshida, et al.,⁽⁸⁾ reported that creep fracture of salt coated specimens occurred as a result of only a few aggressive intergranular penetrations of sulfides initiating main cracks which then propagated rapidly. Other investigators⁽⁴⁾⁽¹¹⁾ have observed that most grain boundaries show no cracking and that deep cracks containing sulfide particles occurred along only a few grain boundaries. However, in this study, deep intergranular spikes were not observed. Only a few instances of intergranular attack of the type shown in Figure 25 were observed in all the specimens. The hot corrosion attack typically seen in this study was along a relatively uniform front advancing inward from the specimen surface. This type of attack and the absence of massive, deep intergranular penetration was most likely due to the many grain boundaries present in the microstructure of the wrought IN 718. Because of the numerous accessible grain boundary paths for diffusion, the inward penetration was "averaged" around the circumference of the specimen along all grain boundaries. However, it seems that if the

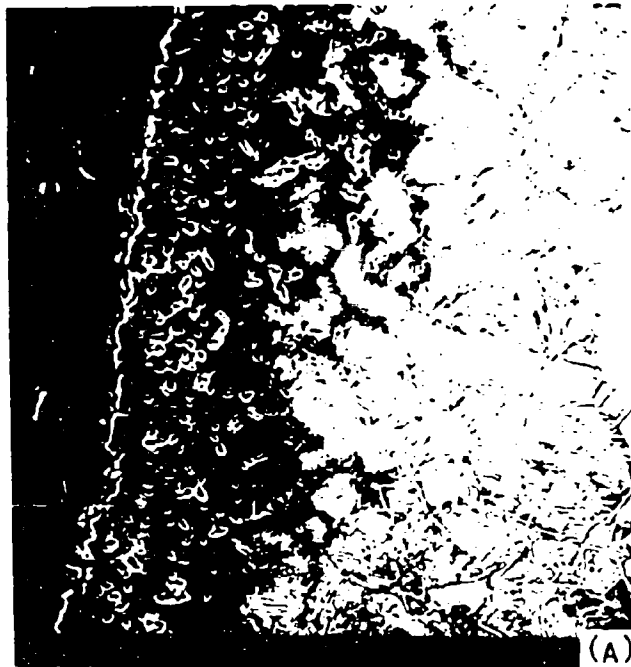


FIG. 25. SCANNING ELECTRON MICROGRAPHS (A) 500x AND (B) 1000x SHOWING INTERGRANULAR PENETRATION AND GRAIN BOUNDARY CRACKING

material tested had larger grains such as in a cast alloy with large columnar grains, the inward diffusion of corrosive species would concentrate at these fewer grain boundaries, and deep intergranular penetration would more likely occur.

An elemental analysis of the corrosion products was conducted using X-ray energy spectroscopy. The results are summarized graphically in Figures 26 and 27. The oxide formed on the surface of the IN 718 specimens was rich in chromium which is to be expected because of the high chromium content of the alloy. Cr_2O_3 is the thermodynamically stable oxide compound for chromium. Much of the titanium and columbium in the alloy also formed oxide compounds. Thermodynamic data suggest that TiO and CbO are most likely the compounds formed. In addition, nickel was found in the oxide layer presumably as the compound NiO . Chromium and titanium were also found in the sulfide particles. Although Figure 26 shows the sulfide containing significant nickel and iron, this is misleading. The sulfide particles were very small and surrounded by metal depleted of alloying elements. The X-ray analysis of a small sulfide particle undoubtedly detected the presence of nickel and iron from the surrounding depleted metal. Note that in the depleted zone, nickel and iron are the main constituents. It is likely that there is indeed some nickel and iron in the sulfide particles, but chromium and titanium appear to be the stronger sulfide formers. The amount of molybdenum and columbium in the sulfide particles could not be determined using X-ray energy spectroscopy since the strong sulfur peak of the energy spectrum masked the presence of molybdenum and columbium. Due to the formation of the oxide layer and internal sulfides, the depleted zone of metal was void of most of the chromium, titanium, and

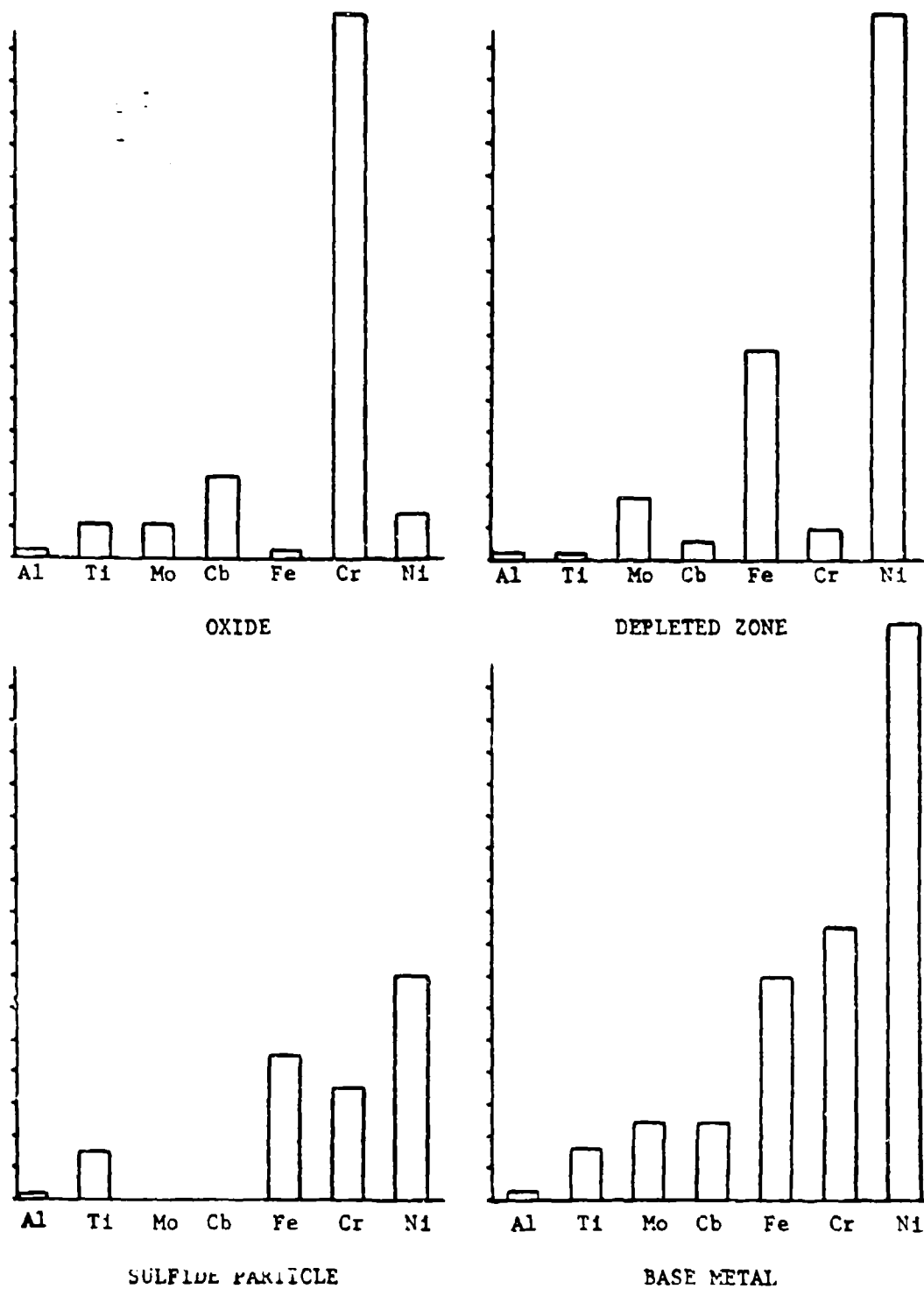


FIG. 26. Elemental analysis of the hot corrosion products for IN 718.

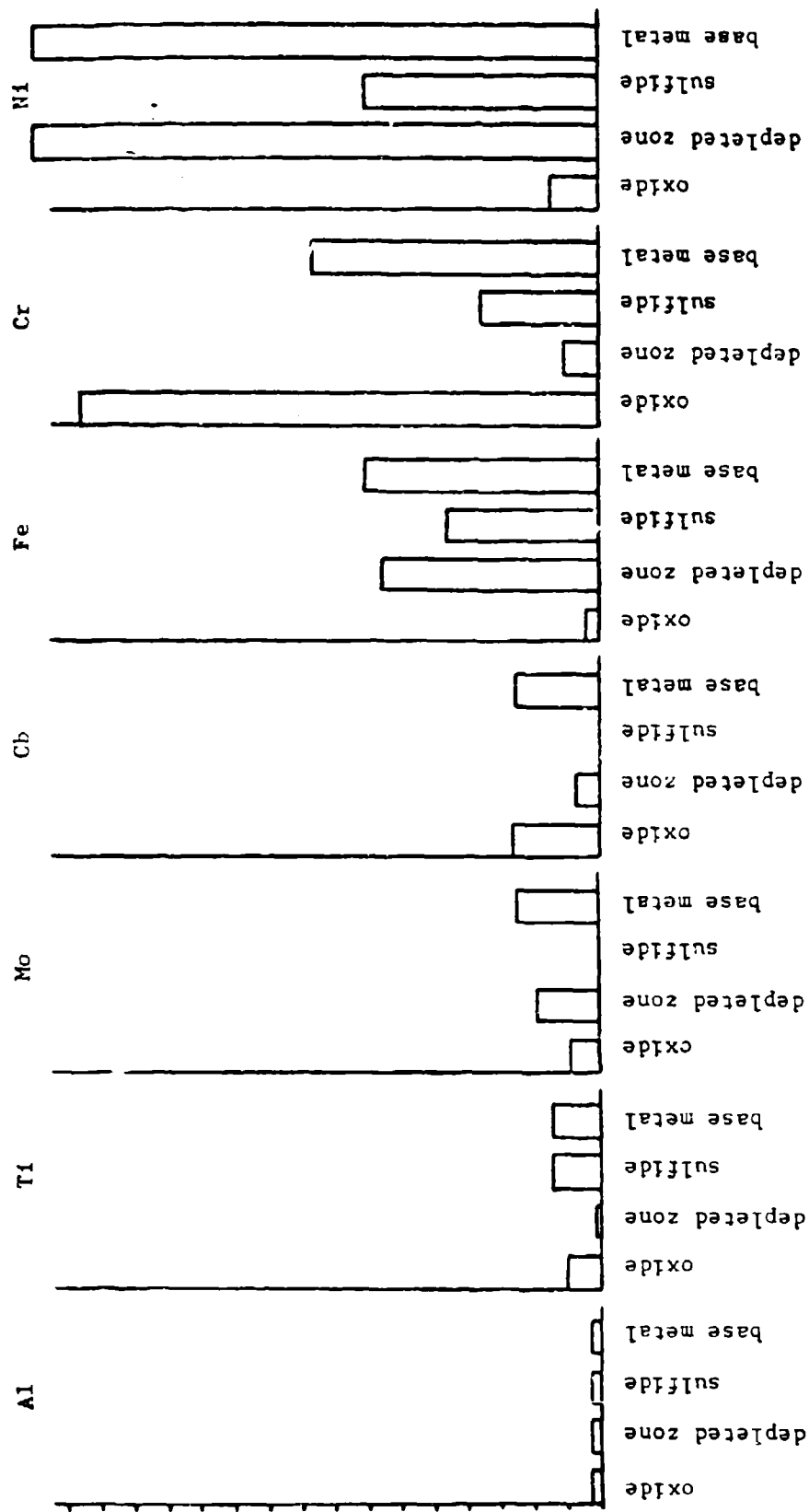


FIG. 27. Elemental analysis of the hot corrosion products for IN 718.

columbium. This left a depleted zone rich in nickel, iron, and molybdenum. The aluminum in the alloy appeared to be uniformly distributed throughout the corrosion products.

3. Summary

The presence of a thin film of molten salt does reduce the creep resistance of Inconel 718 at a temperature of 1472°F (800°C) at stress levels sufficiently large to cause tertiary creep to occur within the 72 hour test period. It is only during tertiary creep that the molten salt affected the creep behavior. Specimens of smaller diameter generally showed a larger environmental degradation of creep properties. It appears that the degree of environmental degradation of creep resistance by molten salt is related to the depth of hot corrosion attack and the ratio of the cross-sectional area affected by corrosion attack to the original cross-sectional area of the specimen. The depth of corrosion attack increased with increasing stress level at the same temperature, and higher minimum rates of creep were found for salt coated specimens than for uncoated specimens tested in laboratory air.

The hot corrosion attack of Inconel 718 resulted in the formation of four distinct zones of corrosion attack. These are (1) a porous, non-adherent oxide layer consisting of mainly chromium and containing titanium, columbium, and nickel; (2) a region of massive penetration of oxide fingers into the depleted metal; (3) a region of metal depleted of its alloying elements and containing sulfide particles of chromium and titanium; and (4) base metal unaffected by hot corrosion attack. The formation of these zones is due to the inward diffusion of sulfur and

oxygen from the molten salt film. The sulfur diffuse inward faster than the oxygen and forms sulfide particles of mostly chromium and titanium. This lowers the chromium content of the alloy and reduces the oxidation resistance of the alloy. The oxygen diffusing inward behind the sulfur forms oxides of nickel, columbium, and chromium. The protective oxide layer of Cr_2O_3 and TiO_2 which forms in high chromium-containing alloys does not form since the chromium content has been lowered and the titanium depleted from the metal by the formation of sulfides. As a result, a non-protective oxide layer containing nickel and columbium in addition to chromium and titanium forms. This oxide layer is very porous, and the molten salt tends to penetrate and dissolve the oxide layer. As the oxygen continues to diffuse inward, the subsurface sulfides of chromium and titanium are converted to oxides. The surface oxides grow inward and link with the oxides converted from sulfides to form the fingerlike penetrations. The released sulfur continues to diffuse inward, depleting the alloy of chromium and titanium and forming new sulfide particles. The columbium left behind in the depleted zone diffuses outward to the oxide layer and is converted to oxide.

Under stress, the associated strain causes cracking in the outer surface oxide layer. Cracking also occurs along the oxide fingers which have penetrated into the depleted metal. This opens new paths for the molten salt to flow inward and attack fresh metal. Internal voids formed by grain boundary sliding occur in the region of metal depleted of alloying elements. The depletion of chromium, titanium, and columbium removes second phase particles and dissolves carbides which pin the grain boundaries and restrict grain boundary sliding. This cracking and grain boundary sliding result in lower creep resistance.

Hot corrosion produces a layer of attack which contains significant cracking and as a result reduces the load carrying capacity of the specimen. Higher stress levels promote deeper oxide penetration and more severe cracking and void formation and magnify the effect of the hot corrosion attack.

Substantial formation of a needlelike orthorhombic Ni_3Cb phase occurred in IN 718 after 72 hours at the test temperature of 1472°F (800°C). Evidence shows that this phase is detrimental to high temperature strength and creep resistance. It appears that the formation of the orthorhombic Ni_3Cb needles begins to nucleate at grain boundaries and that the transformation is stress enhanced.

B. RENÉ 77 AND RENÉ 80

1. Metallographic Analysis

Small cylindrical pins of René 77 and René 80 were tested to examine the oxidation and hot corrosion resistance in an unstressed condition at 1672°F (900°C) for 72 hours. Figure 28 shows the weight change of uncoated and salt coated pins for both alloys. Each bar of Figure 28 represents the average of three pins tested under the same conditions. The data show several trends. Based on weight-change measurements, the René 77 was more oxidation resistant than the René 80. However, the René 80 was superior to the René 77 in hot corrosion resistance. In addition, the data show that the 90% Na_2SO_4 / 10% NaCl salt was slightly more corrosive than the pure 100% Na_2SO_4 .

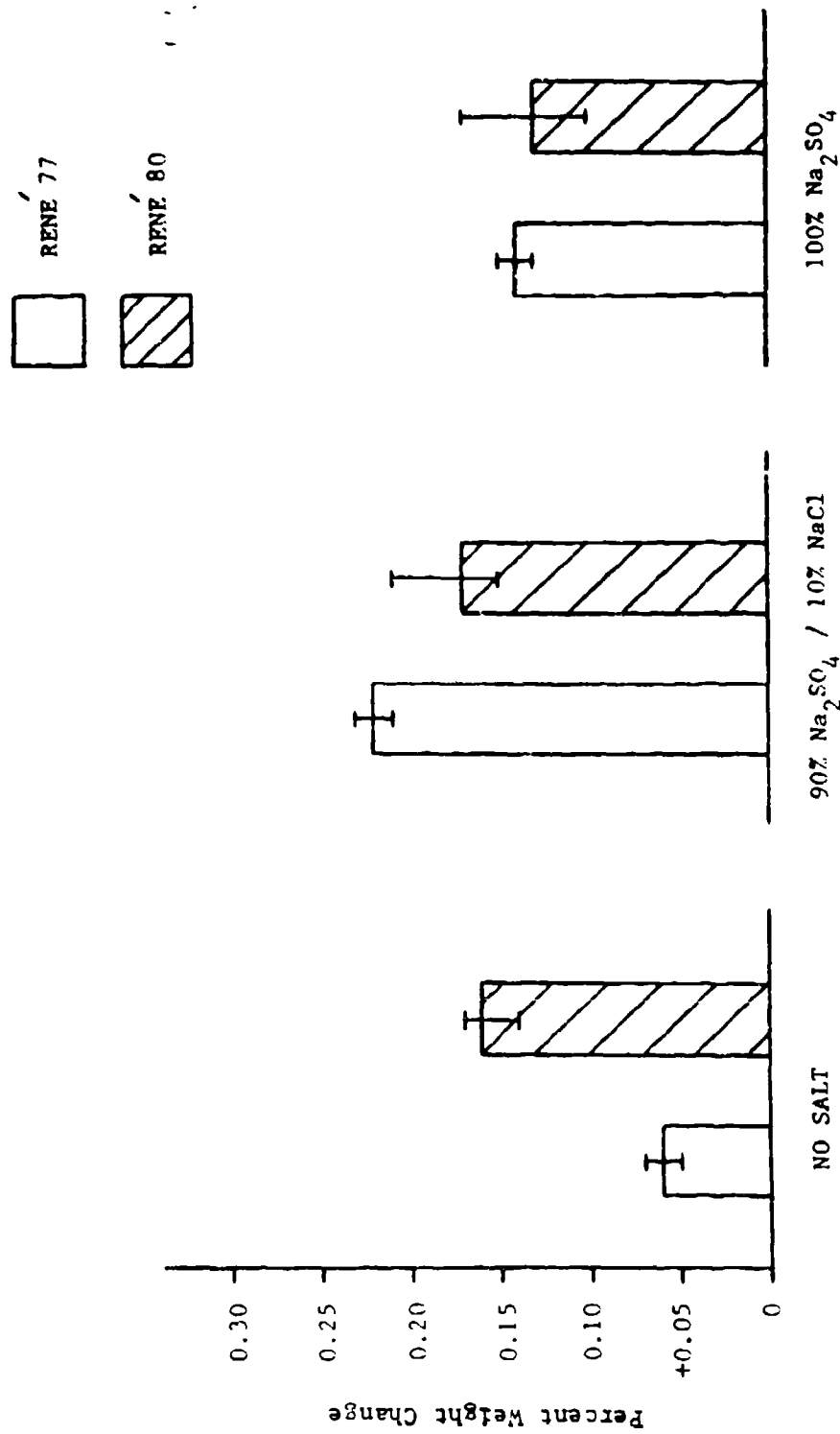


FIG. 28. Weight change of salt coated specimens after 72 hours at 1652°F.

Figure 29 shows the depth of corrosion attack measured on a cross-section as previously described for IN 718. The depth of oxidation attack was considerably less in the René 77 pins than in the René 80 pins. The René 77 was less susceptible to oxidation attack than was the René 80. This agrees with the results of the weight-change measurements. However, in a molten salt environment, René 80 suffered a deeper corrosion attack than did René 77 even though the weight change in René 80 was less than that of the René 77. Also note that the depth of penetration of the hot corrosion attack was approximately equal for both salt compositions.

Figure 30 and Figure 31 show the surface attack caused by molten salt on pins of René 77 and René 80 respectively. In both alloys, the hot corrosion attack caused by the 90% Na_2SO_4 / 10% NaCl salt mixture was virtually identical in appearance to that caused by the 100% Na_2SO_4 salt. In the René 77, three zones of hot corrosion attack can be labelled as shown. Zone I is a tight, adherent oxide layer. There was no evidence of this oxide layer being stripped away from the surface of the specimens even during sectioning for metallographic analysis. Zone II is directly beneath this oxide layer and is a region of metal depleted of some of its alloying elements. Zone II also contains sulfide particles. Zone III is the base metal which was not affected by corrosion attack. This zone contains a fine distribution of the precipitation strengthening gamma-prime phase. Note that for the salt coated specimens, there is little oxide penetration into the depleted zone of metal. However, in the uncoated pin, there was localized penetration of oxide into the depleted zone. The depleted zone was slightly smaller in the uncoated pins than in the salt coated pins, and

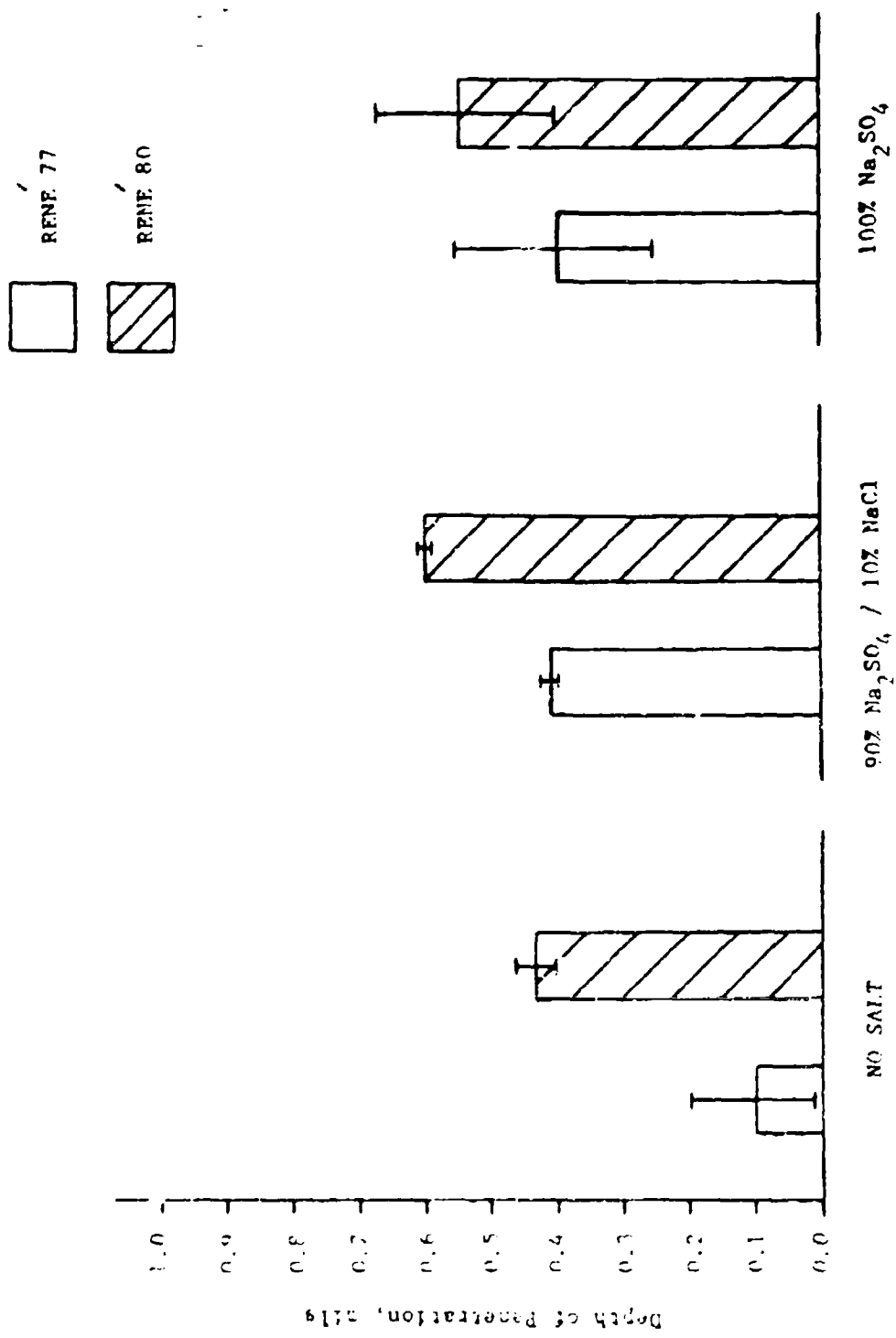


FIG. 29. Depth of hot corrosion attack of salt coated specimens after 72 hours at 1652°F.

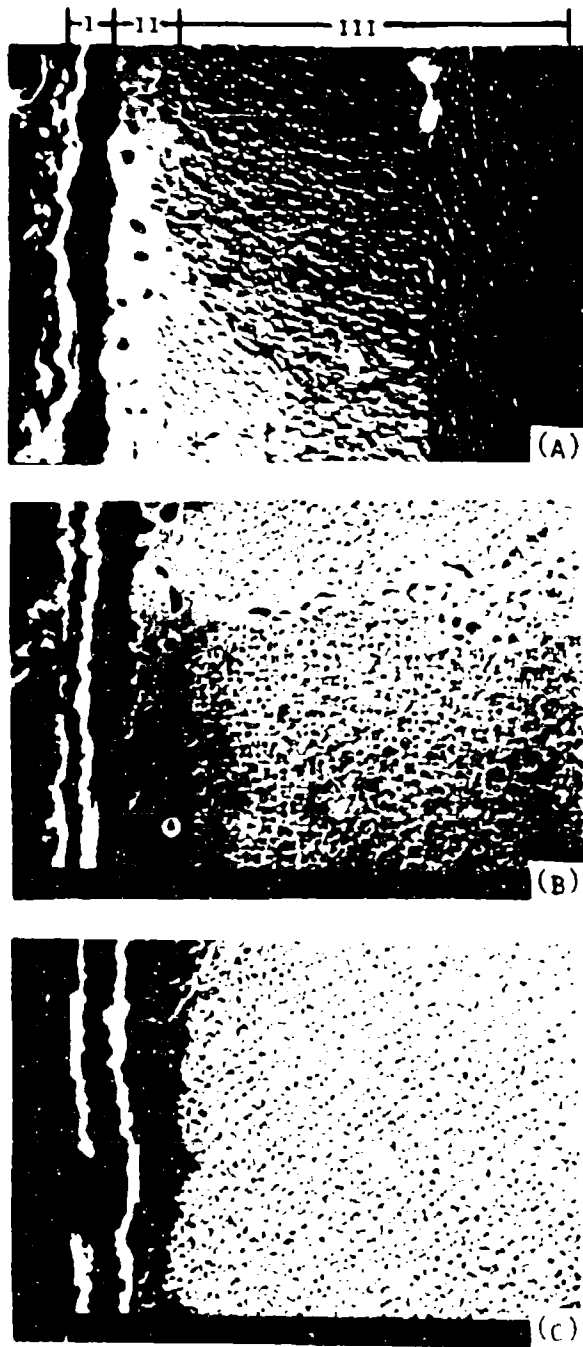


FIG. 30. SCANNING ELECTRON MICROGRAPHS (1000x) SHOWING
HOT CORROSION ATTACK OF RENE '77 COATED WITH
(A) 90% Na_2SO_4 /10% NaCl ; (B) 100% Na_2SO_4 ;
(C) NO SALT; AT 1672°F FOR 72 HOURS

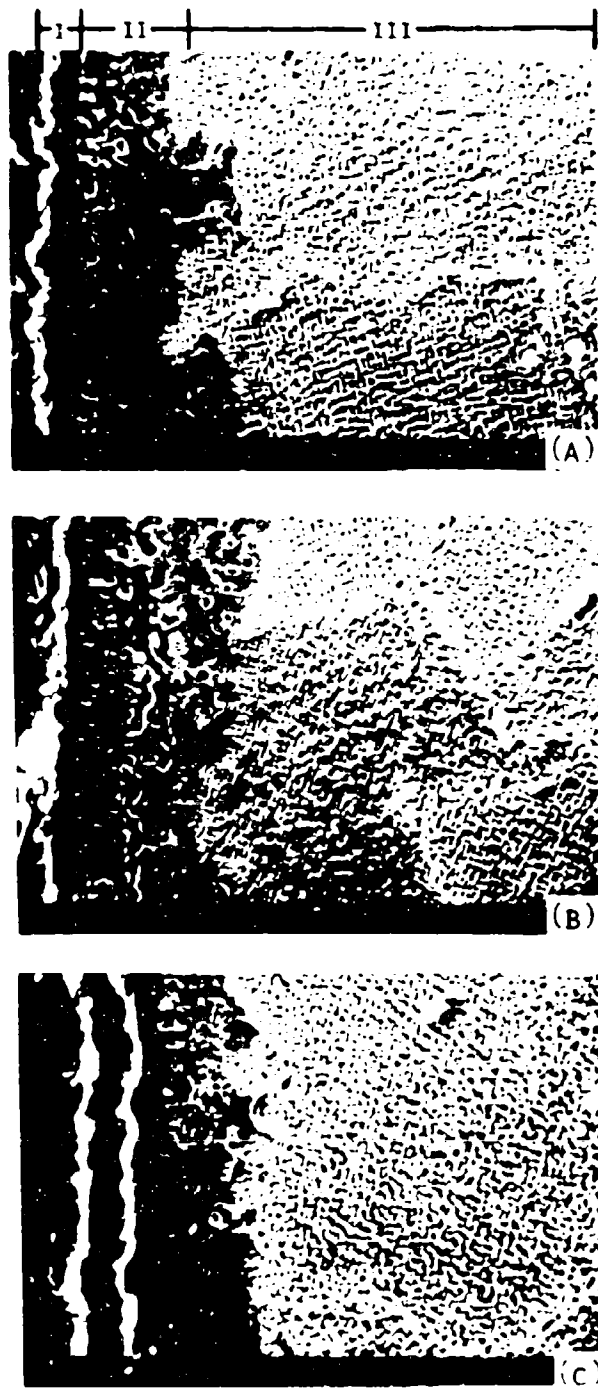


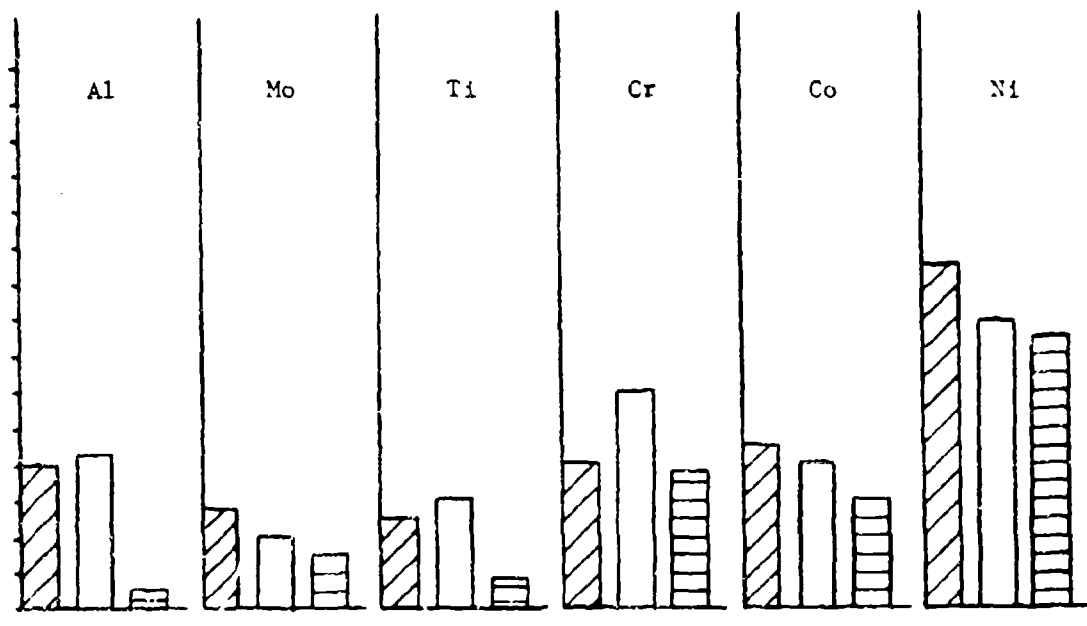
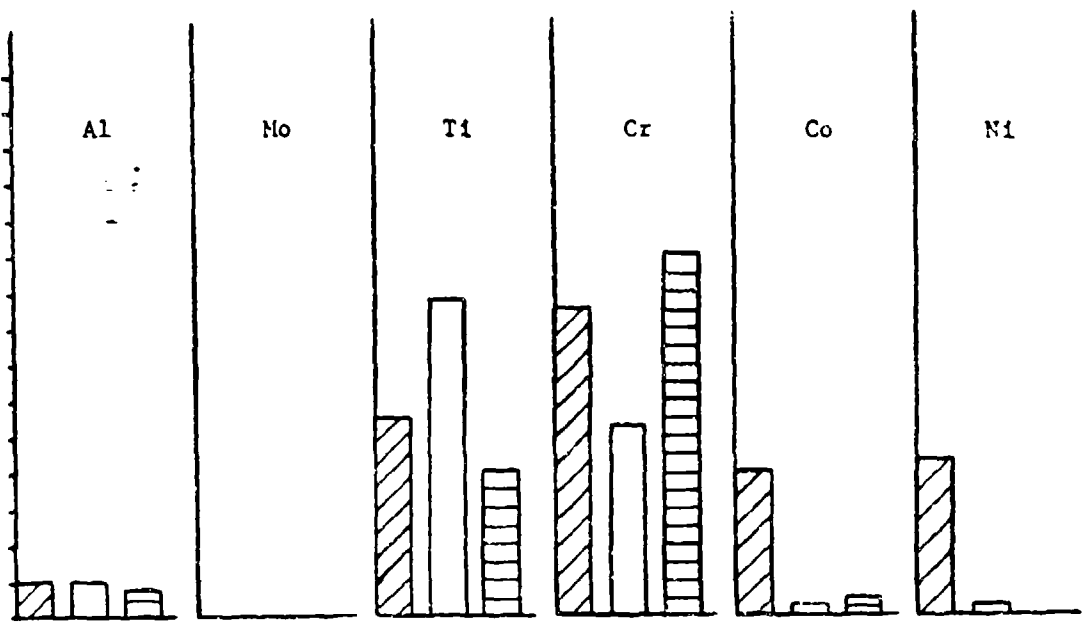
FIG. 31. SCANNING ELECTRON MICROGRAPHS (1000x) SHOWING HOT CORROSION ATTACK OF RENE '80 COATED WITH (A) 90% Na_2SO_4 /10% NaCl ; (B) 100% Na_2SO_4 ; (C) NO SALT; AT 1672°F FOR 72 HOURS

as expected, there were no sulfide particles present in Zone III of the uncoated pins.

The hot corrosion attack in René 80 appears somewhat different than that seen in René 77. Zone I is a layer of tight, adherent oxide similar to the surface oxide layer found on René 77. However, unlike in René 77, the surface oxide in René 80 penetrated into the depleted metal directly under the outer oxide layer. Thus, Zone II contained a region of intertwined oxide and depleted metal. Farther inward, sulfide particles were present in a band of metal depleted of alloying elements. Zone III is the base metal not subjected to hot corrosion attack and shows a fine homogeneous distribution of the gamma-prime precipitation phase. Note that in both the René 77 and René 80 tested in the unstressed condition, there is no evidence of cracking or mechanical damage to the surface oxide layer and no subsurface cracking along oxide-metal interfaces or internal void formation.

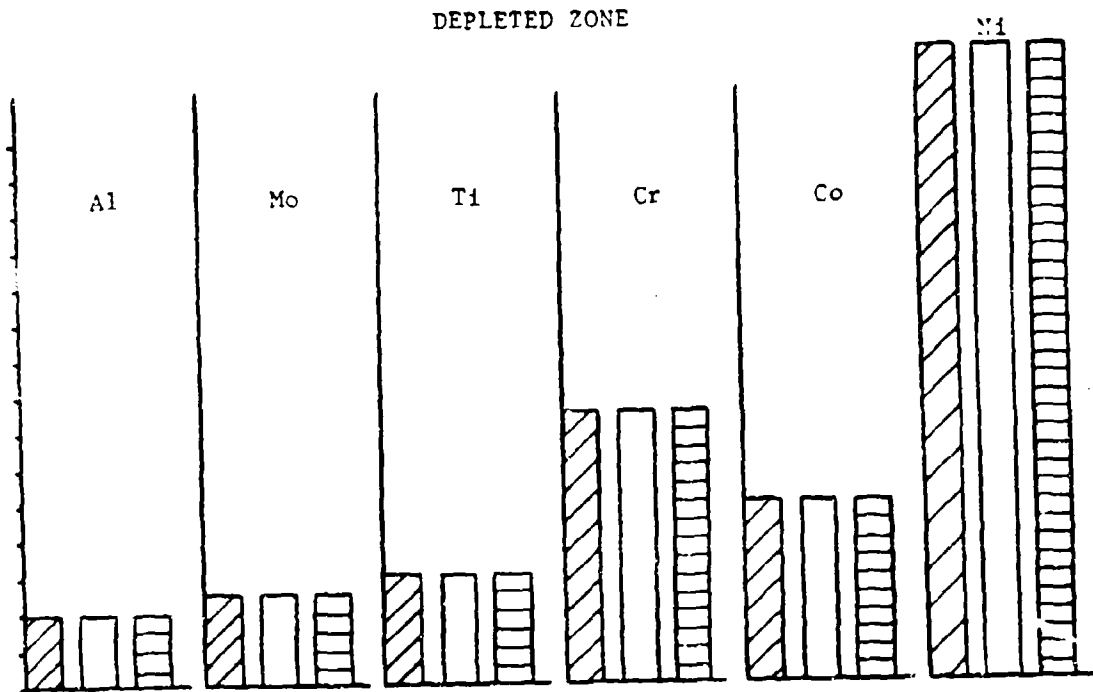
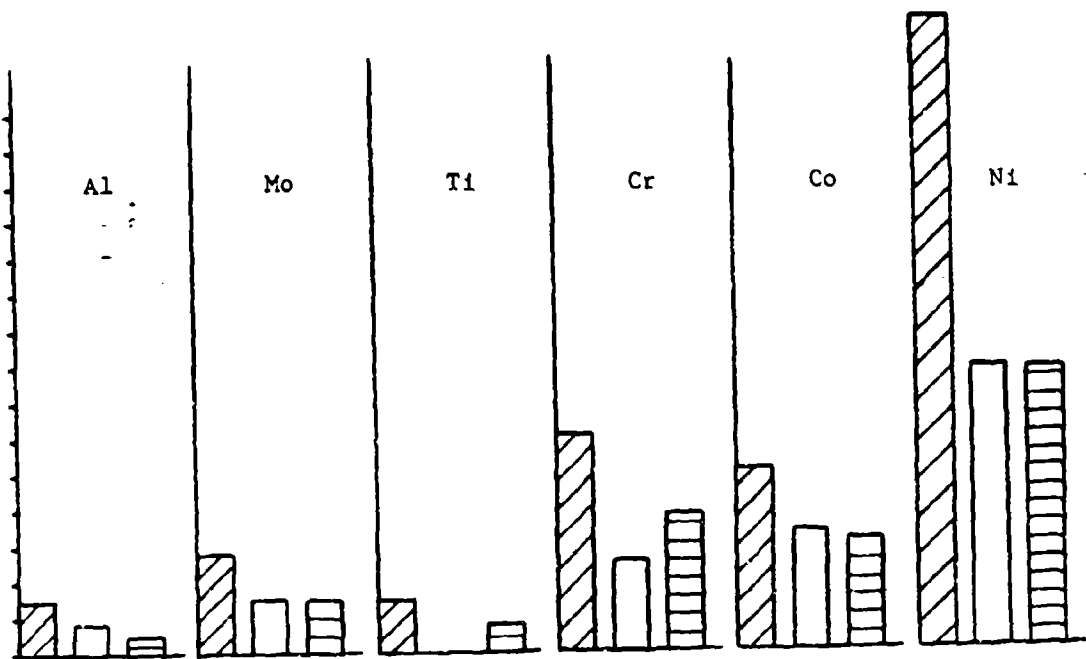
An elemental analysis of the corrosion products was conducted using X-ray energy spectroscopy. Figures 32 and 33 depict graphically the elemental analysis of four regions of the corrosion attack in René 77 and René 80 respectively. These regions are (1) the oxide layer (Zone I); (2) the metal depleted of alloying elements (Zone II); (3) the base metal (Zone III); and (4) the oxide fingers which penetrate into the depleted metal.

In both the René 77 and René 80 pins, the oxide composition was similar. The surface oxide was rich in chromium and titanium. For the pins coated with a salt of 90% Na_2SO_4 / 10% NaCl , the oxide was richer in chromium than in titanium. However, when the pins were tested with a 100% Na_2SO_4 salt coat, the oxide formed contained more titanium than



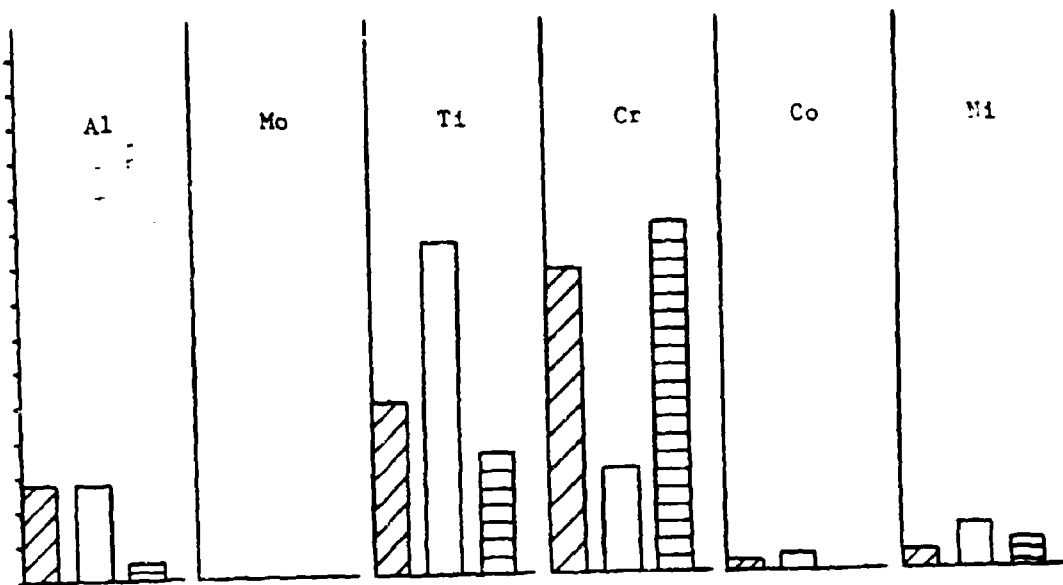
 90% Na₂SO₄ / 10% NaCl
  100% Na₂SO₄
  NO SALT

FIG. 32. Elemental analysis of the hot corrosion products for Rene 77.

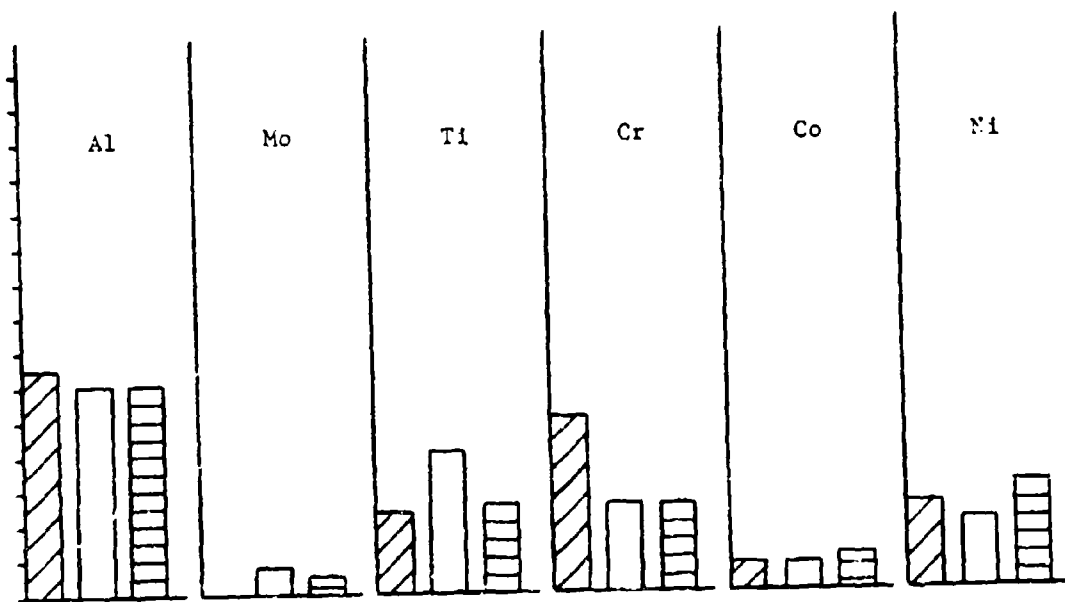


 90% Na₂SO₄ / 10% NaCl
  100% Na₂SO₄
  NO SALT

FIG. 32.(cont)



OXIDE



FINGER REGION



90% Na₂SO₄ / 10% NaCl

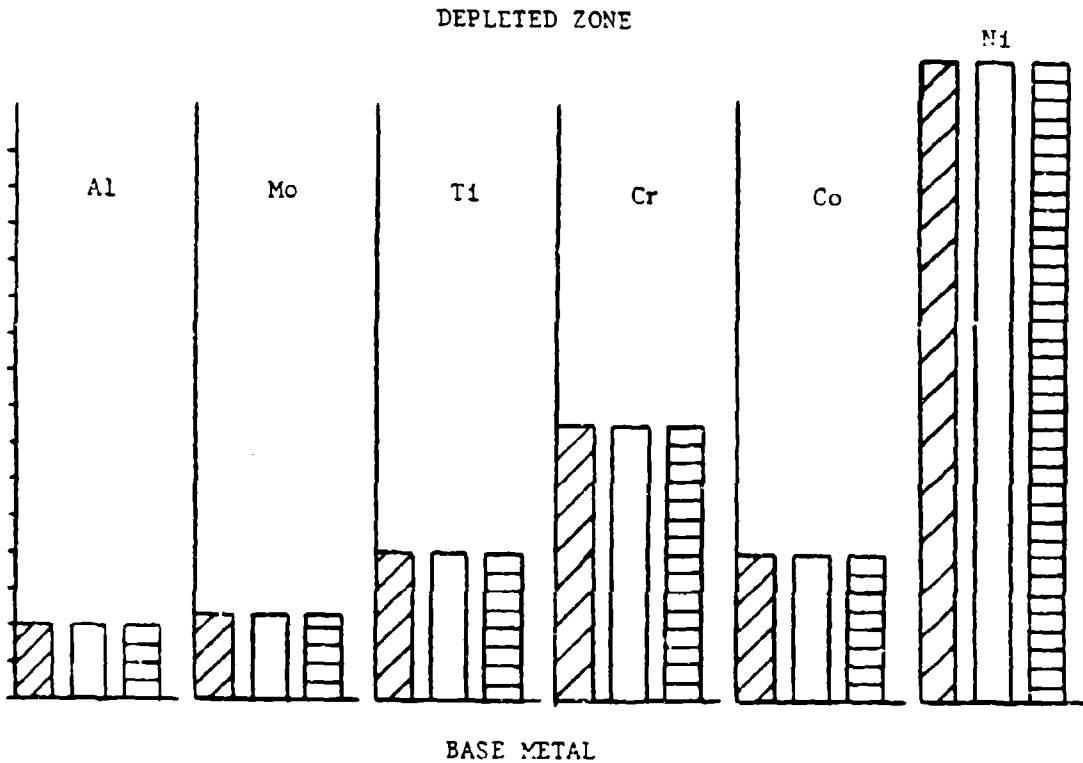
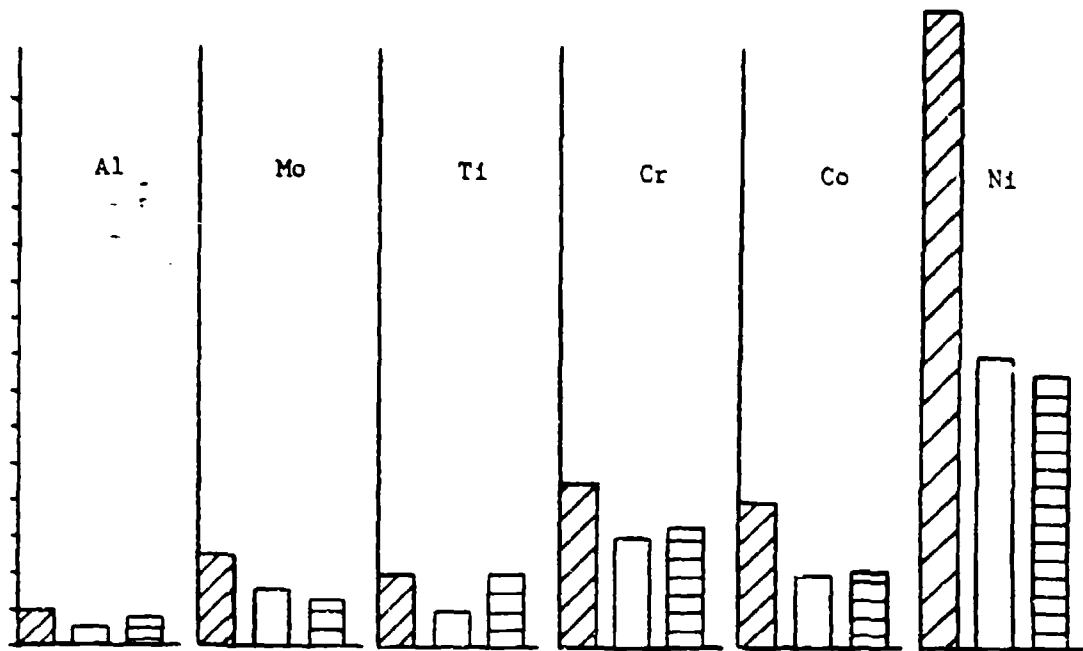


100% Na₂SO₄



NO SALT

FIG. 33. Elemental analysis of the hot corrosion products for Rene 80.



90% Na₂SO₄ / 10% NaCl



100% Na₂SO₄



NO SALT

FIG. 33.(cont)

chromium. Thus, the composition of the molten salt or in this case, the presence of chloride, Cl^- , in the salt mixture affects the composition of the oxide layer. There were some differences in the oxide layers of the two alloys which should be noted. For salt coated pins of René 80, the oxide layer contained a significant amount of aluminum. The aluminum content of the oxide formed on René 77 was less. A second difference was the presence of cobalt and nickel in the oxide formed on René 77 pins coated with 90% Na_2SO_4 / 10% NaCl . Little cobalt or nickel was detected in the oxide layer of René 80 pins tested in any of the three conditions. No molybdenum was found in the oxide layer of either alloy.

In both alloys, X-ray analysis showed a high concentration of aluminum in the region of oxide penetration into the depleted metal. The aluminum was a major constituent in the oxide fingers and in the oxide along the interface of Zone I and Zone II. In the finger region, René 77 contained significant amounts of nickel and cobalt as well as chromium and titanium. However, in René 80, X-ray analysis revealed less nickel and cobalt than in René 77. In addition, the aluminum content was slightly greater than in René 77, while chromium and titanium were less. The depleted zone in both alloys was low in chromium, titanium, and aluminum.

Figure 34 shows the composition of the sulfide particles found in Zone II of both René 77 and René 80 after hot corrosion attack. The sulfides were rich in chromium and titanium. Because the strong sulfur peak in the X-ray energy spectrum masked the presence of aluminum and molybdenum, the presence of these elements in the sulfide particles could not be determined.

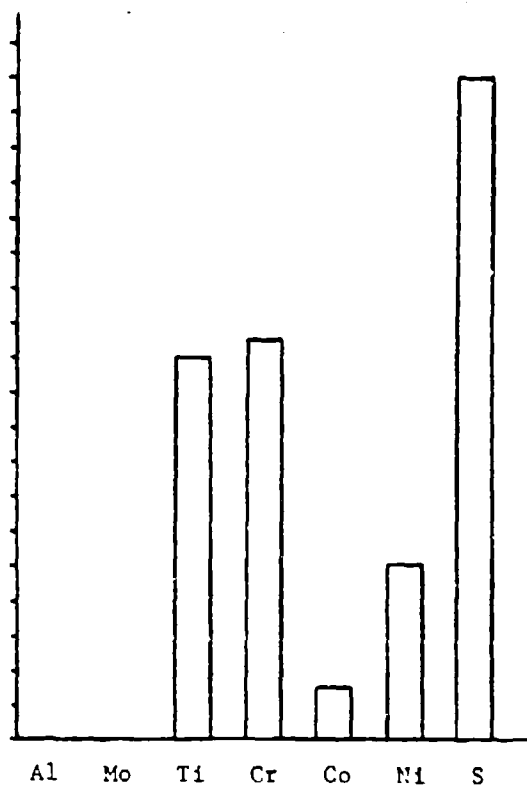


FIG. 34. Elemental analysis of sulfide particles found in René 77 and René 80 after hot corrosion attack.

A set of five René 77 pins were coated with varying amounts of salt ranging from a coverage of approximately 0.5 mg/cm^2 to 10.0 mg/cm^2 . Attempts were made to coat pins with thicker salt layers, but approximately 10 mg/cm^2 proved to be the maximum coverage achievable with the spraying technique used in this study. The salt composition used was 90% Na_2SO_4 / 10% NaCl . Figure 35 shows the pins after 72 hours at a temperature of 1652°F (900°C). It is very apparent from visual examination that salt thickness affects the degree of hot corrosion attack. Note that at the greater salt thicknesses, the oxide which formed was no longer adherent as seen on previous specimens. Figure 36 shows the weight change of the René 77 pins as a function of salt thickness. This graph shows a maximum corrosion attack at a salt coverage of approximately 7.5 mg/cm^2 . These data show a similar trend to that found by Fang and Shores as shown in Figure 1 of this report.

2. Summary

Based on the results of static corrosion tests conducted at 1672°F (900°C) for 72 hours, René 77 showed better oxidation resistance than did René 80. Conversely, weight-change measurements showed the René 80 to resist hot corrosion attack better than René 77. However, the corrosion attack in René 80 exhibited oxide penetration into the depleted metal while the corrosion attack in René 77 resulted in a much more uniform interface. Thus, the depth of corrosion penetration in René 80 was slightly greater than in René 77 even though weight-change measurements showed René 80 to be superior in hot corrosion resistance. Typically, the hot corrosion attack of both alloys exhibited three

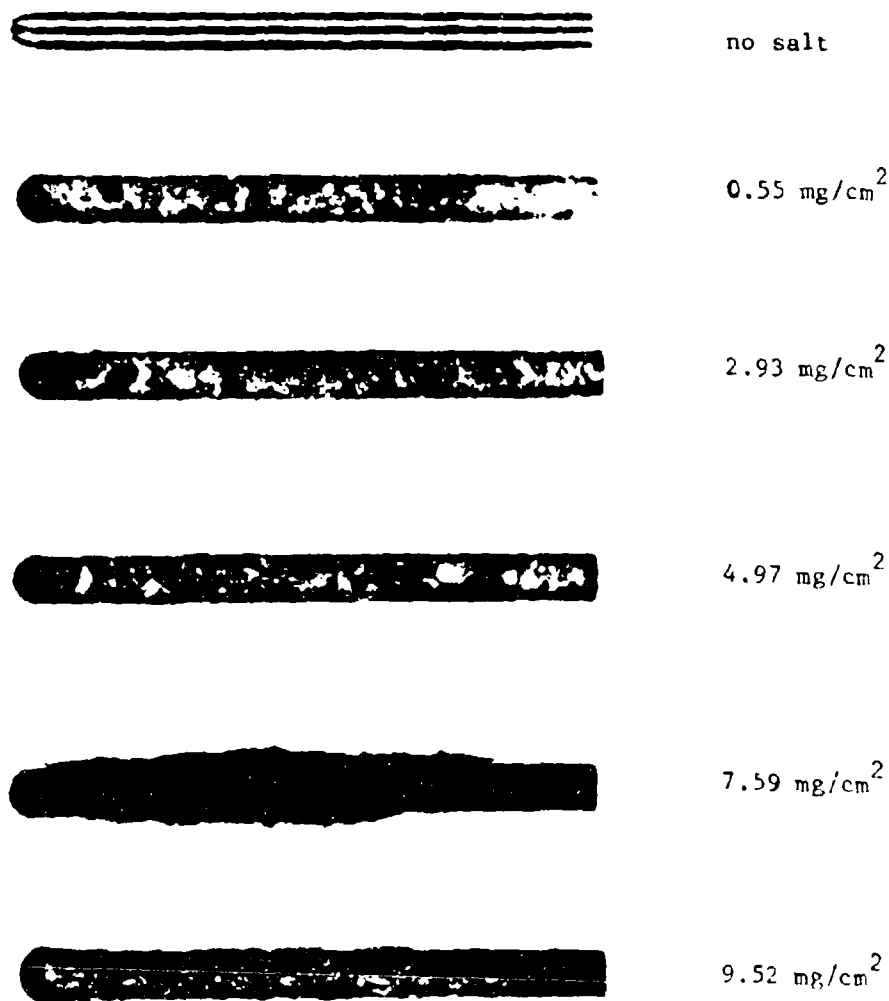


FIG. 35. Rene 77 pins showing the effect of salt thickness on the degree of hot corrosion attack.

EFFECT OF SALT THICKNESS

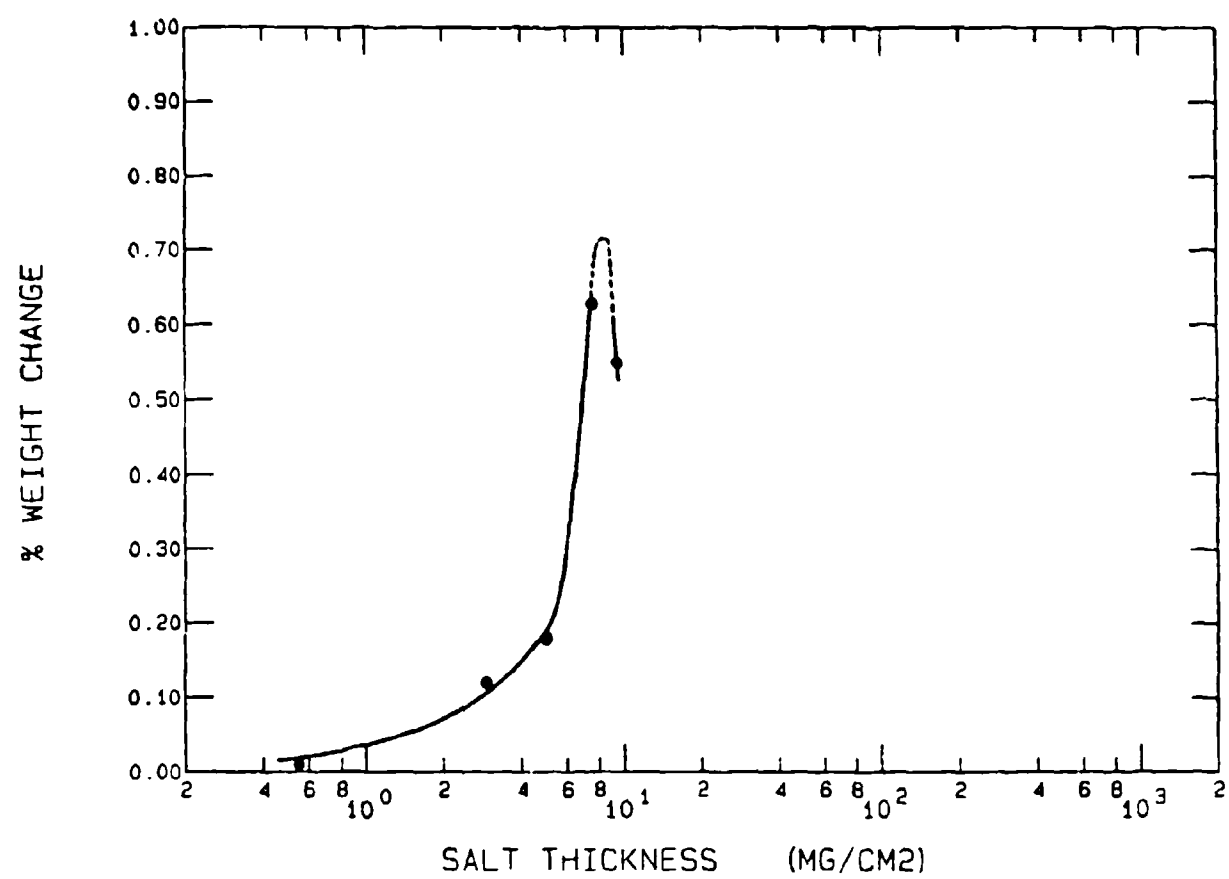


FIG. 36. Effect of salt thickness on the hot corrosion attack of René 77.

distinct zones. These are (1) an adherent oxide layer rich in chromium and titanium; (2) a zone of metal mostly depleted of chromium, titanium, and aluminum and containing sulfide particles of chromium and titanium; and (3) the base metal unaffected by hot corrosion attack.

Based on weight-change measurements, the presence of chloride, Cl^- , in the molten salt results in a slightly more corrosive attack. However, the appearance of the hot corrosion attack was similar for salts with or without the chloride species, and the depth-of-penetration measurements were virtually identical for both salt compositions. Salt thickness, or salt coverage, does affect the degree of hot corrosion. Tests on René 77 showed that an optimum salt thickness exists for maximum corrosion attack, and that as the salt thickness increases, the oxide layer formed is no longer adherent.

V. CONCLUSIONS AND RECOMMENDATIONS

CONCLUSIONS

The presence of a molten salt environment degraded the creep resistance of Inconel 718 only at stress levels sufficiently large to cause substantial tertiary creep to occur within the 72 hour test period. The molten salt showed little effect on the creep behavior of specimens which did not undergo tertiary creep. Higher minimum rates of creep were found for salt coated specimens than for the uncoated specimens tested in laboratory air. However, the steady-state region of creep was not well-defined in the creep tests conducted at the higher stress levels. The difference in the strain rate coefficients indicates that the creep mechanisms which occurred in the salt coated specimens are different from those which occurred in uncoated specimens.

The depth of hot corrosion attack was relatively uniform around the circumference of the round bar specimens. The depth of corrosion attack increased with increasing stress level. The degree of environmental degradation of creep resistance due to the presence of a molten salt appeared to be related to the ratio of the cross-sectional area affected by hot corrosion attack to the original cross-sectional area of the test specimen.

The hot corrosion attack of Inconel 718 resulted in the formation of four distinct zones. These are (1) a porous, non-adherent oxide layer consisting of mainly chromium and also containing titanium, columbium, and nickel; (2) a region of massive penetration of oxide

fingers into metal depleted of alloying elements; (3) a zone of metal which was depleted of chromium, titanium, and columbium and contained sulfide particles rich in chromium and titanium; and (4) base metal which was not affected by hot corrosion attack.

Under stress, the resulting strain caused cracking of the surface oxide layer. Severe cracking was also observed along the oxide-metal interfaces in the region of oxide penetration and intertwined oxide and metal. Internal voids and grain boundary cracking occurred in the zone of depleted metal. This cracking and void formation in the region of hot corrosion attack resulted in a reduction of the load carrying capacity of the specimen and in lower creep resistance. Higher stress levels promoted deeper oxide penetration and more cracking in the region of hot corrosion attack.

At the test temperature of 1472°F (800°C), substantial formation of a needlelike orthorhombic Ni_3Cb phase occurred in the Inconel 718 specimens. It appears that the formation of the orthorhombic Ni_3Cb phase begins to nucleate at grain boundaries and that the transformation is stress enhanced. The presence of this phase was detrimental to creep resistance.

The corrosion tests conducted with René 77 and René 80 showed that René 77 was more oxidation resistant than René 80. However, René 80 had better hot corrosion resistance than René 77. The hot corrosion attack in René 77 resulted in a uniform interface between the surface oxide and the underlying metal, while the hot corrosion attack in René 80 resulted in fingers of oxide penetrating into the underlying metal. The hot corrosion attack in both René 77 and René 80 was divided into three distinct regions. These are (1) a tight, adherent oxide layer rich in

chromium and titanium; (2) a zone of metal depleted mainly of chromium, titanium, and aluminum and containing sulfide particles rich in chromium and titanium; and (3) the base metal which was not affected by hot corrosion attack.

Tests on René 77 showed that the salt thickness affects the degree of hot corrosion attack. There exists a salt thickness that results in a maximum hot corrosion attack. In addition, as the salt thickness increased, the surface oxide layer resulting from the hot corrosion attack became flaky and non-adherent.

RECOMMENDATIONS

Sustained-load creep tests on salt coated and uncoated specimens of René 77 or René 80 should be conducted to study the effect of molten salt on the creep behavior of these alloys. The results of this study on the hot corrosion and oxidation attack of these alloys in the unstressed condition form a good foundation to further characterize hot corrosion mechanisms under stress. In addition, sustained-load creep crack growth experiments using compact tension specimens should be conducted. By testing salt coated and uncoated specimens, the effect of molten salt on creep crack growth characteristics can be studied.

BIBLIOGRAPHY

1. Decker, R. F. "Strengthening Mechanisms in Nickel-Base Superalloys," Steel Strengthening Mechanisms. Greenwich, CO: Climax Molybdenum Co., 1969.
2. Smith, W. F. "Nickel and Cobalt Alloys," Structures and Properties of Engineering Alloys. New York: McGraw-Hill Book Company, 1982.
3. Floreen, S. and R. H. Kane. "Effect of Environment on High Temperature Fatigue Crack Growth in a Superalloy," Metallurgical Trans., 10A: 1745-1751 (November, 1979).
4. Floreen, S. and R. H. Kane. "The Sulfidation Attack of a Nickel-Base Alloy at Intermediate Temperatures," Metallurgical Trans., 15A: 5-10 (January, 1984).
5. Morrow III, H. et al. "The Effects of Molybdenum and Aluminum on the Hot Corrosion (Sulfidation) Behavior of Experimental Nickel-Base Superalloys," Metallurgical Trans., 5A: 673-683 (March, 1974).
6. Allen, J. M. and G. A. Whitlow. "Observations on the Interaction of High Mean Stress and Type II Hot Corrosion on the Fatigue Behavior of a Nickel-Base Superalloy," ASME paper no. 84-GT-149; to be published in ASME Journal of Eng. for Power.
7. Whitlow, G. A. et al. "Intermediate Temperature, Low-Cycle Fatigue Behavior of Coated and Uncoated Nickel-Base Superalloys in Air and Corrosive Sulfate Environments," Journal of Eng. Mats. and Tech., 106: 43-49 (January, 1984).
8. Yoshida, M. et al. "Effect of Hot Corrosion on the Creep Rupture Properties of a Nickel-Base Superalloy," Journal of Iron and Steel Inst. of Japan, 68(1): 120-129 (January, 1982).
9. Spengler, C. J. and R. Viswanathan. "Effect of Sequential Sulfidation and Oxidation on the Propagation of Sulfur in an 85Ni-15Cr Alloy," Metallurgical Trans., 3A: 161-166 (January, 1972).
10. Goebel, J. A. et al. "Mechanisms for the Hot Corrosion of Nickel-Base Alloys," Metallurgical Trans., 4A: 261-278 (January, 1973).
11. Bornstein, N. S. and M. A. DeCrescente. "The Role of Sodium in the Accelerated Oxidation Phenomenon Termed Sulfidation," Metallurgical Trans., 2A: 2875-2883 (October, 1971).
12. Whitlow, G. A. et al. "The Effects of a Liquid Sulfate/Chloride Environment on Superalloy Stress Rupture Properties at 1300^oF (704^oC)," Metallurgical Trans., 15A: 23-28 (January, 1984).
13. Fang, W. C. and D. A. Shores. "The Effect of Salt Deposit Thickness on Hot Corrosion Rates." Extended Abstract. The Electrochemical Society Meeting, Fall 1979.

14. Dieter, G. E. Mechanical Metallurgy (Second Edition). New York: McGraw-Hill Book Company, 1976.
15. Department of Defense. Aerospace Structural Metals Handbook. AFML-TR-68-115 Vol 4. Traverse City, MI: Mechanical Properties Data Center, 1975.
16. Barker, J. F. et al. "Long-Time Stability of Inconel 718," Journal of Metals: 31 (January, 1970).
17. Khobaib, M. University of Dayton Research Institute. Personal Interview. Metals Behavior Branch, Wright-Patterson AFB, OH. January 1985.

APPENDIX

Tabulated Creep Data

JULIAN DATE: 171

MACHINE NUMBER: 9

SPECIMEN ID: 84-253

TIME (HRS)	% STRAIN
0.00000	0.00000
0.83340E-02	0.25975
0.16668E-01	0.33551
0.25002E-01	0.33551
0.33332E-01	0.34634
0.41672E-01	0.33551
0.50002E-01	0.33551
0.58342E-01	0.34634
0.66672E-01	0.34634
0.75002E-01	0.34634
0.83342E-01	0.33551
0.91672E-01	0.34634
0.10001	0.34634
0.10834	0.34634
1.1084	0.34634
2.1085	0.40045
3.1086	0.44374
4.1087	0.48704
5.1088	0.51950
6.1088	0.56280
7.1089	0.61691
8.1090	0.67103
9.1091	0.74679
10.109	0.81173
11.109	0.88749
12.109	0.95242
13.109	1.0390
14.109	1.1256
15.109	1.2230
16.109	1.3312
17.109	1.4503
18.110	1.6018
19.110	1.7209

JULIAN DATE: 192

MACHINE NUMBER: 9

SPECIMEN ID: 84-254

TIME IN HOURS	% STRAIN		
*****	*****		
0.00000000	0.32154344E-01		
0.83339997E-02	0.32154344E-01		
0.16667999E-01	0.16077173		
0.25001999E-01	0.16077173		
0.33335999E-01	0.15005361		
0.41670002E-01	0.15005361	43.070110	1.1789926
0.50003998E-01	0.16077173	44.070190	1.2111470
0.58338001E-01	0.16077173	45.070271	1.2540194
0.66672005E-01	0.16077173	46.070351	1.2968919
1.0667520	0.22508039	47.070431	1.3290462
2.0668321	0.26795286	48.070511	1.3826368
3.0669119	0.28938910	49.070591	1.4362274
4.0669918	0.30010721	50.070671	1.4790999
5.0670714	0.33226156	51.070751	1.5219723
6.0671515	0.35369781	52.070831	1.5755630
7.0672317	0.36441594	53.070911	1.6291535
8.0673122	0.39657024	54.070988	1.6720259
9.0673923	0.40728837	55.071068	1.7256165
10.067472	0.42872462	56.071148	1.7792072
11.067552	0.45016077	57.071228	1.8327975
12.067632	0.47159708	58.071308	1.8863883
13.067713	0.48231521	59.071388	1.9506968
14.067792	0.49303329	60.071468	2.0257239
15.067872	0.50375134	61.071548	2.0900323
16.067951	0.51446950	62.071629	2.1543412
17.068031	0.52518767	63.071709	2.2400861
18.068111	0.53590572	64.071793	2.3043947
19.068192	0.55734193	65.071877	2.3579853
20.068272	0.57877821	66.071953	2.4437301
21.068350	0.60021442	67.072037	2.5187571
22.068430	0.62165070	68.072113	2.6045017
23.068510	0.64308691	69.072189	2.6795287
24.068590	0.66452312	70.072273	2.7652736
25.068670	0.68595934	71.072350	2.8403006
26.068750	0.70739561	72.072433	2.9260452
27.068830	0.72883189	73.072510	3.0117905
28.068911	0.75026804		
29.068991	0.77170426		
30.069071	0.79314047		
31.069151	0.82529473		
32.069229	0.83601296		
33.069309	0.86816734		
34.069389	0.90032154		
35.069469	0.93247592		
36.069550	0.96463042		
37.069630	0.98606658		
38.069710	1.0182209		
39.069790	1.0503753		
40.069870	1.0825296		
41.069950	1.1039660		
42.070030	1.1361202		

JULIAN DATE: 205

MACHINE NUMBER: 9

SPECIMEN ID: 84-250

TIME IN HOURS	% STRAIN		
*****	*****		
0.00000000	0.33670034E-01		
0.83339997E-02	0.56116726E-01		
0.16667999E-01	0.67340069E-01		
0.25001999E-01	0.78563415E-01		
0.33335999E-01	0.89786761E-01		
0.41669998E-01	0.89786761E-01	37.087410	1.2794613
0.50003998E-01	0.89786761E-01	38.087490	1.3243548
0.58337998E-01	0.89786761E-01	39.087570	1.3804716
0.66671997E-01	0.89786761E-01	40.087650	1.4702582
0.75006001E-01	0.89786761E-01	41.088284	1.5263751
0.84451199E-01	0.89786761E-01	42.088364	1.5937150
1.0845312	0.11223345	43.088444	1.6610552
2.0846112	0.14590348	44.088524	1.7171718
3.0846910	0.17957352	45.088604	1.7845118
4.0847712	0.21324356	46.088684	1.8742988
5.0848513	0.23569022	47.088764	1.9640853
6.0849309	0.25813693	48.088844	2.0538721
7.0850110	0.26936027	49.088924	2.1548822
8.0850906	0.30303031	50.089005	2.2334456
9.0851707	0.32547703	51.089085	2.3456790
10.085251	0.33670038	52.089165	2.4354661
11.085331	0.38159376	53.089245	2.5252526
12.085411	0.40404043	54.089325	2.6262629
13.085491	0.41526380	55.089405	2.7497196
14.085570	0.43771049	56.089485	2.8507297
15.085650	0.46015713	57.089565	2.9517398
16.085732	0.48260391	58.089645	3.0639732
17.085810	0.51627386	59.089725	3.1874299
18.085890	0.52749717	60.089806	3.2996635
19.085970	0.54994392	61.089886	3.4231205
20.086050	0.57239062	62.089966	3.5578008
21.086130	0.60606062	63.090046	3.6812570
22.086210	0.63973066	64.090126	3.8159375
23.086290	0.67340070	65.090202	3.9618411
24.086370	0.70707072	66.090286	4.0965209
25.086451	0.74074084	67.090363	4.2199774
26.086531	0.78563422	68.090446	4.3546581
27.086611	0.83052760	69.093857	4.5005612
28.086691	0.87542099	70.097824	4.6576811
29.086771	0.89786762	71.097908	4.8260384
30.086851	0.94276086		
31.086929	0.99887744		
32.087009	1.0325477		
33.087090	1.0886645		
34.087170	1.1335579		
35.087250	1.1896746		
36.087330	1.2345660		

JULIAN DATE: 255

MACHINE NUMBER: 9

SPECIMEN ID: R4-256

TIME (HOURS)	% STRAIN
0.00000000	0.00000000
1.0000800	0.47393363E-01
2.0001597	0.71090043E-01
3.0002398	0.62938381E-01
4.0003200	0.10663506
5.0004001	0.13033174
6.0004802	0.14218009
7.0005598	0.15402842
8.0006399	0.17772511
9.0007200	0.18957345
10.000800	0.20142178
11.000880	0.21327011
12.000959	0.23696680
13.001040	0.24881513
14.001120	0.27251181
15.001200	0.28436017
16.001278	0.28436017
17.001358	0.29620850
18.001438	0.29620850
19.001518	0.29620850
20.001598	0.30805683
21.001678	0.31990519
22.001759	0.33175352
23.001839	0.31990519
24.001919	0.33175352
25.001999	0.34360188
26.002079	0.35545021
27.002159	0.36729854
28.002237	0.36729854
29.002317	0.37914690
30.002398	0.37914690
31.002478	0.39099523
32.002560	0.39099523
33.002640	0.39099523
34.002720	0.40284356
35.002796	0.41469190
36.002876	0.41469190
37.002956	0.42654023
38.003036	0.42654023
39.003117	0.43838859
40.003197	0.45023692
41.003277	0.46208528
42.003357	0.47393361
43.003437	0.47393361
44.003517	0.48578194
45.003597	0.48578194
46.003677	0.48578194

47.003757	0.49763027
48.003838	0.49763027
49.003918	0.50947863
50.003998	0.50947863
51.004078	0.52132696
52.004158	0.52132696
53.004238	0.53317529
54.004318	0.54502362
55.004398	0.54502362
56.004478	0.55687195
57.004559	0.56872034
58.004639	0.58056867
59.004719	0.59241700
60.004799	0.59241700
61.004879	0.60426533
62.004955	0.61611366
63.005035	0.61611366
64.005119	0.63981038
65.005196	0.63981038
66.005280	0.65165871
67.005356	0.67535537
68.005440	0.67535537
69.016548	0.68720001
70.037109	0.69910002
71.037109	0.71090001

JULIAN DATE: 262

MACHINE NUMBER: 9

SPECIMEN ID: 84-257

TIME (HOURS)	% STRAIN		
0.0000000	0.11851150E-01		
0.83339997E-02	0.11851150E-01		
0.16667999E-01	0.23702299E-01		
0.25001999E-01	0.47404598E-01		
0.33335999E-01	0.47404598E-01		
0.41669998E-01	0.59255749E-01		
0.50003998E-01	0.71106903E-01		
0.58337998E-01	0.71106903E-01		
0.66671997E-01	0.71106903E-01		
0.75006001E-01	0.71106903E-01	40.377674	0.39108795
1.0750860	0.82958050E-01	41.419979	0.39108795
2.0907228	0.94809197E-01	42.420612	0.40293911
3.0913582	0.94809197E-01	43.420692	0.41479024
4.0914383	0.11851150	44.434666	0.41479024
5.0915184	0.11851150	45.455299	0.41479024
6.0915980	0.13036264	46.495941	0.42664137
7.0916781	0.14221381	47.496021	0.42664137
8.0917578	0.15406494	48.502213	0.43849254
9.0918379	0.16591610	49.510071	0.43849254
10.091918	0.16591610	50.551266	0.45034370
11.091998	0.17776725	51.551346	0.46219486
12.127636	0.18961839	52.551426	0.47404599
13.128272	0.20146956	53.564285	0.47404599
14.128352	0.21332069	54.582142	0.48589712
15.150656	0.22517185	55.623894	0.49774826
16.170181	0.23702300	56.623974	0.50959945
17.214153	0.20146956	57.624054	0.52145058
18.215345	0.23702300	58.639133	0.53330177
19.215425	0.24887413	59.657551	0.53330177
20.215506	0.23702300	60.703743	0.55700403
21.231142	0.24887413	61.704380	0.55700403
22.261225	0.24887413	62.704460	0.58070636
23.303530	0.26072529	63.723431	0.56885523
24.304165	0.24887413	64.723511	0.58070636
25.313135	0.26072529	65.724701	0.59255749
26.313215	0.28442761	66.724785	0.59255749
27.313295	0.28442761	67.724861	0.59255749
28.313375	0.29627874	68.724945	0.60440862
29.313456	0.29627874	69.725021	0.61625975
30.313536	0.29627874	70.747879	0.61625975
31.313616	0.31998104	71.747963	0.62811085
32.313694	0.33183220		
33.313774	0.34368336		
34.313854	0.34368336		
35.314491	0.36738563		
36.337906	0.35553449		
37.337986	0.36738563		
38.338066	0.37923679		
39.359257	0.39108795		

JULIAN DATE: 290

MACHINE NUMBER: 9

SPECIMEN ID: 84-258

TIME (HOURS)	% STRAIN
*****	*****
0.00000000	0.00000000
0.83339997E-02	0.24151680E-01
0.16668000E-01	0.24151680
0.25002000E-01	0.25359264
0.33335999E-01	0.25359264
1.0334160	0.38642688
2.0334959	0.49510944
3.0335759	0.59171616
4.0336559	0.67624704
5.0337358	0.76077792
6.0338158	0.85738464
7.0338958	0.95399136
8.0339757	1.0747498
8.8996005	1.1834323
9.8996805	1.3162666
10.899760	1.4732525
11.899840	1.6543901
12.899920	1.8234518
13.900000	2.0045894
14.900080	2.2340304
15.900160	2.4996989
16.900240	2.8015949
17.900320	3.1638701
18.900400	3.5623728
19.900480	4.1057856
20.900560	4.6975017
21.900640	5.4220521
22.900720	6.2552851
23.900800	7.2938073
24.900880	8.1874195
25.400920	8.7549840

JULIAN DATE: 303

MACHINE NUMBER: 9

SPECIMEN ID: 84-259

TIME (HOURS)	% STRAIN		

0.00000000	0.00000000		
0.83340000E-02	0.11076921		
0.16668000E-01	0.12307690		
0.25001999E-01	0.12307690		
0.33335999E-01	0.12307690		
0.41669999E-01	0.12307690		
0.52226402E-01	0.12307690		
1.0523064	0.14769228		
2.0523863	0.17230766	42.647299	0.77538448
3.0524663	0.18461535	43.647379	0.79999986
4.0525463	0.20923073	44.647459	0.81230755
5.0526262	0.22153842	45.647539	0.83692293
6.0527062	0.24615380	46.647619	0.84923062
7.0527862	0.25846149	47.647699	0.86153831
8.0528661	0.27076918	48.647779	0.88615369
9.0529461	0.29538456	49.647859	0.91076907
10.053026	0.30769225	50.647939	0.93538445
11.053106	0.31999994	51.648019	0.94769214
12.053186	0.33230763	52.648099	0.97230752
13.053266	0.34461532	53.648179	1.0092306
14.053346	0.36923070	54.648259	1.0338460
15.053426	0.38153839	55.648339	1.0584613
16.053506	0.39384608	56.648419	1.0830767
17.053586	0.39384608	57.648498	1.1076921
18.053666	0.40615377	58.648578	1.1446152
19.053746	0.43076915	59.648658	1.1692306
20.053826	0.44307684	60.648738	1.1938459
21.053906	0.45538453	61.648818	1.2184613
22.053986	0.46769222	62.648898	1.2430767
23.054066	0.47999991	63.648978	1.2799998
24.054146	0.50461529	64.649058	1.3046151
25.054226	0.51692298	65.649138	1.3292305
26.054306	0.54153836	66.649218	1.3661536
27.054386	0.55384605	67.649298	1.3907690
28.054466	0.56615374	68.649378	1.4153844
29.054546	0.59076912	69.649458	1.4399997
30.054626	0.60307681	70.649538	1.4769228
31.054706	0.61538450	71.649618	1.5015382
31.646417	0.62769219		
32.646499	0.63999988		
33.646579	0.65230757		
34.646659	0.67692295		
35.646739	0.68923064		
36.646819	0.70153833		
37.646899	0.71384602		
38.646979	0.73846141		
39.647059	0.75076910		
40.647139	0.75076910		
41.647219	0.76307679		

JULIAN DATE: 307

MACHINE NUMBER: 9

SPECIMEN ID: 84-260

TIME (HOURS) % STRAIN

0.00000000 0.15126839
0.83340000E-02 0.15126839
0.16668000E-01 0.15126839
0.25001999E-01 0.15126839
0.33335999E-01 0.16290442
1.0334160 0.20944854
2.0334959 0.23272060
3.0335759 0.25599266
4.0336559 0.26762869
5.0337358 0.27926472
6.0338158 0.30253678
7.0338958 0.31417281
8.0339757 0.32580884
9.0340557 0.33744487
10.034136 0.34908090
11.034216 0.34908090
12.034296 0.36071693
13.034376 0.37235296
14.034456 0.38398899
15.034535 0.39562502
16.034615 0.40726105
17.034695 0.41889708
18.034775 0.41889708
19.034855 0.43053311
20.034935 0.44216914
21.035015 0.45380517
22.035095 0.46544120
23.035175 0.46544120
24.035255 0.47707723
25.035335 0.48871326
26.035415 0.50034929
27.035495 0.51198532
28.035575 0.52362135
29.035655 0.53525738
30.035735 0.53525738
31.035815 0.54689341
32.035895 0.55852944
33.035975 0.57016547
34.036055 0.58180150
35.036135 0.59343753
36.036215 0.60507356
37.036295 0.61670959
38.036375 0.62834562
39.036455 0.63998165
40.036535 0.65161768
41.036615 0.66325371
42.036695 0.67488974
43.036775 0.69816180
44.036855 0.70979783

45.036934 0.70979783
46.037014 0.73306989
47.037094 0.74470592
48.037174 0.76797798
49.037254 0.77961401
50.037334 0.80288607
51.037414 0.81452210
52.037494 0.82615812
53.037574 0.84943018
54.037654 0.87270224
55.037734 0.88433827
56.037814 0.90761033
57.037894 0.91924636
58.037974 0.94251842
59.038054 0.96579048
60.038134 0.97742651
61.038214 1.0006986
62.038294 1.0239706
63.038374 1.0472427
64.038454 1.0821508
65.038534 1.0937868
66.038614 1.1170589
67.038694 1.1403309
68.038774 1.1636030
69.038854 1.1868751
70.038934 1.2101471
71.039014 1.2334192
72.039094 1.2566912

JULIAN DATE: 332

MACHINE NUMBER: 9

SPECIMEN ID: 84-261

TIME IN HOURS	% STRAIN		
*****	*****		
0.000000000	0.00000000		
0.83339982E-02	0.14857142		
0.16667998E-01	0.15999999		
0.25557598E-01	0.15999999		
0.33891597E-01	0.15999999		
0.42781197E-01	0.17142856		
0.51115197E-01	0.17142856		
0.60004796E-01	0.17142856		
1.0600848	0.18285713		
2.0601647	0.20571428		
3.0602447	0.21714285		
4.0603247	0.25142856		
5.0609602	0.26285713		
6.0610402	0.28571427		
7.0611202	0.31999999		
8.0612001	0.33142856		
9.0612801	0.35428570		
10.061360	0.37714284		
11.061440	0.39999998		
12.061520	0.42285712		
13.061600	0.44571427		
14.061680	0.46857141		
15.062315	0.49142855		
16.062395	0.52571426		
17.062475	0.54857140		
18.062555	0.57142855		
19.062635	0.59428569		
20.062715	0.61714283		
21.062795	0.63999997		
22.063431	0.68571426		
23.063511	0.69714283		
24.063591	0.73142854		
25.063671	0.75428568		
26.063751	0.78857139		
27.063831	0.82285711		
28.063911	0.85714282		
29.063991	0.90285710		
30.064071	0.93714282		
31.064151	0.97142853		
32.064231	1.0057142		
33.064310	1.0514285		
34.064390	1.0971428		
35.064470	1.1428571		
36.064550	1.1999999		
37.065186	1.2457142		
38.065266	1.3028571		
39.065346	1.3485714		
40.065426	1.4057142		
41.065506	1.4628571		
		42.066141	1.5314285
		43.066221	1.5885714
		44.066301	1.6571428
		45.066381	1.7142856
		46.066461	1.7828571
		47.067097	1.8514285
		48.067177	1.9199999
		49.067257	1.9999999
		50.067337	2.0685713
		51.067417	2.1485713
		52.067497	2.2399999
		53.067577	2.3199999
		54.067657	2.3999999
		55.067737	2.4799999
		56.067817	2.5599999
		57.067896	2.6399999
		58.068532	2.7314284
		59.068612	2.8114284
		60.068692	2.9142856
		61.068772	3.0057142
		62.068852	3.1085713
		63.068932	3.1999999
		64.069012	3.3142856
		65.069092	3.4057141
		66.069172	3.5199998
		67.069807	3.6228570
		68.069887	3.7371427
		69.069967	3.8628570
		70.070047	3.9885713
		71.070127	4.1142855
		71.683510	4.1942855
		72.183550	4.2628570
		72.683590	4.3314284
		73.183630	4.3999998
		73.684225	4.4685712
		74.184265	4.5257141
		74.684305	4.5942855

TIME IN HOURS % STRAIN

 0.0000000 0.17100000
 1.0000800 0.27993248
 2.0007155 0.27993248
 3.0007955 0.27993248
 4.0008755 0.27993248
 5.0009554 0.29354904
 6.0010354 0.30716560
 7.0011154 0.30716560
 8.0011953 0.30716560
 9.0012753 0.32078216
 10.001911 0.33439872
 11.001991 0.33439872
 12.002071 0.34801529
 13.002151 0.34801529
 14.002786 0.36163185
 15.002866 0.37524841
 16.002946 0.37524841
 17.003026 0.38886497
 18.003106 0.40248153
 19.003186 0.40248153
 20.003822 0.41609809
 21.003902 0.42971465
 22.003982 0.42971465
 23.004062 0.44333121
 23.504103 0.45694777
 24.504183 0.47056433
 25.504818 0.47056433
 26.504898 0.49779745
 27.504978 0.49779745
 28.505058 0.51141402
 29.505138 0.52503058
 30.505218 0.52503058
 31.505854 0.53864714
 32.505934 0.55226370
 33.506014 0.56588026
 34.506093 0.57949682
 35.506173 0.59311338
 36.506253 0.60672994
 37.506333 0.62034650
 38.506969 0.62034650
 39.507049 0.63396306
 40.507129 0.64757962
 41.507209 0.66119618
 42.507289 0.67481274
 43.507369 0.68842930
 44.508004 0.71566242
 45.508084 0.72927898
 46.508164 0.74289554
 47.508244 0.75651211

48.508324	0.77012867
49.508960	0.78374523
50.509040	0.81097835
51.509120	0.82459491
52.509200	0.83821147
53.509280	0.85182803
54.509360	0.86544459
55.509440	0.89267771
56.510075	0.90629427
57.510155	0.91991083
58.510235	0.93352739
59.510315	0.96076051
60.510395	0.97437708
61.510475	0.98799364
62.510555	1.0016102
63.510635	1.0288433
64.510715	1.0560764
65.510795	1.0696930
66.510875	1.0833096
67.510955	1.0969261
68.511035	1.1241592
69.511115	1.1513924
70.511195	1.1786255
71.511830	1.1922420
72.511910	1.2330917

TIME IN HOURS . % STRAIN

0.00000000 0.00000000

0.83339997E-02. 0.12799180

1.0084140 0.15359015

2.0084939 0.16638933

3.0085739 0.17918851

4.1292191 0.17918851

5.1298546 0.20478687

6.1299346 0.21758605

7.1300146 0.23038523

8.1300945 0.24318441

9.1301745 0.25598359

10.130254 0.26878277

11.130334 0.28158195

12.130970 0.29438113

13.131050 0.30718031

14.131130 0.33277867

15.131210 0.34557785

16.131290 0.35837703

17.131370 0.35837703

18.131450 0.37117621

19.131530 0.38397539

20.132165 0.39677457

21.132245 0.40957375

22.132325 0.42237293

23.132405 0.43517210

24.132485 0.43517210

25.133121 0.44797128

26.133201 0.46077046

27.133281 0.48636882

28.133361 0.48636882

29.133996 0.51196718

30.134076 0.52476636

31.134156 0.53756554

32.134792 0.55036472

33.134872 0.56316390

34.134952 0.57596308

35.135032 0.60156144

36.135112 0.61436062

37.135192 0.62715980

38.135272 0.63995898

39.135351 0.65275816

40.135987 0.66555734

41.136067 0.69115570

42.136147 0.70395488

43.136227 0.71675406

44.136307 0.74235241

45.136387 0.75515159

46.136467 0.76795077

47.136547 0.79354913

48.137182	0.80634831
49.137262	0.83194667
50.137342	0.84474585
51.137422	0.87034421
52.137502	0.88314339
53.137582	0.90874175
54.137662	0.93434011
55.137742	0.95993847
56.137822	0.97273765
57.137902	0.99833601
58.137982	1.0239344
59.138062	1.0495327
60.138142	1.0623319
61.138222	1.1007294
62.138858	1.1263276
63.138937	1.1391270
64.139017	1.1775245
65.139097	1.2031229
66.139177	1.2267212
67.139257	1.2543196
68.139893	1.2799180
69.139973	1.3055163
70.140608	1.3311147
71.140688	1.3567130
72.140768	1.3951106
73.140848	1.4335081

TIME (HOURS)	% STRAIN		

0.0000000	0.0000000		
0.16667999E-01	0.10138136		
0.33891599E-01	0.11405403		
0.51115198E-01	0.12672670		
1.0600848	0.15207204		
2.0601647	0.16474471		
3.0602447	0.19009005		
4.0603247	0.21543539	46.065350	1.9769365
5.0604046	0.22810806	47.065430	2.0783179
6.0604846	0.25345340	48.065510	2.1796993
7.0605646	0.26612607	49.066146	2.2810806
8.0606445	0.29147141	50.066226	2.3951347
9.0607245	0.31681675	51.066305	2.5218614
10.060804	0.32948942	52.066941	2.6485881
11.060884	0.35483477	53.067021	2.7626421
12.060964	0.38018011	54.067101	2.8766961
13.061044	0.39285278	55.067181	3.0160955
14.061124	0.41819812	56.067817	3.1428222
15.061204	0.44354346	57.067896	3.2948942
16.061284	0.46888880	58.067976	3.4469663
17.061364	0.49423414	59.068056	3.5990383
18.061444	0.51957948	60.068136	3.7511104
19.061524	0.54492482	61.068216	3.9158551
20.061604	0.57027016	62.068852	4.0679271
21.062240	0.59561550	63.068932	4.2326718
22.062320	0.62096084	64.069012	4.4100892
23.062400	0.65897885	65.069092	4.6001793
24.062480	0.67165152	66.069172	4.7649240
25.063115	0.68432419	67.069252	4.9423414
26.063195	0.73501487	68.069332	5.1451041
27.063275	0.76036021	69.069412	5.3351941
28.063355	0.82372356	70.070047	5.5379569
29.063435	0.86174157	71.070127	5.7533923
30.063515	0.89975958	72.070207	5.9688277
31.063595	0.93777759	72.090764	5.9688277
32.063675	0.98846827		
33.063755	1.0391590		
34.063835	1.0898496		
35.063915	1.1532130		
36.064550	1.2039037		
37.064630	1.2672670		
38.064710	1.3306304		
39.064790	1.4066664		
40.064870	1.4827024		
41.064950	1.5587384		
42.065030	1.6347745		
43.065110	1.7108105		
44.065190	1.7995192		
45.065270	1.8882279		

JULIAN DATE:

4

MACHINE NUMBER: 9

SPECIMEN ID: 84-239

TIME (HOURS) % STRAIN

0.00000000	0.00000000		
0.86117997E-02	0.10343935		
0.16945799E-01	0.11636927		
0.43336799E-01	0.11636927		
1.0434168	0.15515903		
2.0434967	0.16808895		
3.0438545	0.18101887		
4.0439345	0.19394879		
5.0442922	0.21980863		
6.0446500	0.23273855	46.051738	1.4352210
7.0447300	0.24566847	47.051818	1.4869407
8.0448099	0.27152831	48.052176	1.5645202
9.0451677	0.28445823	49.052256	1.6162399
10.045525	0.29738815	50.052613	1.6938194
11.045605	0.32324798	51.052693	1.7584690
12.045963	0.34910782	52.053051	1.8360485
13.046043	0.36203774	53.053409	1.9136281
14.046123	0.40082750	54.053489	1.9912076
15.046481	0.41375742	55.053569	2.0687871
16.046561	0.43961726	56.053649	2.1592965
17.046641	0.45254718	57.053729	2.2368760
18.046999	0.47840702	58.054086	2.3273855
19.047079	0.49133694	59.054444	2.4308248
20.047159	0.51719677	60.054524	2.5213343
21.047516	0.54305661	61.054604	2.6247736
22.047596	0.55598653	62.054684	2.7282130
23.047954	0.58184637	63.054764	2.8316523
24.048034	0.60770621	64.054844	2.9350917
25.048114	0.63356605	65.054924	3.0643909
26.048472	0.65942589	66.055004	3.1807602
27.048829	0.68528573	67.055084	3.2971294
28.048909	0.72407548	68.055164	3.4264286
29.048989	0.74993532	69.055244	3.5557278
30.049069	0.77579516	70.055602	3.6850270
31.049149	0.80165500	71.055682	3.8143262
32.049229	0.82751484	72.055762	3.9565553
33.049309	0.86630460	73.055842	4.0987844
34.049667	0.89216444	74.055922	4.2410136
35.049747	0.93095419	74.535404	4.3056631
36.050105	0.95681403		
37.050185	1.0085337		
38.050265	1.0343935		
39.050345	1.0861132		
40.050702	1.1249030		
41.051060	1.1766227		
42.051140	1.2154124		
43.051220	1.2671321		
44.051300	1.3188518		
45.051380	1.3835014		

VITA

1Lt Stephen J. Balsone was born on 20 October 1960 in Butler, Pennsylvania. He graduated from Ford City High School in Ford City, Pennsylvania, in 1978. He enrolled at Carnegie-Mellon University (C-MU), Pittsburgh, Pennsylvania, on a four-year AFROTC scholarship. In May, 1982, he received a Bachelor of Science degree in Metallurgical Engineering and Materials Science and upon graduation was commissioned in the United States Air Force. He was employed at C-MU as a metallurgical research engineer until called to active duty in August, 1982. His first duty assignment was to the School of Engineering, Air Force Institute of Technology (AFIT), Wright-Patterson AFB, Ohio, where he received a Bachelor of Science degree in Aeronautical Engineering in March, 1984. Upon graduation he was assigned to the Metals Behavior Branch of the Air Force Materials Laboratory, Wright-Patterson AFB, Ohio. He is presently working as a structural materials engineer and enrolled at AFIT as a part-time Masters of Science degree candidate in Aeronautical Engineering.

permanent address: 2233 Manor Drive

Ford City, PA 16226

UNCLASSIFIED

SECURITY CLASSIFICATION OF THIS PAGE

REPORT DOCUMENTATION PAGE

1a. REPORT SECURITY CLASSIFICATION UNCLASSIFIED			1b. RESTRICTIVE MARKINGS			
2a. SECURITY CLASSIFICATION AUTHORITY			3. DISTRIBUTION/AVAILABILITY OF REPORT APPROVED FOR PUBLIC RELEASE; DISTRIBUTION UNLIMITED			
2b. DECLASSIFICATION/DOWNGRADING SCHEDULE						
4. PERFORMING ORGANIZATION REPORT NUMBER(S) AFIT/GAE/AA/85M-1			5. MONITORING ORGANIZATION REPORT NUMBER(S)			
6a. NAME OF PERFORMING ORGANIZATION SCHOOL OF ENGINEERING		6b. OFFICE SYMBOL (If applicable) AFIT/ENY		7a. NAME OF MONITORING ORGANIZATION		
6c. ADDRESS (City, State and ZIP Code) AIR FORCE INSTITUTE OF TECHNOLOGY WRIGHT-PATTERSON AFB, OHIO 45433			7b. ADDRESS (City, State and ZIP Code)			
8a. NAME OF FUNDING/SPONSORING ORGANIZATION METALS BEHAVIOR BRANCH		8b. OFFICE SYMBOL (If applicable) AFWAL/MLLN		9. PROCUREMENT INSTRUMENT IDENTIFICATION NUMBER		
8c. ADDRESS (City, State and ZIP Code) AIR FORCE MATERIALS LABORATORY WRIGHT-PATTERSON AFB, OHIO 45433			10. SOURCE OF FUNDING NOS.			
11. TITLE (Include Security Classification) SEE BOX 19			PROGRAM ELEMENT NO. 61102F	PROJECT NO. 2302	TASK NO. P1	WORK UNIT NO. 01
PERSONAL AUTHOR(S) STEPHEN J. BALSONE, 1LT, USAF						
13a. TYPE OF REPORT MS THESIS		13b. TIME COVERED FROM _____ TO _____		14. DATE OF REPORT (Yr., Mo., Day) 1985 MARCH		15. PAGE COUNT 116
16. SUPPLEMENTARY NOTATION						
17. COSATI CODES			18. SUBJECT TERMS (Continue on reverse if necessary and identify by block number)			
FIELD	GROUP	SUB GR.	NICKEL-BASE SUPERALLOY, HOT CORROSION, CREEP STRENGTH, GAS TURBINES, ENVIRONMENTAL TESTS			
11	06	1				
11	06	5				
19. ABSTRACT (Continue on reverse if necessary and identify by block number)						
TITLE: THE EFFECT OF STRESS AND HOT CORROSION ON NICKEL-BASE SUPERALLOYS						
THESIS CHAIRMAN: GEORGE W. WATT, LT COL, USAF						
<p>THIS STUDY EXAMINES THE EFFECT OF A MOLTEN SALT ENVIRONMENT ON THE HIGH TEMPERATURE CREEP PROPERTIES OF INCONEL 718. SUSTAINED-LOAD CREEP TESTS WERE CONDUCTED AT A TEMPERATURE OF 1472°F (800°C) IN LABORATORY AIR AT STRESS LEVELS IN THE RANGE OF 10 KSI TO 30 KSI. ROUND BAR TENSILE SPECIMENS WERE COATED WITH A 90% Na₂SO₄/10% NaCl SALT MIXTURE BY SPRAYING A HEATED SPECIMEN WITH AN AQUEOUS SALT SOLUTION. CREEP DATA WERE THEN COLLECTED OVER A 72-HOUR TEST PERIOD. TESTS CONDUCTED WITH SALT COATED SPECIMENS WERE</p>						
20. DISTRIBUTION/AVAILABILITY OF ABSTRACT UNCLASSIFIED/UNLIMITED <input checked="" type="checkbox"/> SAME AS RPT. <input type="checkbox"/> DTIC USERS <input type="checkbox"/>				21. ABSTRACT SECURITY CLASSIFICATION UNCLASSIFIED		
22a. NAME OF RESPONSIBLE INDIVIDUAL GEORGE W. WATT, LT COL, USAF			22b. TELEPHONE NUMBER (Include Area Code) (513) 255-3517		22c. OFFICE SYMBOL AFIT/ENY	

DD FORM 1473, 83 APR

EDITION OF 1 JAN 73 IS OBSOLETE.

UNCLASSIFIED

SECURITY CLASSIFICATION OF THIS PAGE

19. (Cont.)

COMPARED WITH TESTS CONDUCTED WITH UNCOATED SPECIMENS. SPECIMENS WERE SUBSEQUENTLY SECTIONED AND MOUNTED, AND A METALLOGRAPHIC ANALYSIS OF THE CORROSION ATTACK WAS CONDUCTED.

EVIDENCE SHOWS A DEGRADATION OF THE HIGH TEMPERATURE CREEP PROPERTIES OF INCONEL 718 DUE TO THE PRESENCE OF MOLTEN SALT. THIS IS DUE PRIMARILY TO OXIDE PENETRATION INTO METAL WHICH HAS BEEN DEPLETED OF ALLOYING ELEMENTS AND SUBSEQUENT CRACKING ALONG OXIDE-METAL INTERFACES. IN ADDITION, GRAIN BOUNDARY SLIDING AND VOID FORMATION ALONG THE GRAIN BOUNDARIES OCCURRED IN THE ALLOY DEPLETED ZONE OF CORROSION ATTACK. THIS REPORT EXAMINES THE EFFECT OF STRESS IN THE CORROSION PROCESS AND THE MICROSTRUCTURAL CHANGES AND MECHANISMS WHICH OCCUR DURING CORROSION-MECHANICAL PROPERTY INTERACTIONS.

STATIC HOT CORROSION TESTS ON SPECIMENS OF RENE 77 AND RENE 80 WERE ALSO CONDUCTED. CYLINDRICAL PINS WERE SALT COATED AND TESTED FOR 72 HOURS AT A TEMPERATURE OF 1652°F (900°C) IN LABORATORY AIR. WEIGHT CHANGE CALCULATIONS AND DEPTH OF CORROSION ATTACK MEASUREMENTS WERE MADE, AND A METALLOGRAPHIC ANALYSIS WAS DONE.